ESPOO 2006 VTT PUBLICATIONS 613

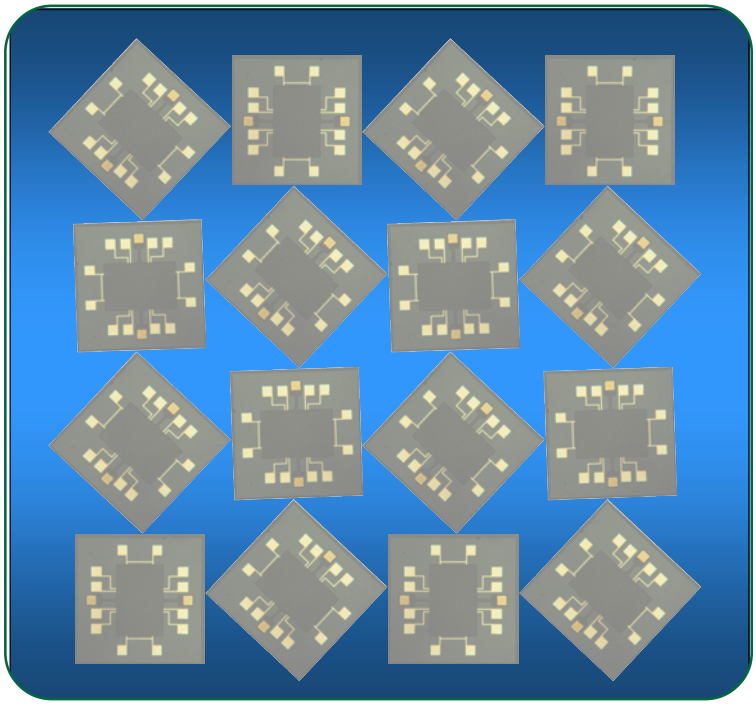

Anna-Maija Kärkkäinen

MEMS based voltage references

VTT PUBLICATIONS 613

MEMS based voltage references

Anna-Maija Kärkkäinen

Dissertation for the degree of Doctor of Philosophy to be presented with due permission of the Department of Electrical and Communications Engineering for public examination and debate in the Large Seminar Hall of Micronova (Tietotie 3) at Helsinki University of Technology (Espoo, Finland) on the 3rd of November, 2006, at 12 o'clock noon.

ISBN 951–38–6859–1 (soft back ed.)
ISSN 1235–0621 (soft back ed.)

ISBN 951–38–6860–5 (URL: http://www.vtt.fi/inf/pdf/)
ISSN 1455–0849 (URL: http://www.vtt.fi/inf/pdf/)

JULKAISIJA – UTGIVARE – PUBLISHER

VTT, Vuorimiehentie 3, PL 1000, 02044 VTT
puh. vaihde 020 722 111, faksi 020 722 4374

VTT, Bergsmansvägen 3, PB 1000, 02044 VTT
tel. växel 020 722 111, fax 020 722 4374

VTT Technical Research Centre of Finland, Vuorimiehentie 3, P.O. Box 1000, FI-02044 VTT, Finland
phone internat. +358 20 722 111, fax +358 20 722 4374

VTT, Tietotie 3, PL 1000, 02044 VTT
puh. vaihde 020 722 111, faksi 020 722 7012

VTT, Datavägen 3, PB 1000, 02044 VTT
tel. växel 020 722 111, fax 020 722 7012

VTT Technical Research Centre of Finland, Tietotie 3, P.O. Box 1000, FI-02044 VTT, Finland
phone internat. +358 20 722 111, fax +358 20 722 7012

Technical editing Maini Manninen

Edita Prima Oy, Helsinki 2006

Kärkkäinen, Anna-Maija. MEMS based voltage references [MEMSiin perustuvat jännite-referenssit]. Espoo 2006. VTT Publications 613. 109 p. + app. 42 p.

Keywords MEMS, micro electromechanical systems, DC voltage reference, AC voltage reference, electrostatic charging, pull-in voltage, long-term stability, micromachining

Abstract

Voltage references are fundamental building blocks in many instruments like data logging systems, digital multimeters, and calibrators. State-of-the-art DC voltage references are large and expensive Josephson voltage standards, operated at cryogenic temperatures. On the other hand, small and affordable Zener diodes are noisy and require temperature compensation, so there is a gap to be filled between these devices. The situation regarding AC voltage references is even worse. There are no references fundamentally based on AC, beside the AC Josephson voltage standard. Usually AC references are based on generating an AC voltage from DC, and respectively, an AC voltage is measured by converting it to DC. Hence, a small and affordable MEMS based AC voltage reference would be a very unique device.

The excellent mechanical properties of silicon microelectromechanical systems (MEMS) have been demonstrated in many commercial applications. Currently the performance of the components is limited by electrostatic instability phenomena and mechanical stress effects arising from component mounting and packaging. However, when these problems are solved, new application areas open up for micromechanical components, for example, in voltage metrology. The stability of a MEMS based voltage reference is ultimately based on mechanical properties of one of the most stable materials: single crystal silicon.

This dissertation reports a DC voltage reference and an AC voltage reference based on the pull-in voltage, a characteristic property of an electrostatic MEMS component. First a brief introduction to voltage metrology and MEMS is given, then methods available for making MEMS based voltage references are discussed, and finally results are presented. The results are divided into three Sections: design and manufacturing of the components, readout electronics, and measurement results of the reference long-term stability.

The stability of the reference voltage is of major importance in metrological applications and it is studied both theoretically and experimentally in this work. A detailed analysis of the electromechanical coupling of MEMS components is presented. Due to the lack of an appropriate text book, a majority of the formulas are derived from the basic equations by the author, including also those presented in the Methods Section. Component manufacturing, design and materials choices are also discussed focusing on the stability issue.

In the experimental part of this work a DC voltage reference and an AC voltage reference were designed, manufactured and characterized. Also two MEMS moving plate capacitors were designed: one optimised for use as a DC reference and the other optimised for use as an AC reference. The capacitor electrodes required metallizing which could not be manufactured using the existing processes. Hence a new silicon-on-insulator (SOI) manufacturing process utilising low temperature fusion bonding was developed.

The stability of the AC voltage reference presented in this dissertation is at ppm-level (10^{-6}). This level of performance is sufficient for several applications and outstanding compared to results published earlier for MEMS based voltage references. In the beginning of this work, a slow electrostatic charging effect of the MEMS component was the major factor limiting the device stability. The charging was significantly reduced by using AC voltage (instead of DC) to actuate the component to the pull-in point. However, even in the absence of an external DC voltage, there is an internal DC voltage due to the component built-in voltage. AC voltage actuation together with built-in voltage compensation removed the charging effect in the first order and reduced the drift of the reference below 2 ppm during the three week measurement period. The next challenge is to improve the component mechanical stability including the reduction of the component temperature coefficient. Before commercialisation component mounting and hermetic packaging need further attention as well.

Also, the DC voltage reference showed a significant improvement compared to results published earlier. In addition to the actions mentioned above, the DC voltage reference would still require improvement in the feedback electronics.

Kärkkäinen, Anna-Maija. MEMS based voltage references [MEMSiin perustuvat jännitereferenssit]. Espoo 2006. VTT Publications 613. 109 s. + liitt. 42 s.

Avainsanat MEMS, micro electromechanical systems, DC voltage reference, AC voltage reference, electrostatic charging, pull-in voltage, long-term stability, micromachining

Tiivistelmä

Mikroelektromekaanisiin systeemeihin, eli MEMSiin, perustuvat jännitereferenssit ovat ainutlaatuisia sekä ominaisuuksiltaan että toimintaperiaatteeltaan. Ne ovat pieniä ja tarkkoja, ja niillä on hyvä hinta-laatusuhde. Referenssin toiminta perustuu mikromekaanisesti valmistettuun levykondensaattoriin, jonka toinen levy on ripustettu piijousien varaan. Levyjen väliin kytketty jännite pyrkii lähentämään levyjä toisiinsa, kun taas piijousi vastustaa tätä liikettä. Voimatasapainoa levyjen välillä voidaan kuvata massa-jousi-vaimennin-mallilla ja sillä on kaksi keskeistä ominaisuutta. Sähköstaattinen voima levyjen välillä on verrannollinen jännitteen neliöön, eli sitä voidaan käyttää todellisena tehollisarvomuuntimena. Lisäksi kondensaattorin ulostulojännitteellä on maksimi, jota voidaan käyttää stabiilina jännitereferenssinä, sillä sen arvo riippuu vain yksikiteisen piin materiaalivakiosta ja jousen geometriasta. Koska referenssijännite on samalla myös käännepiste, ohjausjännitteen pienet vaihtelut eivät vaikuta referenssijännitteen arvoon ensimmäisessä kertaluvussa. Näiden ominaisuuksien ansiosta MEMS-jännitereferenssit tulevat haastamaan olemassa olevat jännitereferenssit, esimerkiksi Zenerdiodit.

Väitöskirjassa tutkitaan sekä teoreettisesti että kokeellisesti kahta jännitereferenssiä, joista toinen on suunniteltu tasajännitteelle ja toinen vaihtojännitteelle. Molemmille suunniteltiin omat MEMS-komponentit. Niiden suunnittelu, valmistus ja ominaisuudet on kuvattu yksityiskohtaisesti samoin kuin referenssien lukuelektroniikat ja valmiiden laitteiden ominaisuudet. Erityisesti huomiota on kiinnitetty referenssien sähköiseen stabiilisuuteen, joka on myös nykyisin kaupallisessa tuotannossa olevien MEMS-komponenttien ongelma. Väitöstyön merkittävin saavutus on MEMS-komponenttien sähköisen stabiilisuuden parantaminen tasolle, joka mahdollistaa niiden hyödyntämisen vaativissa metrologisissa sovelluksissa. Näitä innovaatioita, samoin kuin työssä kehitettyä uutta valmistusmenetelmää, voidaan geneerisesti hyödyntää myös muihin MEMS-sovelluksiin.

Preface

The research work covered by this dissertation has been carried out at VTT Information Technology MEMS sensors group (former VTT Automation, Measurement technology group) during 2001–2005. The research work was mainly done within the EMMA project (ElectroMechanical Microcomponents for presicion Applications) funded by the EU IST programme and by the Technology Development Centre of Finland (Tekes). The work has been done in close collaboration with the co-workers in the MEMS sensors group, the Centre for Metrology and Accreditation (MIKES) and VTI Technologies Oy. Also other EMMA partners Fluke P.M, Twente University, NMi – Van Swinden Laboratorium, and Physikalisch-Technische Bundesanstalt (PTB) are acknowledged.

First of all, I thank Professor Heikki Seppä and Research Professor Aarne Oja for the challenging research topic and guidance in the work. In addition Aarne Oja has instructed the dissertation work which has been a pleasure to me. Also, I wish to thank my supervisor, Professor Ilkka Tittonen from the Helsinki University of Technology for his advice as well as Professor Heli Jantunen and Professor Jukka Lekkala for carefully pre-examining the manuscript.

I thank Heikki Kuisma from VTI Technologies Oy for providing test components and helpful discussions (since 1986, when I joined the legendary MEMS group at Vaisala Oyj). I thank all my co-authors at VTT, MIKES, VTI Technologies Ltd., and NPL for good collaboration: Jukka Kyynäräinen, Nadine Pesonen, Panu Pekko, James Dekker, Mika Suhonen, Antti Manninen, Nikolai Tisnek, Shakil Awan and the previously mentioned names above. Particularly the collaboration with Jukka Kyynäräinen and Nadine Pesonen has been very inspiring and helpful to me. I have also greatly benefited from the help of other members in the MEMS sensor group Teuvo Sillanpää, Ville Kaajakari, Tomi Mattila, and Paula Holmlund and other members of the Microsensing group. I thank Jari J. Penttilä and Ari Häärä for their technical assistance. Also, Seija Lepistö, Aija Kaski and Kaisa Falenius are acknowledged.

Finally, I would like to thank my family and friends for their support and bringing so much love and joy in my life.

Contents

List of acronyms and symbols

ABS	Antilock Braking system
AC	Alternating current
CMOS	Complementary metal-oxide semiconductor
DC	Direct current
DIL	Dual in-line package
DMM	Digital multimeter
DRIE	Deep reactive ion etch
DVM	Digital volt meter
C-V	Capacitance *vs*. voltage (curve)
C4	Controlled Collapse Chip Connection technology (flip-chip)
emf	electromotive force
EDP	Ethylene diamine pyrocatechol, anisotropic silicon wet etchant
ESP	Electronic Stability Program
FGA	Floating gate analog technology
IC	Integrated circuit
JVS	Josephson voltage standard
KOH	Potassium hydroxide, anisotropic silicon wet etchant
LIGA	Litographie galvanoformung, abformung
LPCVD	Low pressure chemical vapour deposition
LTCC	Low temperature co-fired ceramic
MEMS	Microelectromechanical system
MOSFET	Metal oxide semiconductor field effect transistor
MST	Microsystem technology
NBTI	Negative bias temperature instability
PCB	Printed circuit board
PECVD	Plasma enchanged chemical vapour deposition
PID	Proportional, plus integral, plus derivative controller

PMJTC	Planar multijunction thermal converter
ppm	Parts per million
RMS	Root mean square
RF	Radio frequency
SD	Sputter deposition
SI	System of units
SOI	Silicon on insulator
TC	Linear coefficient of thermal expansion
TMAH	Tetramethylammonium hydroxide, anisotropic silicon wet etchant
A	Surface area
C	Capacitance
d	Gap (between a moving and a fixed electrode)
e	Elementary charge
E	Young's modulus
E_e	Electrostatic energy
E_C	Bottom of conduction band
E_F	Fermi energy level
E_V	Top of valence band
f	Frequency
F	Force
g	acceleration
G	Shear modulus
h	Plank constant
I	Current, Moment of inertia
J	Current density
k	Spring constant
k_B	Boltzmann's constant
m	Mass
n	Density of free electrons

N_A	Acceptor density
P	Pressure
p	Density of free holes
q	Charge
Q	Mechanical quality factor
Q_{it}	Interface-trapped charge
Q_f	Fixed oxide charge
R	Resistance
t	Time
T	Temperature, Torque
V	Voltage
V_{bi}	Built-in voltage
V_{pi}	Pull-in voltage
x	Deflection from the rest position
x_d	Extent of the space charge
α	Phase, silicon linear coefficient of thermal expansion
β	Young's modulus linear coefficient of thermal expansion
γ	Diffusion constant
δ_N	Noise displacement
ε	Permittivity
ε_0	Permittivity in vacuum
κ	Spring torsion coefficient
λ	Damping coefficient
ρ	Density
ρ_s	Space charge density
σ	Surface charge density
τ	Time constant of charging
φ	Tilt angle
ω	Angular frequency

List of publications

This dissertation includes the following publications, which are referred to in the text by Roman numerials I–V.

I. Kärkkäinen, A., Oja, A., Kyynäräinen, J., Kuisma, H. and Seppä, H. Stability of Electrostatic Actuation of MEMS. Physica Scripta, Vol. T114, 2004, pp. 193–194.

II. Kärkkäinen, A., Pekko, P., Dekker, J., Pesonen, N., Suhonen, M., Oja, A., Kyynäräinen, J. and Seppä, H. Stable SOI Micromachined Electrostatic AC Voltage Reference. Microsystem Technologies, Vol. 12, Dec. 2005, pp. 169–172.

III. Kärkkäinen, A., Pesonen, N., Suhonen, M., Oja, A., Manninen, A., Tisnek, N. and Seppä, H. MEMS-Based AC Voltage Reference. IEEE Transactions on Instrumentation and Measurement, Vol. 54, Apr. 2005, pp. 595–599.

IV. Kärkkäinen, A., Awan, S.A., Kyynäräinen, J., Pekko, P., Oja, A. and Seppä, H. Optimized Design and Process for Making a DC Voltage Reference Based on MEMS. IEEE Transactions on Instrumentation and Measurement, Vol. 54, Apr. 2005, pp. 563–566.

V. Kärkkäinen, A., Tisnek, N., Manninen, A., Pesonen, N., Oja, A. and Seppä, H. Electrical stability of a MEMS-based AC voltage reference. Submitted to Sensors and Actuators A.

Author's contribution

The results presented in this dissertation are obtained in collaboration with several other persons from VTT and the Centre for Metrology and Accreditation (MIKES). The author has been the main writer in all of the publications I–V. The author has designed both the DC and the AC reference components. All the calculations and simulations related to the components are done by the author except the theoretical AC reference frequency response (Fig. 4) in publication III. Due to the lack of an appropriate text book, a majority of the formulas are derived from the basic equations by the author, including also those presented in the Methods Section. The author has participated in the EMMA process development by defining the targets for the structures and suggested processing methods, but not in the component manufacturing in the clean room. The author has designed the built-in voltage compensation for the AC reference readout electronics. She is also a co-author in the patent application related to that innovation. The author has participated in the development of the measurement systems and performed most of the measurements, except those in publication IV and the AC reference long-term stability measurement in publications II, III, and V.

1. Introduction

1.1 MEMS

The acronym for Microelectromechanical systems, MEMS, lacks a definition, but it is used to describe simultaneously a toolbox, a physical product, and a methodology all in one [1]. Typical MEMS products are mechanical actuators, sensors and other devices, which are microscopic in scale and are fabricated by integrated circuit technology. The operation principle of these components can be based on various physical phenomena and the sensors can be thermal, optical, mechanical, magnetic, etc. [2]. The devices may be either independent components or integrated into circuit devices. Microsystem technology (MST) is a platform which enables manufacturing of MEMS components characterised for their small size, low cost, low power consumption, reliability and integrability with electronics.

Currently MEMS components are applied in communication technology, automotive and transportation industry, medical and biological technologies, environmental control, etc. Hard disc drive read/write heads, inkjet printer heads, accelerometers and pressure sensors are the traditional mass market applications. Today an average car comprises more than 50 sensors, luxury models more than 100 sensors, and roughly one third of them are based on MST [3]. MEMS accelerometers are applied as air bag inflators, in Antilock Braking Systems (ABS), and in Electronic Stability Programs (ESP). MEMS based angular rate sensors or gyroscopes measure rotational motion about vertical axis (yaw rate) or longitudinal axis (rollover) of vehicles. Manifold absolute pressure sensors are also employed in the air intake manifold, where they measure the engine load by detecting the sub pressure as well as the turbo charge pressure.

Accelerometer and pressure sensors based on MEMS usually exploit micromachined beams, membranes or cantilevers. The movement is detected either capacitively or piezo-resistively. The advantages of these structures are that there is no mechanical contact causing wearing, damping can be controlled with the residual gas pressure inside the component enclosure, the characteristics of the components are predicted by conventional mechanical theory, high resonant frequencies and hence large band-widths are obtainable. The challenges

are sensitivity of microstructures to mechanical stress and fairly low capacitance values which require careful design of the readout electronics.

MEMS sensors are not only miniaturized mechanical sensors because scaling down in dimensions (d) results in stronger electrostatic force which scales as d^{-2}. A direct consequence of this is that the voltage level of capacitive transducers, as well as resolution, is usually limited by the pull-in phenomenon, not by the electric breakdown. The mechanical, the material and the electric properties as well as the sensor readout electronics and manufacturing process are tightly interconnected which makes the design of a MEMS component interesting and challenging.

1.2 Voltage metrology

The volt is defined in the International System of Units (SI) as: "*The volt is the electromotive force between two points on a conductor carrying a constant current of 1 ampere when the power dissipated between the two points is 1 watt*"[4]. Realisation of the volt depends on the experiments that relate the ampere and the volt to the mechanical units of length, force and power. Before the early 1970s Weston cells, based on electromotive force (emf), were used as voltage standards. The Weston cell consists of a cadmium amalgam anode and a mercury-mercurous sulfate cathode with a saturated cadmium sulfate solution as the electrolyte. Drift and transportability problems limited their accuracy to about 1 part in 10^6 (ppm) [5]. This accuracy was dramatically improved after Brian Josephson discovered that electrons can tunnel in pairs (Cooper pairs) between two superconductors separated by a thin insulating barrier in the superconducting state. The Josephson effect was first used with the existing Weston cell voltage standard to improve the accuracy of the measurement constant $2e/h$, where e is the elementary charge and h is the Planck constant. Soon the single-junction Josephson cells, based on fundamental physical constants rather than artefacts, replaced the electrochemical cells as voltage standards. However, the disadvantage was that they could only generate very small voltages, about 1 to 10 mV. The output voltage was increased by connecting up to about 20 junctions in series, which was difficult because of the junction non-uniformity. All the junctions required to be individually biased. In 1977, M. T. Levinson and colleagues showed that unbiased Josephson junctions

would spontaneously develop quantized DC voltages when irradiated with microwaves, opening the path to successful Josephson junction arrays [6]. Only in the last ten years the junction technology has developed to the level which enables output voltages of ±10 V with common bias current in series-array Josephson standards [5]. Currently the relative voltage uncertainty is less than 10^{-9} at 10 V level. National metrology laboratories decided in 1990 that the AC Josephson effect is the representation of the volt and agreed that the value of the Josephson constant $2e/h$ is $K_{J\text{-}900}$ = 483597.9 GHz/V.

1.3 DC voltage references

Voltage references are fundamental building blocks in a variety of instruments operating over a very wide range of accuracies. Applications range from data logging systems to digital multimeters (DMM) and precision laboratory references. Many lower precision instruments, such as handheld DMMs, do not employ separate voltage references. Their analog to digital converter usually includes a voltage reference.

Voltage reference instruments are used by calibration laboratories to maintain a local standard for voltage. Lower level equipment is calibrated against these instruments. They are also used as a means of importing traceability from higher levels within the traceability chain, usually the Josephson standard, which is the state-of-the-art instrument today.

The key performance criterion for a voltage reference is the stability with time and temperature, in particular the predictability of temporal drift, immunity to effects of humidity and atmospheric pressure, and immunity to effects of transportation in some applications.

Zener diodes and bandgap references are the most common DC voltage references either used alone or as a part of an integrated voltage reference circuit. A new reference device based on CMOS floating gate analog technology has recently been introduced. General characteristics of these references and the Josephson voltage standard shall be discussed next.

1.3.1 Josephson voltage reference

The Josephson voltage standard is the state of the art voltage reference as discussed in Section 1.2. The basic element of the reference is the Josephson junction which consists of two superconductor electrodes separated by a thin insulator layer. In a superconducting state, electrons are attracted to each other and form bound pairs, Cooper pairs, which tunnel through the junction. An applied DC voltage V across the barrier would generate an AC current at the frequency $f = 2eV/h$, where e is the elementar'y charge and h is Planck's constant. During each cycle of the oscillation, a single quantum of magnetic flux ($h/2e$) passes through the junction. It is difficult to directly observe this small oscillation. However, if an AC current is applied to the junction, there is a range of bias current for which the flow of flux quanta will phase-lock to the applied frequency. An applied AC current of frequency f would generate a DC voltage V_n at the quantized values $V_n = nhf/2e$, where n is an integer. This effect is known as the AC Josephson effect. The stability of the Josephson volt depends only on the stability of f. In other words, a Josephson junction is a frequency-to-DC voltage converter. The best devices today consist of 19 000 junctions and they are able to produce a series of very accurate quantized voltages up to 12 V [6].

Josephson-junction-based voltage standard systems are rather expensive and large devices mainly used by National Standards Laboratories to maintain the local standard for voltage. They consist of microwave source and feed, cryostat, probe, chip, and readout and control system. Microwave energy is fed into the chip mounted in the probe's chip carrier and the chip is cooled by liquid helium.

1.3.2 Zener diodes

1.3.2.1 Principle of operation

A Zener reference is based on the breakdown of a reverse biased p-n junction [7]. Any reverse biased p-n junction has a small reverse current flow due to the presence of minority carrier holes and electrons in the vicinity of the depletion region. As the reverse bias voltage across the junction is increased, the carriers acquire an increasing amount of energy between lattice collisions. At a certain voltage, the breakdown voltage, the carriers have enough energy to create new

electron-hole pairs in collisions with the silicon atoms. This is called the avalanche process in which the current in a reverse-biased diode dramatically increases at a certain voltage threshold. A resistor in series with the diode establishes a constant current, allowing the Zener to operate as a stable reference voltage. The Zener reference behaves as a typical shunt, or two-terminal, reference.

The operation of a Zener diode can also be based on Zener breakdown which is different from the avalanche effect described above. The Zener breakdown occurs only in very heavily doped junctions if the electric field is large enough for a valence electron to make a transition form the valence band to the conduction band. This process is a tunneling effect, but there is no multiplication effect involved. Although the Zener breakdown mechanism is only important for breakdown voltages below about 6 V, all breakdown diodes are commonly referred to as Zener diodes.

1.3.2.2 Zener diode characteristics

Lower precision Zener references offer outputs in the range from 1.2 V to 10 V with accuracies from 0.2% to 5%, and temperature coefficients in the range between 10 ppm/°C and 150 ppm/°C.

The drawbacks of the low precision Zener diodes are the substantial noise associated with surface effects, poor voltage tolerance and the dependence of Zener voltage on current and temperature. To reduce these problems, two-terminal and three-terminal reference circuits have been developed which include a number of active devices to compensate the temperature effects, provide constant current to the Zener diode, and buffer the output voltage, etc. [8].

1.3.2.3 IC Zeners

The best commercially available voltage reference integrated circuits (IC) are based on burn-in and careful selection of the Zener diode component, temperature-stabilized housing and integrated electronics.

The temperature stability of a Zener diode, which is about 0.5 ppm/°C, can be improved by an order of magnitude by utilizing the component TO-package as a temperature stabilized oven. A reference Zener, a temperature compensation

transistor, a temperature sensor transistor and a heater resistor are all on a single chip, which is mounted in a TO-package. An external circuit is required to implement a temperature control circuit to maintain the chip at a constant elevated operating temperature and supply a constant current to the reference Zener. For example the LTZ1000/100A (Linear Technology) reference utilises this technology and the temperature coefficient of the component is less than 0.05 ppm/°C and long term stability is about 1 ppm/year [8].

An even better way is to mount the whole reference circuitry in a metal box and maintain the box at an elevated temperature. This enables a temperature stability of ±50 mC at room environment, but it is bulky, slow and has high power consumption [8].

1.3.3 Bandgap references

Voltage reference circuits usually fail to provide small temperature coefficients without a temperature control circuit, which is undesirable especially if small size and low power consumption are desired. Instead of trying to control the temperature of the circuit it is also possible to eliminate the temperature coefficient by adding the reference voltage to another voltage that has a temperature coefficient of the same order of magnitude but with different sign. The bandgap voltage reference circuit is based on compensating the negative temperature coefficient of a transistor base-emitter voltage V_{BE} with a positive temperature coefficient of the thermal voltage V_T. The thermal voltage source is realised using two identical p-n junctions having different collector current densities J_C. The base-emitter voltage difference of these two transistors is $\Delta V_{BE} = kT/e\ln(J_{C1}/J_{C2})$, were k is Bolzmann's constant and e the elementary charge and T temperature [7]. The temperature coefficients for V_{BE} and for ΔV_{BE} are about -2 mV/°C and +0.085 mV/°C respectively at room temperature T_R. When the positive temperature coefficient is multiplied with a constant K, about 23.5, the sum of these voltages has a zero temperature coefficient at T_R as shown in Fig. 1. The bandgap voltage reference compensates only the linear term of temperature coefficient and hence the temperature coefficient is zero only at one temperature T_R. Nevertheless, fairly small, about 50 ppm/°C, temperature coefficients are achievable with this technique.

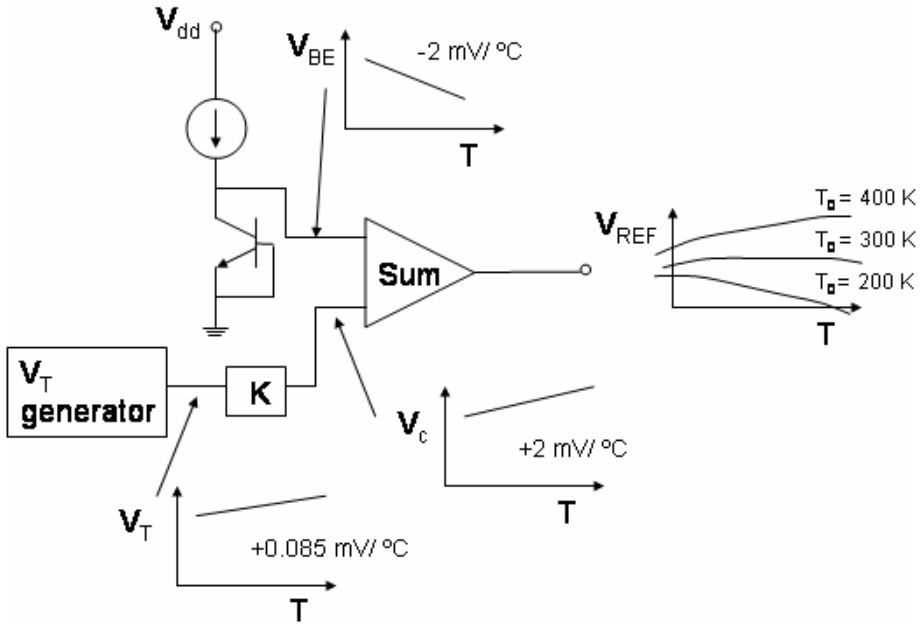

Figure 1. Bandgap voltage reference (redrawn after [7]).

1.3.4 Floating gate technology

A new commercial reference device has recently been announced by Intersil Corporation based on floating gate analog (FGA) technology, an extension of non-volatile memory [9]. FGA technology is based on storing a precise charge in a floating gate cell. The reference voltage is output from the buffered floating gate voltage. The devices, as well as the amplifier circuitry, are manufactured using CMOS process. The advantage of the FGA technology is that the reference voltage is not determined by the breakdown voltage or bandgap voltage but can be designed for a wide range of voltages.

The components are specified from 1.25 V to 5 V output with temperature coefficients from 1 to 20 ppm/°C, accuracy from 0.5 mV to 5 mV, stability of 10 ppm/sqrt(1000h), noise of 30 µV p/p (0.1–10 Hz), at a 500 nA supply current.

1.4 AC voltage references

There are only two voltage references, which are fundamentally based on AC voltage, namely the AC voltage Josephson reference and the MEMS based AC voltage reference described in this dissertation.

Usually AC voltage sources are based on generating an AC voltage from DC and respectively an AC voltage is measured by converting the AC to DC. AC converters are fundamental building blocks in a variety of instrumentation operating over a very wide range of accuracies, like DC references discussed in Section 1.3. The middle and lower accuracy devices are simple rectifier circuits, which detect the signal peak values. The output is calibrated to give the equivalent RMS value of a sinusoidal signal. If the signal is noisy or the signal shape differs from sinusoidal, substantial errors can occur. Higher precision devices utilise sampling with fast A/D converters and RMS to DC converters realised with discrete components. Thin film or planar multijunction thermal converters (PMJTC), based on thin-film technology, can realise a zero AC-DC difference with an uncertainty below 0.1 ppm at 1 kHz [10]. However, thermal conversion is a complicated and a time consuming measurement method. The inherent limitation of thermal sensors is the need to generate heat for signal detection and ultimately the accuracy is limited by the phonon noise.

All major National Standards Laboratories are presently developing AC voltage standards based on Josephson junction arrays, discussed in Section 1.3.1. The approach is to generate a programmable digital-to-analog converter capable of synthesizing arbitrary waveforms. One of the major challenges is to fabricate uniform junctions for large arrays [5]. The AC Josephson standard suffers from the same limitations as the DC Josephson voltage standard: they are expensive, large devices, which need to be operated at cryogenic temperatures.

1.5 MEMS in voltage metrology

Microsystem technology has enabled improvement of existing voltage standards and creation of new standards based on quantum phenomena or characteristic properties of micromechanical moving plate capacitors. Two state-of-the-art standards, namely Josephson junctions and multijunction thermal converters, are

manufactured using MST as already mentioned in the previous Section. Manufacturing of a Josephson junction requires an extremely thin (few nanometers) insulator layer, which is not possible without semiconductor fabrication technologies. Multijunction thermal converters can be manufactured using traditional technologies, but MST has enabled a substantial improvement in device performance. The decreased device size (thermal mass) and reproducible manufacturing process, utilising well characterised materials, creates more accurate, faster, and less expensive MJTCs.

The potential of MEMS in metrology is discussed in [11]. During the last 10 years several new devices based on micromechanical moving plate capacitors have been suggested. The principle of operation of a true RMS-to-DC converter was first published in 1995 [12]. The operation of the device has been demonstrated using surface micromachined [13] and bulk micromachined [14] devices. Also a RMS-to-DC converter based on a SOI process and comb-structure has been presented in [15].

The principle of operation of a DC voltage reference and an AC voltage reference, both based on the pull-in phenomenon of a moving plate capacitor, were first published in 1998 [16]. Further analysis of the voltage references, as well as the principle of operation of a DC current reference, a low frequency voltage divider, and a microwave detector, are presented in [17]. The first experimental results of a DC voltage reference and an AC voltage reference are published in [17] and [18]. Those results are based on commercial bulk micromachined angular rate sensors. A surface micromachined beam designed to be used as a DC voltage reference is reported in [19] and later analysed in more detail in [20].

The previous studies demonstrated the feasibility of the idea, *i.e.* the use of the pull-in voltage as a voltage reference, but the stability of the devices has not been sufficient. This dissertation, including the publications, concentrates on analysing and solving this problem.

The approximate accuracy levels for different voltage references are compared in Fig. 2. The best standards before the invention of the Josephson voltage standard (JVS) in the early 1970s could reach an accuracy of 10^{-6}. This level of accuracy is currently achieved by high quality (HQ) Zener diodes. However, the

characteristics of the high quality Zener diodes have remained the same for tens of years, whereas the MEMS references are in the beginning of their life cycle and there is a huge potential for improvement. In addition to accuracy, also long-term stability, temperature coefficient, and noise voltage level are important characteristics of the references.

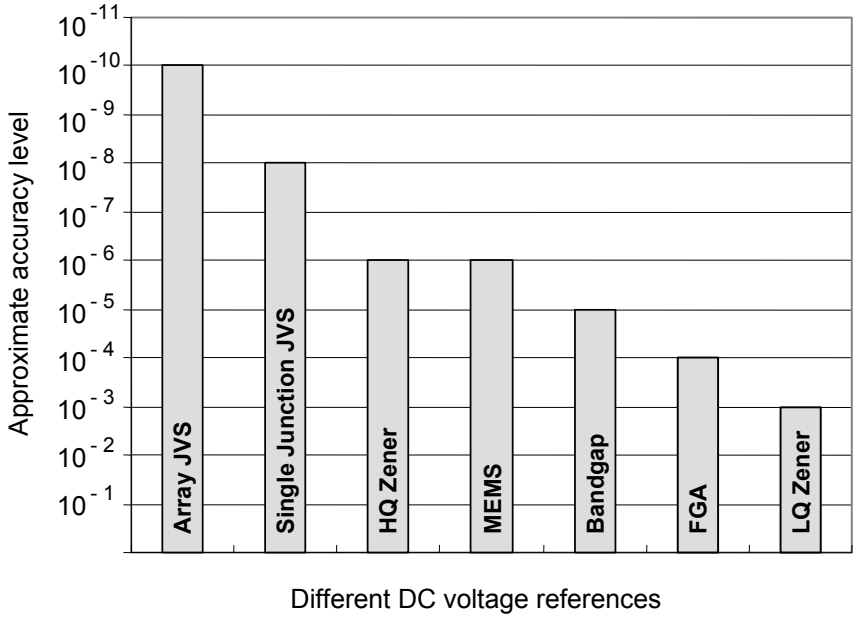

Figure 2. The approximate accuracy levels of different DC voltage references.

2. Methods

2.1 Electromechanical coupling in MEMS components

Electromechanical coupling of a moving plate capacitor, especially the pull-in phenomenon, is well known both theoretically and experimentally, for a review see [21] and [22]. However, the dynamics of a current driven microactuator in the low frequency range has not been published and will be discussed here in more detail.

2.1.1 Static analysis

A MEMS moving plate capacitor, shown in Fig. 3, is manufactured from two silicon wafers, where the upper one is etched to form a moving mass suspended by three elastic springs. The spring-mass system can be described by the dynamic equation of a forced oscillator

$$F_{\mathrm{e}}(t) = m\frac{d^2x}{dt^2} + \lambda\frac{dx}{dt} + kx - F_{\mathrm{m}}, \tag{1}$$

where m is the mass of the moving plate, λ is the damping coefficient, related to gas damping of the component, and k is the spring constant [23]. F_{m} describes the force the capacitor experiences, for example due to the ambient gravity or any other external force, and F_{e} the electrostatic force acting on the moving plate. In the static analysis of a parallel plate capacitor it is assumed that the variation of the actuation is slow enough, so that the system is in equilibrium all the time, *i.e.* the time-dependent terms in (1) vanish. The plate movement is analysed both in translational and rotational modes.

2.1.1.1 Translational mode

The electrostatic force F_{e} acting on the moving plate of the parallel plate capacitor, shown in Fig. 3, due to an external voltage V_{ext} is

$$F_{\mathrm{e}} = \frac{1}{2}V_{\mathrm{ext}}^2\frac{\varepsilon A}{(d-x)^2} = \frac{1}{2}V_{\mathrm{ext}}^2\frac{C}{(d-x)}, \tag{2}$$

where ε is the permittivity of the medium between the capacitor plates, d is the gap between the plates at rest position ($V_{ext} = 0$), x is the deflection from the rest position, and A is the electrode surface area [23]. The parallel plate capacitance C has an expression

$$C = \frac{\varepsilon A}{d - x}. \tag{3}$$

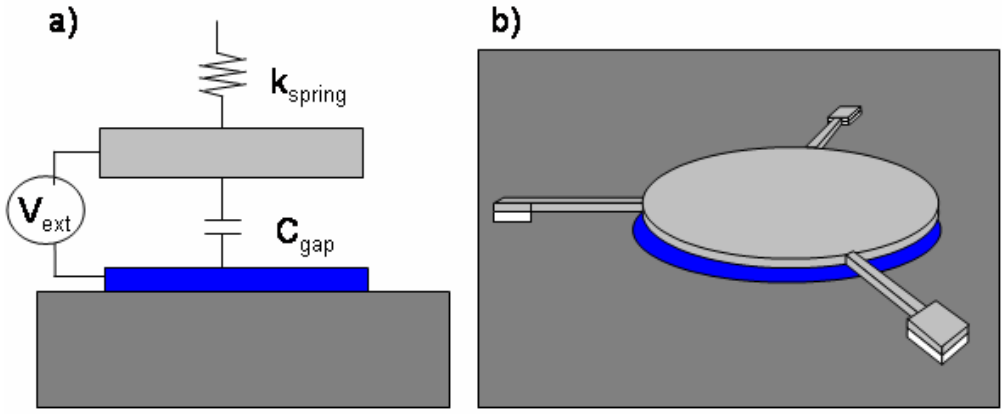

Figure 3. Schematic model for a translationally moving parallel plate capacitor (a) and its realisation with a MEMS component (b).

Assuming that there are no external forces acting on the system, $F_m = 0$, Eq. (1) simplifies to

$$\frac{1}{2} V_{ext}^{\ 2} \frac{\varepsilon A}{(d - x)^2} = kx, \tag{4}$$

where k is the spring constant

$$k = 3\frac{Eh^3 w_s}{l_s^3} \tag{5}$$

for the plate suspended with three springs as shown in Fig. 3 [24]. E is Young's modulus, h the plate thickness, w_s the spring width and l_s the spring length. Equation (5) assumes that the spring is fixed from one end and guided from the other end.

Solving V_{ext} from Eq. (4) results in

$$V_{ext} = \sqrt{\frac{2(d-x)^2 kx}{\varepsilon A}}. \tag{6}$$

The maximum of V_{ext}, *i.e.* the pull-in voltage V_{pi}, is

$$V_{pi} = \sqrt{\frac{8kd^2}{27C_0}}, \tag{7}$$

which occurs at $x = d/3$. C_0 is the nominal capacitance ($x = 0$)

$$C_0 = \frac{\varepsilon A}{d}. \tag{8}$$

The eigencurve of the moving plate capacitor is shown in Fig. 4.

The pull-in voltage can be used as a voltage reference since the relative uncertainty of the pull-in voltage $\Delta V_{pi}/V_{pi}$ is proportional to the relative uncertainty of the displacement $\Delta x/d$ squared

$$\frac{\Delta V_{pi}}{V_{pi}} \approx -\frac{27}{8}\left(\frac{\Delta x}{d}\right)^2, \tag{9}$$

which results from derivation of (7). The relative displacement can easily be controlled at a level of 10^{-4} resulting to relative voltage accuracy in the order of 10^{-8}.

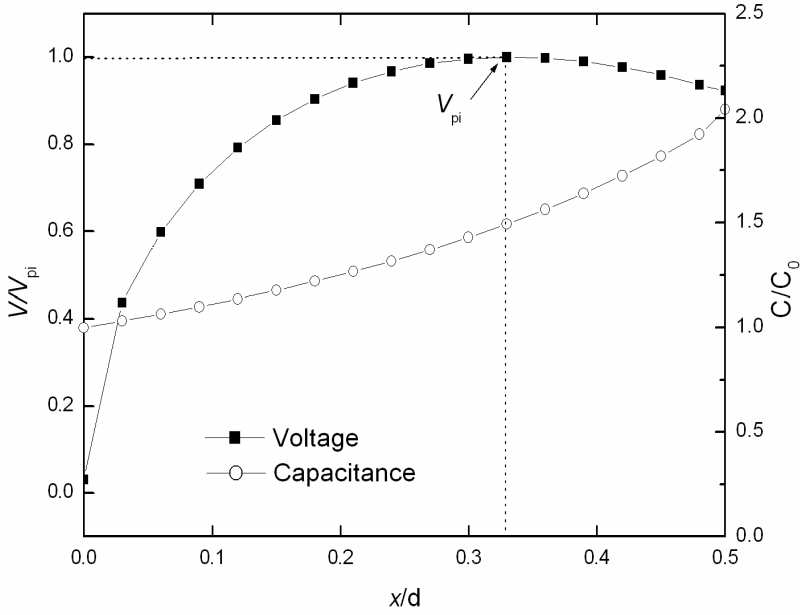

Figure 4. Eigencurve of a moving plate capacitor. The pull-in voltage is the maximum of the voltage curve.

2.1.1.2 Rotational mode

If the moving capacitor plate is suspended with two springs from the centre of the mass, as shown in Fig. 5, the plate moves in a rotational mode, *i.e.* tilts. In that case the equilibrium equation is

$$T = \kappa\varphi\,, \tag{10}$$

where φ is the tilt angle, κ is the spring torsion coefficient, and T is an external torque [24]. For rectangular springs, as shown in Fig. 5, the total spring torsion coefficient is

$$\kappa = 2\frac{G}{l_s}ab^3\left[\frac{16}{3} - 3.36\frac{b}{a}\left(1 - \frac{b^4}{12a^4}\right)\right], \tag{11}$$

where G is the shear modulus of silicon, l_s is the length and $a \times b$ is the cross section of a single spring ($a \geq b$) [24]. The torque can be calculated as

$$T = \int_{c-e/2}^{c+e/2} F_{dl}\,dl = \int_{c-e/2}^{c+e/2} \frac{1}{2}\frac{\varepsilon H V_{ext}^2\, l dl}{(d - l\tan\varphi)^2} = \tag{12}$$

$$\frac{\varepsilon H V_{ext}^2}{2\tan^2\varphi}\left[\ln\left(\frac{1-a_1\tan\varphi}{1-a_2\tan\varphi}\right) + \frac{1}{1-a_1\tan\varphi} - \frac{1}{1-a_2\tan\varphi}\right],$$

where c is the distance to the centre of the electrode, z is the length of the electrode,

$$a_1 = \frac{c + z/2}{d}, \text{ and } a_2 = \frac{c - z/2}{d}. \tag{13}$$

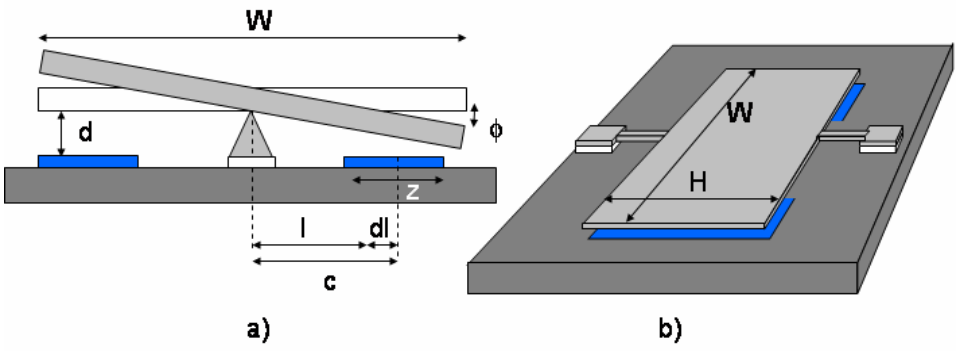

Figure 5. Rotationally moving capacitor, side view (a) including notations used in the text and a component (b).

By combining Equations (10) and (12), V_{ext} gets the expression

$$V_{ext} = \left\{\frac{2\kappa\varphi\tan^2\varphi}{\varepsilon H}\left[\ln\left(\frac{1-a_1\tan\varphi}{1-a_2\tan\varphi}\right) + \frac{1}{1-a_1\tan\varphi} - \frac{1}{1-a_2\tan\varphi}\right]^{-1}\right\}^{1/2}. \tag{14}$$

This equation can be solved numerically. The eigencurve of a rotationally moving capacitor is shown for different lengths of the electrode (z) in Fig. 6, and for different heights of the gap (d) in Fig. 7.

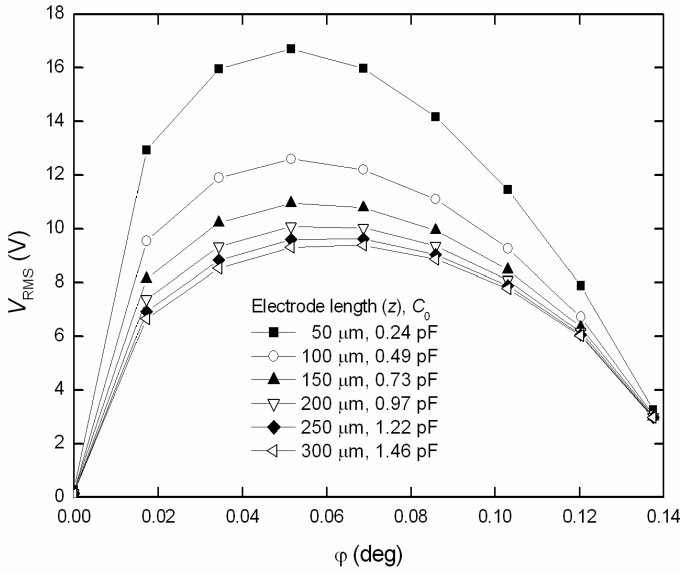

Figure 6. Eigencurve of a MEMS capacitor as a function of the rotation angle φ for different lengths of the electrode. The electrode length determines also the value of nominal capacitance C_0, which is displayed in the legend. Other parameters used in the calculation are listed in Table 3 in Section 3.2.1.

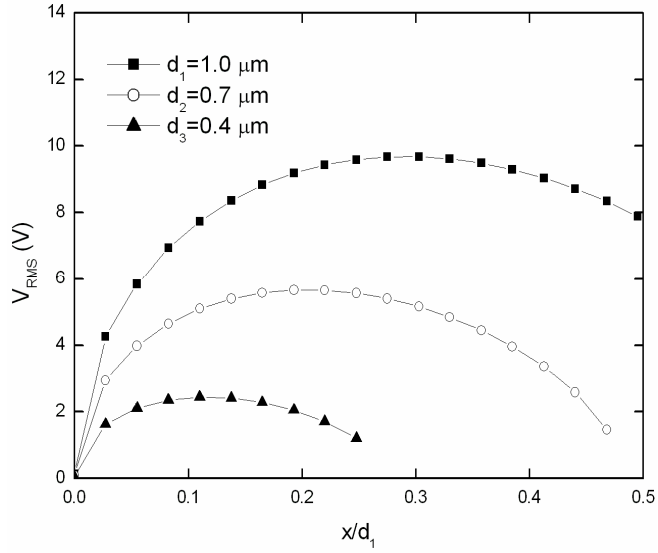

Figure 7. Component eigencurve as a function of relative displacement x/d_1 for different heights of the gap (displayed in the legend). Other parameters used in the calculations are listed in Table 3 in Section 3.2.1.

2.1.1.3 DC voltage actuation

When DC voltage is used to actuate a parallel plate capacitor, like the one shown in Fig. 3, the system is stable only below the pull-in voltage, *i.e.* for displacements $x < d/3$. The instability originates from the positive feedback to the system, which is provided by the voltage source. When the plate deflects, the capacitance increases and the voltage source adds more charge causing the plate to deflect even further. There are a number of techniques to increase the stable actuation range, for a review see [21] and [25]. The most feasible techniques for the voltage reference use are the voltage feedback, discussed below, and the actuation with an AC current source, which is discussed in the next Section.

A feedback loop enables stable actuation in the region which is unstable using a simple DC voltage source. A basic understanding of this phenomenon is obtained considering a system model illustrated in Fig. 8. The output of the system *Y(s)* is determined by the feedback function *H(s)* if $|K_0G(S)H(s)| >> 1$,

$$\frac{Y(s)}{R(s)} = \frac{K_0 G(s)}{1 + K_0 G(s)H(s)} = \frac{1}{1/K_0 G(s) + H(s)} \approx \frac{1}{H(s)}, \qquad (15)$$

where K_0 and *G(s)* are the controller and plant functions respectively. Thus, with a high open loop gain K_0, the overall transfer function is sensitive to variations in the feedback gain factor, but relatively insensitive to variations in the transfer function [26].

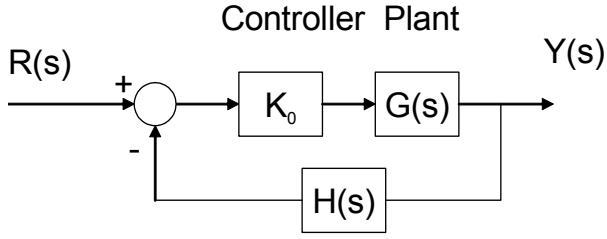

Figure 8. A general graphical presentation of a feedback loop.

A control system model for a DC voltage actuated capacitor is displayed in Fig. 9. The aim of the circuit is to keep the position of the moving plate at the pull-in point, x_{pi}, which is the system input. The controller defines the position

change *dx* needed to minimize the position error $e = x_{pi} - x_m$, where x_m is the measured displacement. Different kinds of controllers can be used. For a linear controller the transfer function is $G_1 = K_0$ and for a PID controller $G_1 = K_0 + K_d s + Ki/s$ [26]. The transfer function for the actuation voltage is obtained from Eq. (4), $G_2 = C_0 V_{ext}^2 / 2d(1 - x/d)^2$. The component dynamics is described by Eq. (1) and the Laplace transformation of it is

$$F(x) = ms^2 X(s) + \lambda s X(s) + kX(s), \tag{16}$$

assuming that the initial displacement and velocity vanish, *i.e.* $X(0) = 0$ and $\dot{X}(0) = 0$, as well as the external force acting on the system, $F_m = 0$. The component dynamic transfer function G_3 is then

$$G_3 = \frac{X(s)}{F(x)} = \frac{1}{m}\left(\frac{1}{s^2 + \lambda s/m + k/m}\right). \tag{17}$$

Finally, the position detection transfer function G_4 depends on the readout electronics used. For an electronics described in Section 4.1, the transfer function is

$$G_4 = \frac{\mathrm{Re}\{V\}}{\delta x} = \frac{27}{16}\frac{V_{\mathrm{ext,RMS}}}{d}\frac{\left(\frac{C_A}{C_m} + \frac{9}{4}\right)}{\left(\frac{C_A}{C_m} + \frac{9}{4}\right)^2 + \left(\frac{9}{4} R_s \omega C_A\right)^2}, \tag{18}$$

where C_A is the amplifier input capacitance, C_m is the nominal capacitance of the plate deflection detection electrode and R_s is the resistance of the silicon spring (it has been assumed that the parasitic capacitance C_p is negligible).

The overall transfer function of the feedback control system is then

$$\frac{x_{pi}(s)}{V_{out}(s)} = \frac{G_1 G_2 G_3}{1 + G_1 G_2 G_3 G_4}. \tag{19}$$

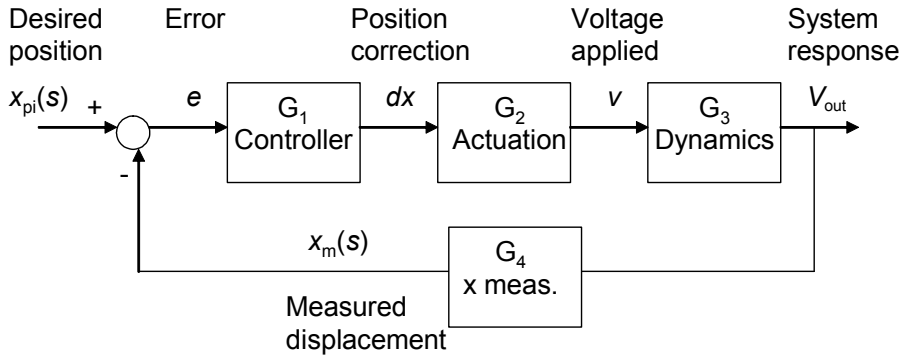

Figure 9. A feedback control system diagram for a DC voltage actuated moving plate capacitor.

2.1.1.4 AC current actuation

A DC voltage actuated MEMS capacitor is unstable at the pull-in point and the displacement x of the moving plate is limited to $d/3$ unless a feedback loop is used. The feedback system usually requires additional electrodes for the plate displacement detection and an advanced electronics for the feedback circuit implementation. These problems can be avoided by using AC current actuation. When the displacement of the capacitor is controlled using charge drive instead of voltage drive the electrostatic force between the capacitor plates does not depend on the remaining gap and hence the system is stable. It has been theoretically shown that if the AC current drive is ideal, any position across the gap is stable. In practice the maximum displacement is limited by the parasitic capacitance and leakage currents of the device [27].

If a sinusoidal current with an amplitude $\hat{I}$ and angular frequency ω, $I = \hat{I}\sin(\omega t)$, is driven through a capacitor, the force acting on the moving plate is

$$F_e(t) = -\frac{\partial E_e}{\partial x} = -\frac{\partial}{\partial x}\left(\frac{q^2(t)}{2C}\right) = \frac{1}{2}\frac{q^2(t)}{\varepsilon A} = \frac{\hat{I}^2}{2\varepsilon A\omega^2}\cos^2(\omega t), \qquad (20)$$

where $q(t)$ is the capacitor charge integrated from the current equation above assuming that the time average of the capacitor charge is zero, which corresponds to a vanishing DC voltage across the capacitor. The average force acting on the component is

$$\overline{F}_{\mathrm{e}} = \frac{1}{\pi}\int_0^{\pi} \frac{\hat{I}^2}{2\varepsilon A\omega^2}\cos^2(\omega t)dt = \frac{\hat{I}^2}{4\varepsilon A\omega^2} = \frac{I_{\mathrm{RMS}}^2}{2\varepsilon A\omega^2}. \tag{21}$$

The Equation of motion (1) for a moving plate capacitor, shown in Fig. 3, is now

$$\frac{I_{\mathrm{RMS}}^2}{2\varepsilon A\omega^2} = kx - F_{\mathrm{m}} \tag{22}$$

in the static case. Solving x from (22) and substituting it into the equilibrium equation

$$\frac{1}{2}V_{\mathrm{ext}}{}^2\frac{\varepsilon A}{(d-x)^2} = kx - F_{\mathrm{m}} \tag{23}$$

results in an expression for the amplitude of the AC RMS voltage, V_{AC}, across the plate

$$V_{\mathrm{AC}} = V_{\mathrm{ext,RMS}} = \frac{I_{\mathrm{RMS}}}{\omega C_0}\left[1 - \frac{4}{27}\left(\frac{I_{\mathrm{RMS}}}{\omega C_0 V_{\mathrm{pi}}}\right)^2 - \frac{F_{\mathrm{m}}}{kd}\right]. \tag{24}$$

The amplitude V_{AC} reaches a maximum value

$$V_{\mathrm{AC}}^{\max} = V_{\mathrm{pi}}\left(1 - \frac{F_{\mathrm{m}}}{kd}\right)^{3/2}, \tag{25}$$

where $V_{\mathrm{pi}} = \sqrt{8kd^2/27C_0}$, at $I_{\mathrm{RMS}} = (3/2)\omega C_0 V_{\mathrm{pi}}\sqrt{1 - F_{\mathrm{m}}/kd}$. This voltage amplitude value can be utilised as a reference voltage since the relative uncertainty of the reference voltage is proportional to the relative uncertainty of the driving current squared

$$\frac{\Delta V_{\mathrm{AC}}}{V_{\mathrm{AC}}^{\max}} \approx -\frac{3}{2}\left(\frac{\Delta I}{I_{\mathrm{RMS,max}}}\right)^2. \tag{26}$$

In Fig. 10 the RMS voltage V_{AC} is shown as a function of the RMS current I_{RMS} for a typical component with different frequency values of the driving current.

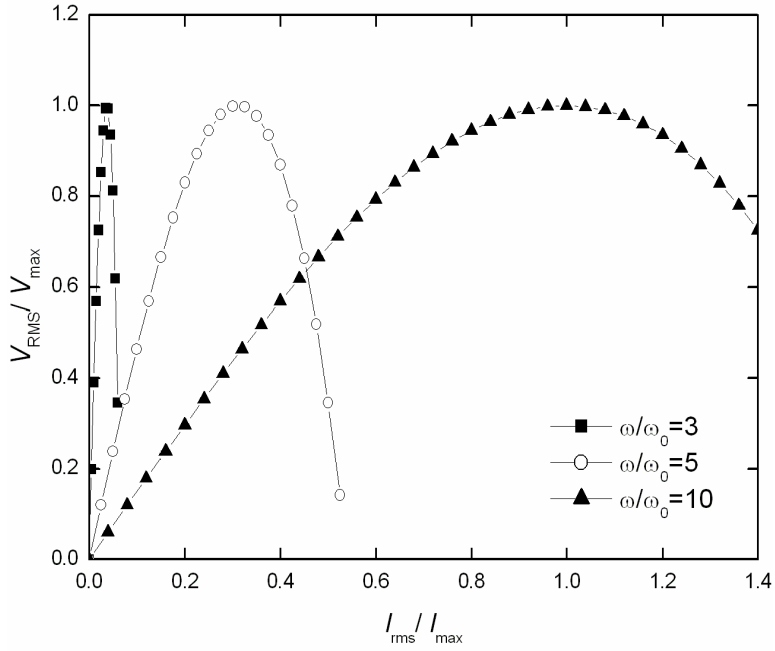

Figure 10. Eigencurves for a MEMS component with different frequency values of the driving current I_{RMS} assuming that $F_m = 0$. The undamped resonance frequency is ω_0.

2.1.2 Dynamic analysis

In the previous analysis, it has been assumed that either the frequency of the actuation is much higher than the component mechanical resonance frequency or the motion of the moving electrode is sufficiently damped, so that the position of the moving electrode is stationary. In that case the time-dependent terms in the equation of motion (1) will vanish. However, if either of these assumptions is not valid, the plate oscillation can not be omitted. The plate movement will also generate other harmonic frequencies into the output signal in addition to the original frequency of the sinusoidal input signal. If the AC voltage is not measured using the phase locking technique, the additional frequency components will cause an error in the AC RMS value.

In order to find out the effect of plate oscillation on the reference voltage, the equation of forced oscillation needs to be solved. In the case of AC current actuation, the electrostatic force F_e acting on the component when sinusoidal current with an amplitude $\hat{I}$ and angular frequency ω, $I=\hat{I}\sin(\omega t)$, is driven through a capacitor, is (see Eq. (20))

$$F_e = \frac{\hat{I}^2}{2\varepsilon A\omega^2}\cos^2(\omega t) = \frac{{I_{RMS}}^2}{2\varepsilon A\omega^2}(1+\cos(2\omega t)). \tag{27}$$

The equation of the forced oscillator is now

$$\frac{d^2x}{dt^2} + 2\gamma\frac{dx}{dt} + \omega_0^2 x = \frac{{I_{RMS}}^2}{2m\varepsilon A\omega^2}(1+\cos(2\omega t)), \tag{28}$$

where $\gamma = \lambda/2m$ and $\omega_0 = \sqrt{k/m}$. The external force term F_m has assumed to be negligible. Equation (28) has the solution

$$x(t) = \hat{x}_0\left(1+\frac{1}{\Omega}\sin(2\omega t-\alpha)\right), \tag{29}$$

where

$$\Omega = \sqrt{\left(4\left(\frac{\omega}{\omega_0}\right)^2-1\right)^2+\left(\frac{4\gamma\omega}{\omega_0^2}\right)^2} = \sqrt{\left(4\left(\frac{\omega}{\omega_0}\right)^2-1\right)^2+\left(\frac{2\omega}{\omega_0 Q}\right)^2}, \tag{30}$$

$$\hat{x}_0 = \frac{1}{2\varepsilon Ak}\left(\frac{I_{RMS}}{\omega}\right)^2, \tag{31}$$

and

$$\tan(\alpha) = \frac{4\omega^2-\omega_0^2}{4\gamma\omega}. \tag{32}$$

The amplitude ratio between the oscillating component $\hat{x}_0 / \Omega$ and the non-oscillating component $\hat{x}_0$ as a function of the driving angular frequency ω is shown in Fig. 11 for different Q values of the component. The component mechanical Q value, $Q = \sqrt{km} / \lambda = \omega_0 / 2\gamma$, varies from about 0.01 for well damped components up to 10^6 for vacuum packaged components. It can be observed that the oscillating component dominates at the energy resonance $\omega_0/2$, *i.e.* when the driving frequency equals the natural frequency of the oscillation without damping and hence the energy transfer from the applied force to the oscillator is at maximum. Above the resonance the amplitude ratio decreases as $1/\omega^2$.

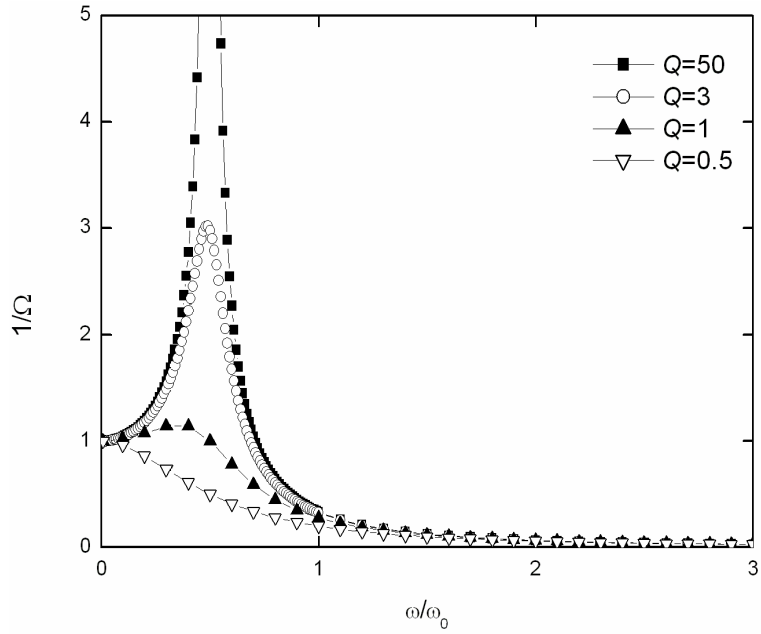

Figure 11. The amplitude ratio between the oscillating and the non-oscillating components of the capacitor plate displacement x actuated by current $I = \hat{I}\sin(\omega t)$ *as function of the normalized angular frequency ω/ ω0.*

The phase α, calculated using Eq. (32), as a function of the relative angular frequency ω/ω_0, is displayed in Fig. 12 for different Q values.

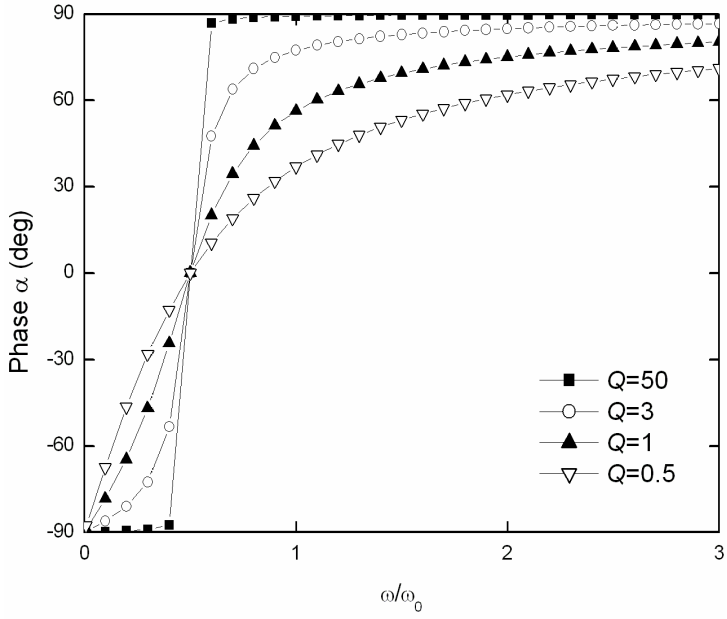

Figure 12. The phase α as function of the relative angular frequency ω/ω_0 for different Q values.

The voltage over the capacitor can now be calculated

$$V = \frac{q(t)}{C(t)} = \frac{\sqrt{2}}{\varepsilon A}\left(\frac{I_{\mathrm{RMS}}}{\omega}\right)(d - x(t))\cos\omega t \\ = \hat{U}_{\omega}\sin(\omega t - \beta) - \hat{U}_{3\omega}\sin(3\omega t - \alpha) = U_{\omega} + U_{3\omega} \tag{33}$$

where

$$\hat{U}_{\omega} = \frac{\sqrt{2}I_{\mathrm{RMS}}}{\omega\varepsilon A}\left[\left(d - \hat{x}_0\left(1 - \frac{\sin\alpha}{2\Omega}\right)\right)^2 + \hat{x}_0{}^2\left(\frac{\cos\alpha}{2\Omega}\right)^2\right]^{1/2} \tag{34}$$

and

$$\hat{U}_{3\omega} = \frac{\sqrt{2}}{k(2\varepsilon A)^2\Omega}\left(\frac{I_{\mathrm{RMS}}}{\omega}\right)^3. \tag{35}$$

The phase α is given in Eq. (32) and β is

$$\beta = \arcsin\left(\frac{-d + \hat{x}_0\left(1 - \frac{\sin\alpha}{2\Omega}\right)}{\left[\left(d - \hat{x}_0\left(1 - \frac{\sin\alpha}{2\Omega}\right)\right)^2 + \hat{x}_0{}^2\left(\frac{\cos\alpha}{2\Omega}\right)^2\right]^{1/2}} \right). \tag{36}$$

According to Eq. (33) the voltage across the capacitor oscillates with the driving frequency $f = \omega/2\pi$ and with the third harmonic $3f$. The amplitude ratio of these components is

$$\frac{\hat{U}_{3\omega}}{\hat{U}_{\omega}} = \frac{\hat{x}_0}{2\Omega\left[\left(d - \hat{x}_0\left(1 + \frac{\sin\alpha}{2\Omega}\right)\right)^2 + \hat{x}_0{}^2\left(\frac{\cos\alpha}{2\Omega}\right)^2\right]^{1/2}}. \tag{37}$$

This ratio at the maximum point of the voltage-current curve is shown for a typical component in Fig. 13.

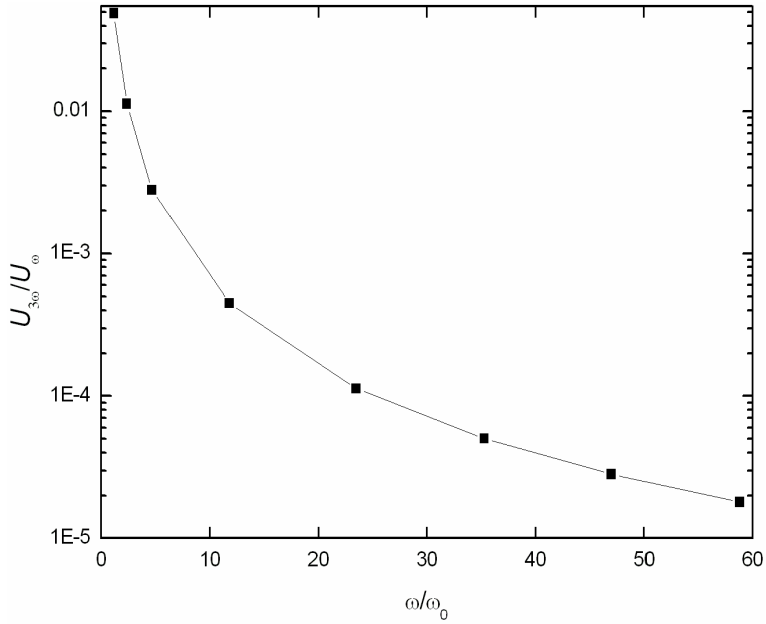

Figure 13. Amplitude ratio of the voltage components at driving frequency and the third harmonic $\hat{U}_{3\omega}/\hat{U}_{\omega}$. *The following numerical values have been used:* $m = 1.45\times10^{-6}$ *kg,* $A = 1.45\times10^{-6}$ m^2, $\varepsilon = 8.85\times10^{-6}$ C^2/Nm, $d = 2\times10^{-6}$ *m and* $k = 105$ *N/m.*

At high frequencies, $\omega \gg \omega_0$, $\alpha \approx 90°$ as can bee seen in Fig.12, and Eq. (37) simplifies to

$$\frac{\hat{U}_{3\omega}}{\hat{U}_{\omega}} \approx \frac{1}{2\Omega}\frac{\frac{\hat{x}_0}{d}}{1-\frac{\hat{x}_0}{d}}. \tag{38}$$

The RMS voltage over the moving plate is then

$$V_{\mathrm{RMS}}^2 = U_{\omega,\mathrm{RMS}}^2 + U_{3\omega,\mathrm{RMS}}^2 \tag{39}$$
$$\approx \left(\frac{I_{\mathrm{RMS}}}{\omega C_0}\right)^2\left[\left(1-\frac{\hat{x}_0}{d}\left(1-\frac{1}{2\Omega}\right)\right)^2 + \left(\frac{\hat{x}_0}{d}\frac{1}{2\Omega}\right)^2\right].$$

Hence both components, *i.e.* U_ω and $U_{3\omega}$, contribute to the reference voltage value. The distortion will change the value of the voltage maximum V_{RMS} and its position I_{RMS}. The voltage ratio V_{RMS}/V_{max} is shown in Fig. 14 for different Q values, when the driving frequency f equals the mechanical resonance frequency f_0. V_{max} corresponds to Q value 3.

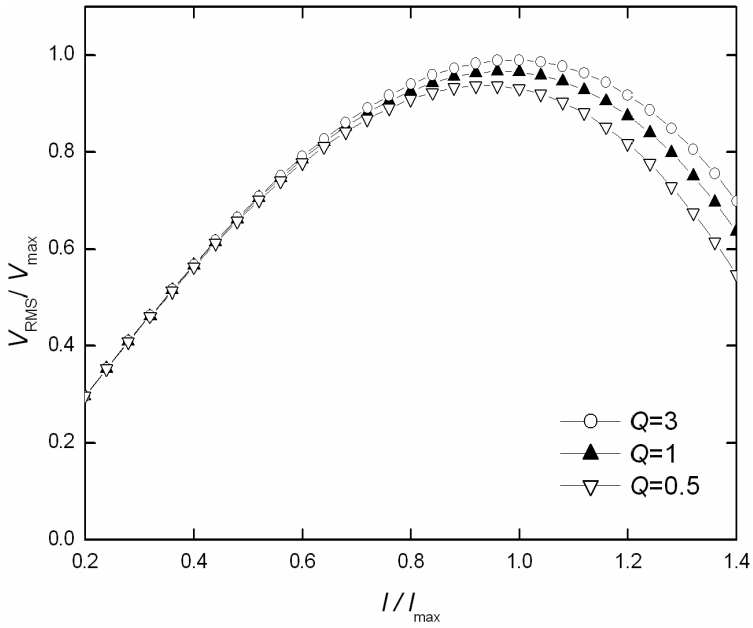

Figure 14. Reference voltage change due to the distortion with different Q values, $f = f_0$.

At high frequencies the component U_ω dominates and the case equals to the static case presented in Section 2.1.1.4 Only close to the mechanical resonance frequency the third harmonic component becomes significant.

2.1.3 Damping

The mechanical Q value of the moving plate capacitor can be controlled by adjusting the gas pressure inside the component enclosure. In the analysis above it was assumed that the damping coefficient is constant, which is a valid assumption for a qualitative analysis. However, for a quantitative analysis the

compressibility of the gas needs to be taken into account. In that case two different frequency domains can be observed. Below the cut-off frequency the gas has enough time to flow away from the gap, thus causing dissipation, whereas above the cut-off frequency the gas film is trapped and squeezed between the electrodes and behaves like a spring with low dissipation [28]. Further refinement of the model also includes the surface reflections of the gas molecules from the silicon and metal interfaces [29]. The major differences in the simulation results compared to the ideal harmonic oscillator model are the larger phase shift at low frequencies and generation of a new resonance in the high frequency area [28].

In voltage reference applications the component is usually actuated to the pull-in point with a frequency much higher than the mechanical resonance frequency in order to avoid the distortion caused by the third harmonic which is a potential error source in two different ways. First, if the RMS voltage is not measured using a phase-locked voltage detector, the higher harmonic will increase the voltage maximum, i.e. the value of the reference voltage, as seen from Eq. (39). Second, this voltage increase depends on the mechanical Q value related to the gas pressure in the component enclosure. As it is difficult to control the gas pressure inside the package after closing and if the hermetic package leaks with time, the reference voltage will change.

Gas damping will also increase the mechanical noise of the component [30]. The molecules in any material at a temperature above absolute zero are constantly vibrating, which gives rise to small random motions in the micro structure. The mechanical noise of the component sets the fundamental noise floor of the voltage reference [17], [18]. According to equipartion theorem the noise displacement δ_N at DC for a singly clamped cantilever, like the VTI accelerometer, is [30]

$$|\delta_N| = \sqrt{\frac{2k_B T}{\pi f_0 k Q}} = \sqrt{\frac{2k_B T}{\pi^3 f_0^3 m Q}} \quad \text{in} \left[\frac{\text{m}}{\sqrt{\text{Hz}}}\right], \tag{40}$$

where T is the absolute temperature and k_B is the Boltzmann's constant. For typical values of T = 300 K, f_0 = 0.5 kHz, k = 30 N/m, f = 1 Hz, and Q = 1 the noise displacement is 4×10^{-7} μm corresponding to noise voltage of 6×10^{-12}V near

the pull-in point (10 V). It has been assumed that the bandwidth is 1 Hz. The noise spectrum is flat (white noise), but shaped by the force-to-displacement transfer function of the resonator (Eq. 17) such that it peaks at the resonance frequency f_0. Equation (40) demonstrates the fundamental relationship between mechanical noise and component size. As the component mass decreases the noise will increase. Noise of this nature can be a fundamental problem in some surface micromachined devices [30].

2.2 MEMS manufacturing technologies

Silicon micromechanics is traditionally divided into two categories: surface micromechanics and bulk micromechanics. The silicon-on-insulator (SOI) process is an emerging technology falling in between surface and bulk micromachining as far as the thickness of the structures and the lateral resolution are concerned. The unconventional surface micromachining technique LIGA (Litographie Galvanoformung, Abformung), which also allows fabrication of structures with high aspect ratio, is not discussed here since it requires X-ray lithography equipment that is not commonly available in a process line. There are a number of different variations of these manufacturing technologies and they can be combined in various ways. Hence a strict categorisation is not possible. However, depending on the desired component structure, some manufacturing processes are more feasible than others. The main processing technologies for manufacturing a moving plate capacitor using a silicon wafer is briefly reviewed next.

2.2.1 Bulk micromachining

Bulk micromachining is used in manufacturing large seismic mass devices which have applications for example in high precision, low-g accelerometers. Often the whole wafer thickness is used to process the moving beam/cantilever and the cavity is formed by bonding this wafer with another silicon or glass wafer. Bulk micromachining is based on etching single-crystal silicon. Traditionally wet etchants, like potassium hydroxide (KOH), ethylene diamine pyrocatechol (EDP) or tetramethylammonium hydroxide (TMAH), are used. It enables a good control of the dimensions, but the typical pyramid of V-groove

shapes formed in anisotropic etching limits the freedom of design and increases the device size. The recently developed plasma etching enables narrow line widths and high aspect ratios also for bulk micromachining. With Deep Reactive Ion Etching (DRIE) it is possible to obtain aspect ratios of 20:1 [31]. Loading, *i.e.* reduction of the etch rate with increasing etch area, feature charging and notching are challenges in plasma etching [32].

Single-crystal silicon wafers are stress free. However, high doping concentrations, for example $7x10^{19}$ cm^{-3} boron, used to improve the electric conductivity of the silicon or used as an etch stop layer, can cause high intrinsic tensile stress [33]. Different process steps, like oxidation or annealing at high temperatures, can change the tensile stress to compressive stress. Sandwich structures, *i.e.* a stack of wafers manufactured from different materials bonded together, are susceptible to mechanical stress, which originates from the different temperature coefficients of the materials.

2.2.2 Surface micromachining

Surface micromachining is a mature processing technology generally used in manufacturing of high-g accelerometers, pressure sensors, etc. In surface micromachining the devices are made of thin films deposited on the surface of a silicon wafer, which acts merely as a support for the structure. The most widely used materials are low-pressure chemical vapour deposited (LPCVD) polycrystalline silicon as the structural material and silicon dioxide as the sacrificial layer. The LPCVD polycrystalline layers are typically a few micrometers thick but with an epireactor it is possible to deposit tens of micrometers thick epipoly films [34]. However, stress control becomes more difficult with increasing layer thickness. The major advantages of surface micromachining are the simplicity of the process and the use of standard CMOS fabrication. The major challenge is the internal stress control of the polysilicon film, which is originally under compressive stress, and the variation of the stress along the growth direction [34]. Also, planarity and stiction problems are common in surface micromachining.

2.2.3 SOI

A silicon-on-insulator (SOI) wafer is composed of two single-crystal silicon wafers with a silicon oxide layer in between. The relatively thin (1–2 μm) oxide layer can be used as an etch stop, an isolation layer, or as a sacrificial layer. Hence relatively thick silicon structures can be realised with well defined layer heights. A wide range of thicknesses are available for the structure wafer. The internal stress in SOI wafers is low [32]. Different micromachining technologies are compared in Table 1.

Table 1. Comparison of different micromachining technologies. These values vary depending on the manufacturing equipment and materials used.

	Bulk	**SOI**	**Surface**
Thickness of structures	> 10 μm	> 5 μm	< 5μm
Lateral resolution	1.4 × wafer thickness* / few micrometers (DRIE)	< 2 μm	< 2 μm
Tensile stress	none**	low	moderate/high
IC compatibility	no	yes	yes
Seismic mass	large	medium	small

* In <100> direction with anisotropic wet etch.

** Usually the stress in bulk micromachined structures arises from bonding the bulk wafer to another wafer.

2.3 MEMS component

The manufacturing process sets the rules for the component design, *i.e.* the maximum size of the released area, the minimum height of the gap, the layer thicknesses, etc. Some fundamental design considerations are discussed in this Section.

2.3.1 Component Dimensions

The size of the released structure determines the moving capacitor electrode area and hence the component capacitance value. For the readout electronics it is advantageous to have a large enough capacitance. Depending on the manufacturing design rules, the released structure should typically be smaller than 800 μm × 800 μm in order to avoid the stiction problem.

The area of the released structure and the wafer thickness determine the seismic mass m of the component. The mass together with spring constant k determine the component mechanical resonance frequency $f_0 = \sqrt{k/m}/2\pi$. If a low resonance frequency is preferred, the component size is maximized, assuming that the spring constant remains the same. However, a massive device is more susceptible to external vibrations.

Although with micromachining it is possible to manufacture extremely thin structures or narrow features in nanometer scale, the relative accuracy is only about $10^{-1}\ldots10^{-3}$, *i.e.* orders of magnitude worse than using traditional technologies [35]. The process uniformity is a critical parameter in MEMS fabrication and has a great impact on the component yield. Also, if the dimensions of the component vary, the sensitivity and capacitance will vary accordingly elaborating the design of the readout electronics and final testing of the device.

2.3.2 Materials choices

The selection of materials available for MEMS manufacturing is large. However, in practice only a restricted number of materials is available in one single process line. The most common substrate and device wafer material is silicon, which has well characterised properties and mature processing technology.

2.3.2.1 Single-crystal silicon

Single-crystal silicon has excellent mechanical properties. Silicon shows no drift or hysteresis at normal temperatures. The resistivity of silicon varies from 0.001 to 20 000 Ω-cm depending on the doping level. High-resistivity silicon can in

some applications be used as a dielectric layer whereas high-conductivity silicon is used as an electrode material. However, silicon is brittle. It breaks if the induced stress is higher than the yield stress.

Typical material properties of silicon are presented in Table 2.

Table 2. Typical material properties of Si at 25 ºC used in the calculations.

	Symbol	Si at 25 ºC	Unit	Reference
Density	ρ	2.3×10^{3}	kg/m^3	[36]
TC*	α	2.84×10^{-6}	$ºC^{-1}$	[37]
Intrinsic resistivity		3.3×10^{5}	Ω-cm	[36]
Young's modulus	E	1.3×10^{11}	Pa	[37]
Shear modulus	G	5.75×10^{10} … 7.9×10^{10}**	Pa	[35]
TC of Young's modulus	β	-65×10^{-6}	$ºC^{-1}$	[37]

* Linear coefficient of thermal expansion (TC)

** Depending on the crystal orientation.

2.3.2.2 Polysilicon

Since it is difficult to grow thin films of single-crystal silicon, polycrystalline silicon can be used instead. Polysilicon is widely used in surface micromachining as a structural layer. The internal film stress of polysilicon depends greatly on the deposition process. The stress can be controlled by deposition conditions, post deposition annealing or film doping [32]. Depending on the doping level polysilicon can be used as an insulator or a conductor. Its interface with silicon dioxide is stable and its lithography and etching properties are good [31].

2.3.2.3 Silicon oxide and silicon nitride

The most common insulators used in silicon technology are silicon oxides (SiO_x) and silicon nitrides (SiN). The high-frequency *C-V* curve of thermal SiO_2 shows no hysteresis or displacement of the capacitance-voltage (*C-V*) curve minimum point unlike other insulators. But the high deposition temperature (800…1000 °C) limits its use in later stages of fabrication, especially if metal layers have been deposited. Sputter Deposition (SD) and Plasma Enchanged Chemical Vapour Deposition (PECVD) are processed at temperatures below 400 °C, but the dielectric properties are inferior compared to thermal SiO_2 [33].

2.3.2.4 Metals

Metals in MEMS are needed for the electric contacts and in some cases for the electrode surfaces. Aluminium (Al) is commonly used especially if Al bond wires are used. Aluminium is easy to sputter and it forms a good mechanical contact with silicon. Alloys of aluminium, for example Al-1%Si, are used to increase the stability of the metallization. A disadvantage of aluminium is hillock formation at temperatures above 200 °C, which can short-circuit the narrow gap of a MEMS structure. Hillocks are small protrusions, which are formed when compressive stresses in Al relax [31]. Hillock formation can be reduced by sputtering a thin layer of another metal, molybdenum for example, on the top of the aluminium. Al also forms a native oxide layer.

Other generally used metals in MEMS manufacturing are molybdenum (Mo), tungsten (W), copper (Cu), and tantalum (Ta) and several compounds and alloys like TiW, Al-Cu etc. The electric resistivities vary from 1.92 μohm-cm (Cu) to 48 μohm-cm (Ti) [31]. The thin film resistivity is often much higher than bulk resistivity.

Gold (Au) would be an ideal metal in many MEMS applications since it is a noble metal and thus does not oxidise or form any other compounds with processing chemicals. However, gold is not CMOS compatible and it is not available in many clean rooms.

Some metals can produce a large change in its electric resistivity due to gas adsorption and are therefore used as gas sensors. Metal oxides ZnO, TiO_2 and

In_2O_3 as well as precious catalytic metals Pt and Pd should be avoided when a stable capacitor electrode is desired [2].

2.3.3 Parasitic capacitance

Parasitic capacitance is usually minimized in a MEMS component design, because it causes a loss of sensitivity as will be demonstrated in Section 4.1. The major sources of the parasitics are the anchoring areas of the released structures, which are also used for the electric contact (bonding or flip chip) to the moving electrode and hence need to be at least 100 μm × 100 μm. A typical parasitic capacitance value for a component which has three springs (see Fig. 3) is

$$C_{\mathrm{p}} = 3 \times \frac{\varepsilon_{\mathrm{ox}} A}{d} = 3 \times \frac{3.4 \times 10^{-11}\,\mathrm{F/m} \times (100\mu\mathrm{m})^2}{1\mu\mathrm{m}} = 1.0 \quad \mathrm{pF} \tag{41}$$

assuming that the oxide layer thickness is 1 μm between the upper and lower electrodes. Hence the parasitic capacitance can be the same order of magnitude as the work capacitance of the MEMS component. Other sources for the parasitics are the connection wires, which should be kept as short as possible and well shielded.

2.3.4 Packaging

Packaging provides mechanical support, protection from the environment, and electrical connection to the MEMS component. These functions can also be separated between different levels of packaging. For example, the zero-level package can be wafer-level encapsulation, *i.e.* bonding of an additional silicon or glass wafer on top of the MEMS device wafer, which provides hermetic enclosing and mechanical shield. The first-level package can be a dual in-line (DIP or DIL) package, including also the readout electronics, which provides the electrical connections. In volume production it is economical to use standard packages for further component handling in testing and final mounting on a printed circuit board (PCB).

In the voltage reference application the mechanically induced stress to the component due to rigid mounting is critical. Often an elastic adhesive is used as die-attached material in order to minimize the mechanical stress due to package bending caused by mechanical stress or temperature induced stress [38]. The thermal expansion coefficient (TC) of the package should be equal or slightly greater than the TC of silicon for reliability since thermal shock or thermal cycling may cause die cracking and delamination if the materials are unmatched or if the silicon is subject to tensile stress [39].

An open capacitive structure is very sensitive to changes in humidity, pressure etc. Hence the sensor needs to be encapsulated in vacuum or in a protective gas atmosphere. Inertial gases, like argon or nitrogen, are commonly used. High gas pressure works as a mechanical damper as discussed in Section 2.1.3. Suitable hermetic packages for MEMS components are metal packages (TO-can, DIL, etc.) and ceramic Low Temperature Co-fired Ceramic (LTCC) packages. Also wafer level encapsulation is an economical and high quality option for packaging, which results in a small sensor size. Before the final lid seal, a bake is usually performed to drive out any trapped gas or moisture. This also reduces the moisture related corrosion of metals in the component.

The electric contacts to the MEMS component are usually done using wire bonding, conductive adhesive, soldering or Controlled Collapse Chip Connection technology (C4), generally called flip-chip, depending on the number and size of contact pads, component temperature durability, etc. Soldering and flip-chip connections can cause stress to the component [39] and should hence be avoided in voltage reference use.

2.4 VTI accelerometer

Several measurements presented in this dissertation are performed using bulk micromachined accelerometers manufactured by VTI Technologies Oy [40]. The accelerometer is a cantilever attached at one end as shown in Fig. 15. The component consists of three silicon wafers. A silicon wafer where the moving structure is etched is anodically bonded between two glass-covered silicon wafers. A single component comprises of two identical capacitors which are formed by the surfaces of the moving mass and the fixed electrodes above and

below it. The components are enclosed in a gas atmosphere by wafer level anodic bonding. The pressure inside the cavity is high enough to over damp the cantilever movement, *i.e.* the mechanical Q value is well below 1. The components are sensitive to inclination change, which is characteristic for an accelerometer, and therefore they are not optimal in voltage reference use.

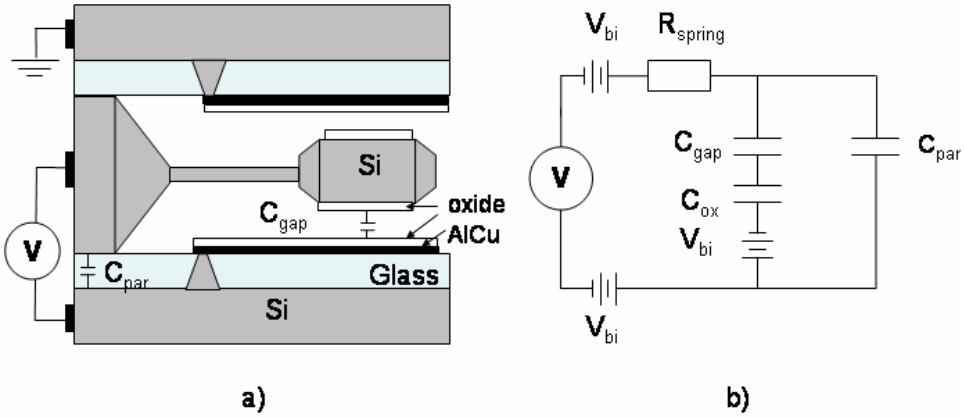

Figure 15. a) A schematic view of an accelerometer by VTI Technologies and b) its equivalent circuit. V is the external voltage source, V_{bi} is the built-in voltage of the metal-silicon junction. C_{gap} is the component capacitance (work capacitance), which has a parasitic capacitance C_{par} in parallel. C_{ox} is the capacitor formed by the dielectric layer (usually SiO_2). R_{spring} is the resistance of the silicon spring.

The electrode materials varied. Most of the components had AlCu, Ta or Mo coating on the non-moving electrode. Some of the components had a dielectric layer processed on top of the metal. Also the moving electrode was metallised in some of the components.

2.5 Stability of a MEMS component

Fundamental factors effecting the stability of the reference voltage, according to Eq. (7), are the stability of the spring constant k, the gap d, the permittivity ε, and the electrode area A of the component. A stable spring constant is achieved by using stress free single-crystal silicon springs. Although single-crystal silicon

is mechanically an extremely stable material, the spring constant has a temperature coefficient arising mainly from the temperature coefficient of the modulus of elasticity (Young's modulus), which is in the order of -6×10^{-5}/°C. However, usually the temperature coefficient of the device is 10–20 times higher, which results from a change in the gap due to mechanical stress.

Voltage references are operated at the pull-in point, which implies that there is a high electric field (about 0.1 MV/cm) between the electrodes. Various electrostatic surface and interface effects are potential sources of electrical instability. Especially metal-silicon interface effects and oxide charging can reduce the stability of the device as will be discussed below.

2.5.1 Component structure

An ideal capacitor, which is desired in the voltage reference application, is mechanically stable and the surface potentials of the electrodes are well defined. A semiconductor surface may be unstable due to surface charges, which will cause energy band bending [36]. Hence metal electrodes are preferred although metallizing the moving electrode significantly complicates the manufacturing process of the component. A cross section of a component with metal electrodes is shown in Fig. 16.

The electric contact to the upper electrode goes through the silicon spring. From an electrical point-of-view it would be advantageous to access the metal directly in order to avoid the built-in voltage V_{bi} between silicon and metal. However, this would require metallizing the spring which would significantly reduce the mechanical stability of the component. A metal layer on the silicon spring would induce stress and also increase the temperature coefficient due to the bi-metallic effect. If the metal contact on top of the moving plate is processed of the same metal as is used for the electrode coating, the built-in voltages should cancel each other.

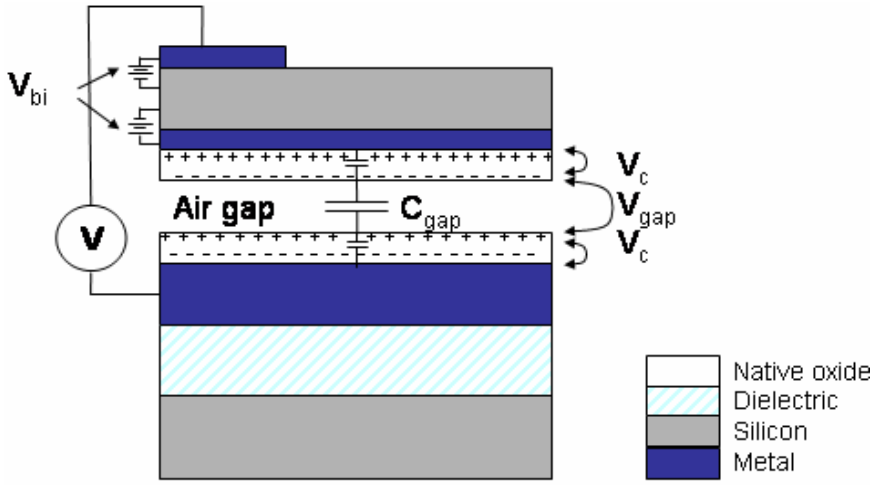

Figure 16. A cross section of an ideal MEMS moving plate capacitor (not in scale). V_{bi} is the built-in voltage between metal and Si and V_c is the potential caused by oxide charging.

Surfaces and interfaces, where defects are concentrated, are areas where charges are preferentially trapped and hence potential sources for instability. The design goal for the moving plate capacitor design presented in Fig. 16 was to minimize these effects. However, still a metal-silicon surface and a native oxide layer exist and their effect on the device stability will be discussed in the next Section.

2.5.2 Built-in voltage

The energy band diagram of a metal and an *n*-type semiconductor interface before and after contact is displayed in Fig. 17. When an n-type semiconductor is attached to metal, electrons will diffuse from the semiconductor to the metal since the Fermi level E_F of the semiconductor is higher than the Fermi level of the metal. A negative surface charge will be created on the metal side whereas a positive charge will be created in the semiconductor depletion region. This charge imbalance will create an electric field which opposes the diffusion current. Electrostatic potential related to this field bends the energy bands on the semiconductor side. At equilibrium the electrostatic potential balances the Fermi level difference.

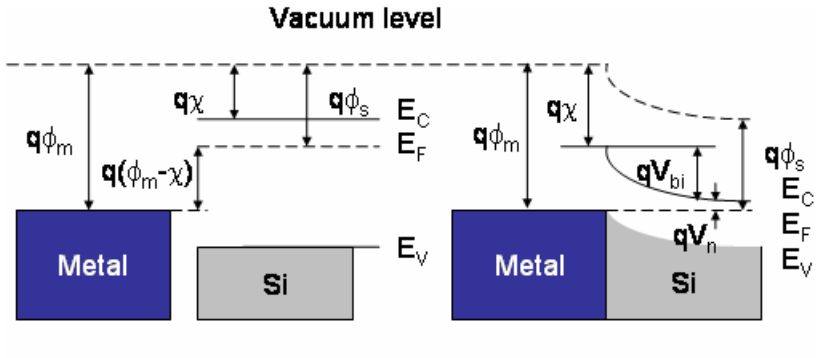

Figure 17. Energy band diagram of an isolated metal adjacent to an n-type semiconductor under thermal non-equilibrium condition and metal-semiconductor contact in thermal equilibrium (redrawn after [36]).

The built-in voltage V_{bi} is defined as the potential seen by the electrons in the conduction band trying to move to the metal

$$V_{bi} = \phi_{Bn} - V_n = \phi_m - \phi_s \,, \tag{42}$$

where qV_n is the difference between the bottom of the conduction band and the Fermi level. Similar results also apply for *p*-type semiconductor. Hence the built-in voltage can be calculated from the work function difference of the materials. The work function difference varies with the doping concentration. For p-type silicon the work function difference increases as a function of the doping level and for n-type silicon the work function difference decreases as a function of the doping level [36]. For example in the case of aluminium and p-type silicon, $N_A = 10^{18}$, $V_{bi} \approx 4.1$ V – 5.1 V = -1.0 V. However, in practice the situation is more complicated. The disruption of the crystal lattice produces a large number of surface energy states located in the forbidden bandgap. These surface states can act as donors or acceptors that influence the final determination of the barrier height [36].

The built-in voltage of the moving plate capacitor can be experimentally determined from the component *C-V* curve as the offset voltage with respect to zero bias voltage as shown in Fig. 18. Hence the built-in voltage translates the *C-V* curve along bias voltage axis, but does not change the shape of the curve.

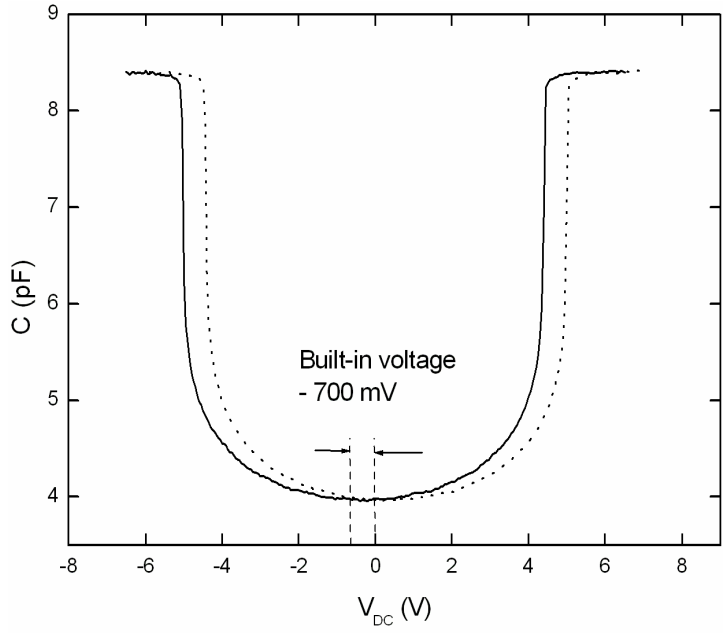

Figure 18. C-V curve of a moving plate capacitor.

Extensive studies on the built-in voltage and its temperature dependence for different MEMS components manufactured by VTI Technologies Oy (mainly accelerometers) have been done [41, 42]. The non-moving electrode of the VTI components is different from the metal-semiconductor structure presented above. The electric contact to the non-moving electrode goes via silicon as shown in Fig. 15 in Section 2.4. Also, in some devices the moving electrode was not coated with metal and some metal electrodes had an additional SiO_2 coating. However, the measurement results still have general applicability. The measured built-in voltage values agreed only partly with theory. Large variations were observed in the built-in voltages, even for components from the same wafer. The built-in voltages and their temperature coefficients were lower in the metal-metal structures, especially in the Mo-Mo structures, than in the metal-Si structures. A SiO_2 layer on top of the metal generally decreased the values of the built-in voltage as well as its temperature dependence. A thick SiO_2 layer could even change the sign of the built-in voltage which suggests that the layer was heavily charged. Theoretically the SiO_2 layer on top of the metal electrode should not have an effect on the temperature dependence. It is suggested in [42] that the trapped charges in the oxide balance the temperature dependence.

However, another explanation is that there are residuals of process chemicals inside the component enclosure, and their adsorbtion on the metal surfaces varies with temperature which causes a change in the surface potential. The SiO_2 layer passivates the electrode surface and hence reduces the temperature dependence. This theory is in agreement with the stability study of a MEMS resonator, where the humidity inside the component enclosure was observed to cause drift of the resonance frequency [43].

2.5.3 Depletion layer capacitance

When a bias voltage is applied to the metal-semiconductor junction the energy band diagram will change as shown in Fig. 19 for a *p*-type semiconductor. When the bias voltage is zero (case a), the band diagram is in thermal equilibrium and the Fermi levels of both materials are equal (as also shown in Fig. 17 for an *n*-type semiconductor).

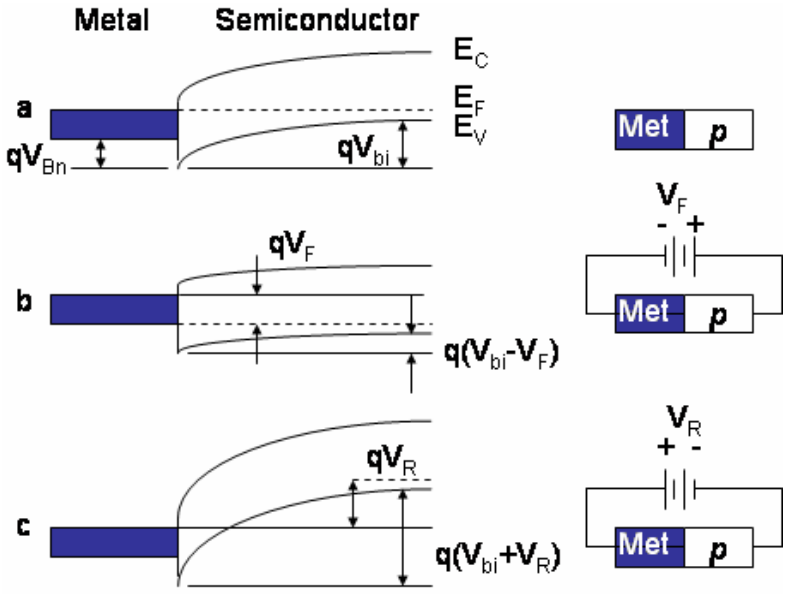

Figure 19. Energy band diagram of a metal p-type semiconductor junction under different bias conditions: a) thermal equilibrium b) forward bias V_F and c) reverse bias V_R.

If a negative voltage V_F (forward bias) is applied to the metal with respect to the semiconductor, electrons can easily move from the semiconductor to the metal because the semiconductor-to-metal barrier height has decreased by voltage V_F (case b). A reverse bias V_R (case c) has the opposite effect. It increases the barrier height by V_R.

The charge and field distributions for a metal-semiconductor contact are shown in Fig. 20 a) and b) respectively.

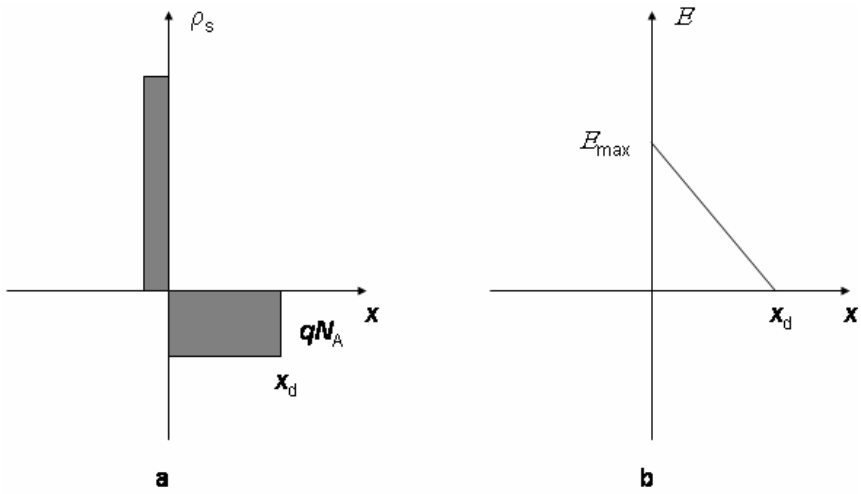

Figure 20. Charge distribution (a) and electric field distribution (b) in a metal p-type semiconductor junction.

Assuming that the metal is a perfect conductor and the extent of the space charge ρ_s in the semiconductor is x_d, *i.e.*, the $\rho_s = - qN_A$ for $x < x_d$ and $\rho_s = 0$ for $x > x_d$, the electric field distribution is given by

$$E(x) = \frac{qN_A}{\varepsilon_s}(x_d - x) = E_{max} - \frac{qN_A}{\varepsilon_s}x \tag{43}$$

where N_A is the acceptor density, ε_s is the permittivity of the semiconductor, and E_{max} is the maximum electric field located at the junction interface. The voltage across the space charge region is

$$V_{\mathrm{bi}} - V_{\mathrm{bias}} = \frac{E_{\max} x_{\mathrm{d}}}{2} = \frac{q N_{\mathrm{A}} x_{\mathrm{d}}}{2\varepsilon_{\mathrm{s}}} \tag{44}$$

where V_{bias} equals $+V_{\mathrm{F}}$ for forward bias and $-V_{\mathrm{R}}$ for reverse bias. The depletion region x_{d} forms a voltage controlled capacitor with capacitance

$$\frac{C_{\mathrm{dep}}}{A} = \frac{\varepsilon_{\mathrm{s}}}{x_{\mathrm{d}}} = \sqrt{\frac{q\varepsilon_{\mathrm{s}} N_{\mathrm{A}}}{2(V_{\mathrm{bi}} - V_{\mathrm{bias}})}} \,. \tag{45}$$

This capacitance is in series with the moving plate capacitance and it can have a significant effect on the reference voltage. The MEMS capacitance is typically order of pF while the depletion layer capacitance is order of nF. The bias voltage required to eliminate the depletion region capacitance is well above the component pull-in voltage due to the voltage division between these capacitances. The relative change of the pull-in capacitance $(C_{\mathrm{pi}}\text{-}C_{\mathrm{tot}})/C_{\mathrm{pi}}$, where $C_{\mathrm{tot}} = C_{\mathrm{pi}}C_{\mathrm{dep}}/(C_{\mathrm{pi}}+C_{\mathrm{dep}})$, as a function of the relative forward bias $V_{\mathrm{bias}}/V_{\mathrm{bi}}$ is shown in Fig. 21.

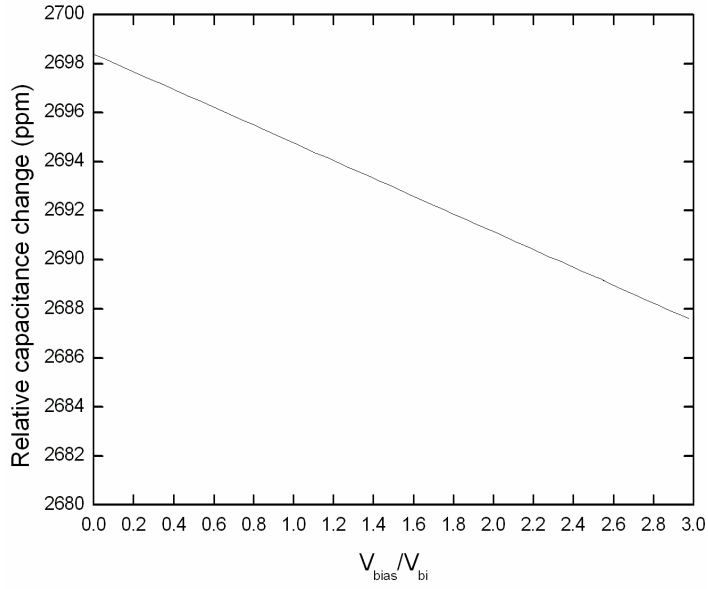

Figure 21. Relative change of the pull-in capacitance as a function of relative forward bias voltage assuming acceptor density $N_A = 2\times10^{18}$(corresponds to Si resistivity of 0.02 Ω-cm), V_{bi} = 0.7 V and gap 1 μm.

The depletion region capacitance can be reduced by a good ohmic contact between the metal-semiconductor interface, *i.e.* low contact resistance, by extra doping the contact area of the silicon [36]. Also, it is advantageous to connect the high potential to the moving mass if *p*-type silicon is used (forward bias).

2.5.4 Electrostatic charging

Formation of a native oxide on the surfaces of electrodes is difficult to avoid even when the electrodes are coated with metal. A dielectric layer can have a considerable amount of trapped charges [45]. A sheet charge causes a voltage V_c between the electrodes [36]

$$V_{\mathrm{c}} = -\frac{d_{\mathrm{ox}}\sigma_{\mathrm{ox}}}{\varepsilon_{\mathrm{ox}}}. \tag{46}$$

If the dielectric layer is native oxide on silicon, V_{c} is typically of the order of -50 mV, assuming that the SiO_2 layer thickness d_{ox} is 1 nm, permittivity is $\varepsilon_{\mathrm{ox}} = 3.8\ \varepsilon_o$ and surface charge density σ_{ox} is 10^{12} e/cm^2. Hence the charges create a potential difference over the component the same way as the built-in voltage does. The offset voltage of a *C*-*V* curve is the sum of these two voltages.

A charged dielectric layer can also have another effect on the *C*-*V* curve since it can reduce the effective gap of the component as shown in Fig. 16. Depending on the location of the charge in the dielectric, the amount of the gap reduction is between the height of the dielectric layer (charges locate on the air-dielectric surface) and zero (charges locate on the metal-dielectric surface). Charges in dielectrics are discussed in the next Section in more detail. The effect of the gap reduction on the component *C*-*V* curve is shown in Fig. 22.

A change in the component parasitic capacitance transfers the *C*-*V* curve along the capacitance axis, but does not change the shape of the curve as seen in Fig. 22.

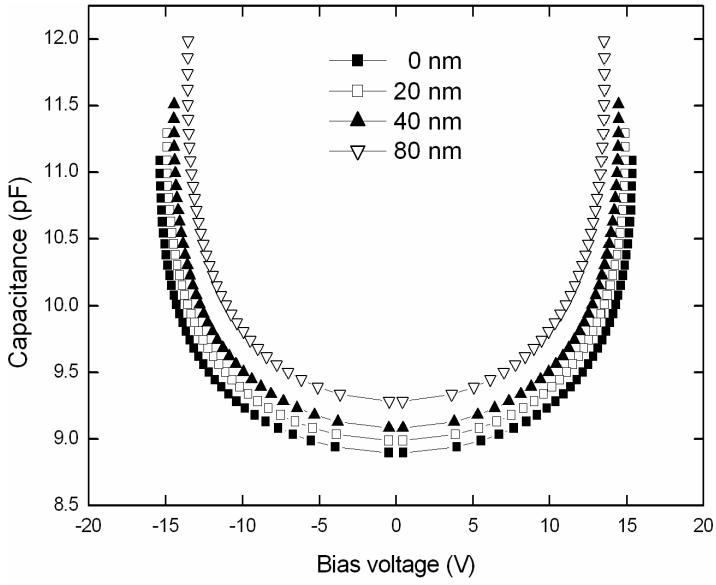

Figure 22. C-V curve for the round component (dimensions listed in Table 5) with a nominal gap value of 1 μm (δg = 0 nm) and reduced gap values. The gap reduction, δg, is 20 nm, 40 nm, and 80 nm. The change of the C-V curve offset (232 mV for 50 nm thick oxide assuming charge density 10^{11} *e*/cm^2) *does not show in this scale.*

2.5.4.1 Charges in dielectrics

Charge trapping mechanisms in dielectrics have been investigated for more than 30 years in association with metal-oxide-semiconductor (MOS) transistors [36]. The scaling down of the MOS devices has recently activated this research field again. The Negative Bias Temperature Instability (NBTI) has been observed to shorten the lifetime of p-channel field-effect MOS transistors when stressed with negative gate voltage at elevated temperatures [46]. Another commercially important application, where dielectric charging degrades the device operation, is a capacitive RF-MEMS switch [47]. Although much effort has recently been dedicated to study the dielectric charging, details of the phenomena are not yet clearly understood.

Traditionally charges in MOS capacitors are classified in four groups: interface-trapped charges, fixed oxide charges, oxide-trapped charges, and mobile ionic charges [36]. In addition to these charges, in moving plate capacitors there are surface charges at the electrode-air interface.

An interface trap charge, Q_{it}, results from the silicon dioxide and silicon (SiO_2-Si) interface properties and it is dependent on the chemical composition of the interface. The trap density in the <100> orientation can be as low as 10^{10} cm^{-2}, about an order of magnitude smaller than in the <111> orientation [36]. Si dangling bonds, *i.e.* trivalent silicon atoms with an unsaturated valence electron, $Si_3 \equiv Si\bullet$, act as interface trap centres, which are usually passivated by low-temperature hydrogen annealing. Subsequent arrival of a positively charged ion at the interface can cause depassivation of the SiH bond, which is suspected to cause the NBTI. There are two basic approaches to explain this phenomenon: the hydrogen model [48] and the chemical reacting model [49]. In the hydrogen model as the SiH bond breaks, due to an electric field for example, H^+ diffuses away and reacts directly with SiH. The products of this reaction are an H_2 molecule and a positively charged dangling bond centre:

$$Si_3 \equiv SiH + H^+ \Leftrightarrow Si_3 \equiv Si\bullet + H_2, \tag{47}$$

where $\equiv SiH$ is a hydrogenated trivalent silicon and H^+ is positively charged hydrogen ion (proton). H_2 can later dissociate and act again as a catalyst to disrupt additional SiH bonds. In the chemical reacting model a species Y diffuses to the SiO_2-Si interface and creates a trap and X. Y can be, for example, a neutral water molecule and a hole at the silicon surface ($Y = H_2O + h^+$) and X is then H^+. The interface trap creation via hydrogen model can be modelled as

$$Si_3 \equiv SiH + Y \Leftrightarrow Si_3 \equiv Si\bullet + X. \tag{48}$$

A fixed oxide charge Q_f can be regarded as a sheet charge locating near the SiO_2-Si interface. This charge is fixed and cannot be affected over a wide variation of surface potential [36]. Generally Q_f is positive and depends on oxidation and annealing conditions and on silicon orientation. For <100> oriented silicon the Q_f is typically 10^{10} …10^{12} cm^{-2}. Similar to interface trap creation model fixed charges can be modelled as

$$O_3 \equiv SiH + h^+ \Leftrightarrow O_3 \equiv Si^+ + H^0, \tag{49}$$

where h^+ is a hole and H^0 is a neutral hydrogen atom. An interface trap and a hydrogenated trivalent silicon defect in SiO_2 are illustrated in Fig. 23. Interface

trap charges and fixed charges can be distinguished with a *C-V* measurement. As the applied bias voltage is varied, the Fermi energy at the oxide-semiconductor interface changes accordingly and affects the occupancy of the surface states. The interface states cause the transition in the capacitance measurement to be less abrupt. The combination of the low frequency and high frequency capacitance allows a calculation of the surface state density [36].

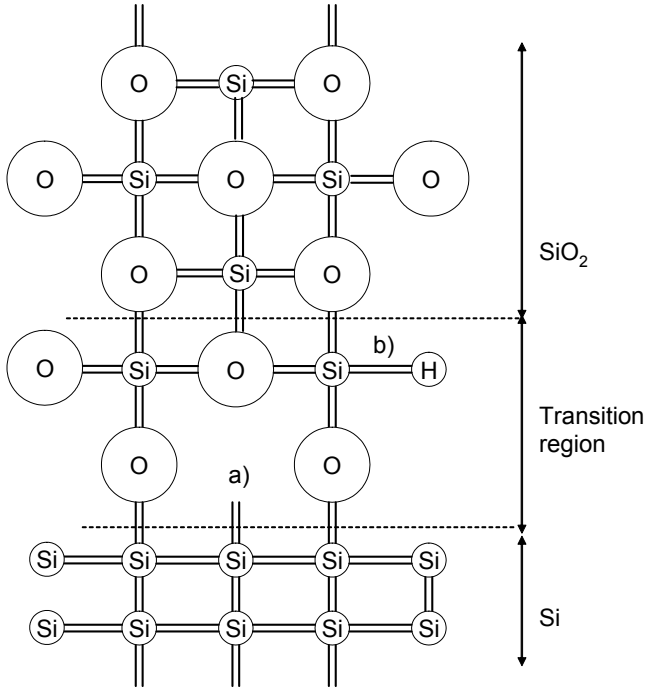

Figure 23. A silicon atom forms a covalent bond with its four nearest neighbours in wafer bulk. The crystal lattice is broken at the SiO_2 interface. In the transition region there are a) interface traps (dangling bonds) and b) $\equiv$SiH *defects. Redrawn after [49].*

Mobile oxide charges result from ionic contamination due to Na^+, Li^+, K^+, Ca^{++}, and Mg^{++}. They are impurities that are carefully controlled in IC processes. Especially sodium was a big concern in early days of MOS manufacturing. The glass used in anodic bonding contains sodium and for this reason anodic bonding is not a CMOS compatible process. Since anodic bonding is used in manufacturing of the VTI sensors they contain mobile sodium ions. Hydrogen is the most common impurity in IC fabrication and cannot easily be avoided.

H^+ can exist for prolonged periods in oxides as a mobile charge [46]. On the other hand, hydrogen is also used to passivate Si dangling bonds as discussed earlier.

As a summary, common to all these charging models is that they depend on the electric field in the oxide and that the charging saturates over time (unlike the oxide-trapped charges, which are due to defects in the SiO_2, and are very stable). Threshold voltage shifts of MOS structures in the NBTI experiments have been found to be proportional to the electric field as E_{ox}^{m}, where m lies in the range of $1.5 \leq m \leq 3$ [46], whereas in RF-MEMS switch reliability studies, the electric field dependency has been measured to be exponential (exp(E)) [50]. The major difference between these experiments is the thickness of the oxide layer, which is in the order of nanometers in the NBTI studies and two orders of magnitude thicker in the RF-MEMS studies. In thin oxides the charges can tunnel from the insulator to the semiconductor and vice versa [51] which could explain the difference. Also the oxide quality and deposition process has a significant impact on the charging properties which complicates the analysis of the charging effect.

The charging analysis above considers only silicon dioxide, which is the most extensively studied dielectric material. Also other materials, especially high dielectric constant (ε) materials like SiON, Al_2O_3, HfO_2, Al2O3, ZrO_2 and silicates, have been experimented. There is no direct relationship between an insulator conductivity and its charging properties since the trapped charges are rather related to the defects in the crystallographic structure than to the nature of the bulk material (ionic or covalent bond) [47]. Still, some of the experiments demonstrate low density of interface defects for high dielectric constant materials. Also a recently proposed model, further developed from the hydrogen model, proposes that the saturation voltage of a MOSFET threshold voltage shift, is proportional to $1/\varepsilon$ [52].

2.5.4.2 Oxide charging models

The time dependence for oxide charging under bias voltage has been studied for both pFETs [52] and for RF-MEMS switches [50]. The first model is based on physical principles of SiO_2 interface (hydrogen model discussed earlier). According to this model the threshold voltage shift ΔV_t of a transistor is

$$\Delta V_{\mathrm{t}} = -\frac{Q_{it} + Q_{\mathrm{f}}}{C_{\mathrm{ox}}} = \Delta V_{\max}\left(1 - \exp\left(-\frac{t}{\tau}\right)^{\gamma}\right), \tag{50}$$

where the $\Delta V_{\max}$ depends on the electric field, initial SiH density, oxide thickness, energy levels of interface and oxide traps and dielectric constant of the oxide. γ is a constant related to dispersive diffusion of bonded and interstitial hydrogen atoms (often assumed to be approximately 1 for thick oxides) and τ is a time constant.

The oxide charging model developed for RF-MEMS switches takes also into account decharging observed to occur during long experiments. If N_0 is the total trap density, e elementary charge, τ_1 time constant for charging, and τ_2 time constant for decharging, the surface charge σ gets an expression

$$\sigma = N_0 e \frac{\tau_1}{\tau_1 + \tau_2}\left(1 - \exp\left(-\frac{\tau_1 + \tau_2}{\tau_1 \tau_2} t\right)\right). \tag{51}$$

In pFETs and switches the moving plate is in contact with the oxide layer but in the voltage reference application the capacitor formed by the air gap, C_{gap}, significantly reduces the voltage over the oxide layer. Since MEMS capacitances are typically in pF-region and the oxide capacitances is in nF-region the voltage over the oxide is three orders of magnitude smaller than the applied bias voltage.

2.5.5 Mechanical stability

Mechanical deformation of the electrodes can change the gap d. Intrinsic stress, inherent in an epi-poly process, strongly influences time and temperature stability of the component. Hence the use of stress-free substrate material, such as SOI, is essential.

Also rigid mounting of the component can cause external stress, as shown in Fig. 24. Package-induced stress to wafer level vacuum encapsulated MEMS resonators have been studied in [44]. The results demonstrate that with a good mechanical design it is possible to reduce the component drift below 0.1 ppm/month, which is sufficient even for high-precision applications.

There are several ways to decrease the package induced stress: an increase in the thickness of the component makes it more rigid, spring shape and suspension can be optimized to release the stress, reinforcing structures can be mounted inside the enclosure, and materials, which have nearly equal thermal expansion coefficients, can be chosen.

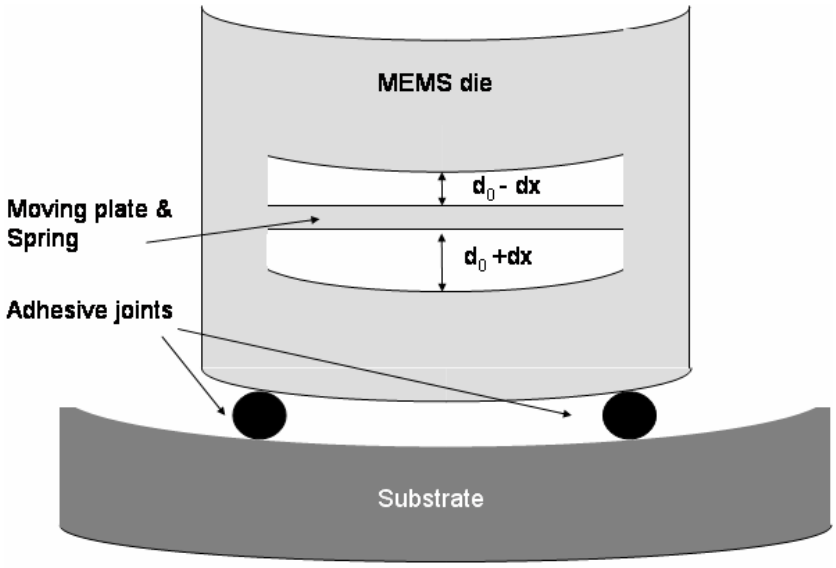

Figure 24. Gap deformation of a component due to package bending (not in scale).

3. Manufacturing and design of the components

Electrode surface quality and mechanical stress are the key factors defining the stability of a MEMS component. A new fabrication process was developed to optimize these factors. The major improvements introduced by the EMMA SOI process are the use of stress-free SOI wafers, and sputtering of both electrode surfaces by thermally and chemically stable metal. Two components were designed for the process. One component was optimized for the DC voltage reference use and the other for the AC voltage reference use.

3.1 EMMA Process

SOI was selected as the starting point of the design because of well defined device layer thickness and buried oxide layer, which was used as etch stop. Although the substrate layer was removed during the process, this manufacturing scheme is expected to give the best results in terms of stability, especially mechanical stress. Further, inertial effects are not important in SOI. A 20 μm SOI-wafer is easily available and thick enough to make the bi-metallic effect negligible. The gap height, determined by the buried oxide layer thickness, is not a critical value in the voltage reference application.

The device wafer was a SOI wafer, which had a 20 μm thick device layer and 1 μm buried oxide layer, and the substrate wafer was a 380 μm thick double side polished Si wafer. Both wafers were highly doped with boron resulting to silicon resistivity of 0.015–0.02 Ω-cm. The metal electrodes were placed in wells to avoid problems in wafer bonding. The well depth and oxide thickness of the substrate wafer defined the gap height which was 1 μm.

The process consisted of four phases: 1) processing of the device (moving part) wafer, 2) processing of the substrate wafer, 3) bonding of the wafers, and 4) processing of the bonded pair as shown in Fig. 25. Low temperature fusion bonding is utilised in bonding of the sputtered wafers. After wafer bonding the handle layer of the SOI wafer and the buried oxide were removed by etching. Then the upper component surface was sputtered and patterned and finally the

moving mass was released with inductively coupled plasma (ICP) etching. The process required 10 lithography steps.

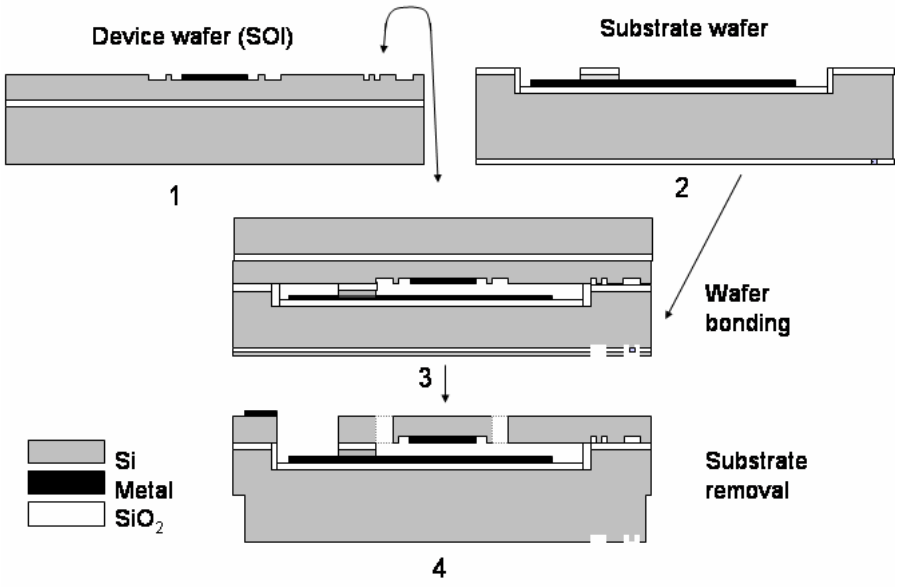

Figure 25. EMMA SOI process.

The most critical step in the process was the wafer bonding. If the surface quality of the wafers were insufficient, large non-bonded areas could be observed in optical or acoustical measurements. In the worst case, the wafers did not bond at all. To keep the surfaces in bondable condition, careful process planning and frequent cleaning procedures were required throughout the process. Metal residues had to be removed from bonding surfaces with great care.

Also, trapped gas bubbles between the bonded wafers can cause large non-bonded areas, as was experienced in the early stage of process development. Those were eventually removed by etching gas outlet grooves in the substrate wafer. The component yield from the successfully bonded areas was very good.

Hillocks on Al electrodes were observed to form even at 200 ºC. Hillock formation could be reduced by sputtering a thin layer of Mo on top of the Al.

3.2 Component for the DC voltage reference

The design of the DC voltage reference component was based on the following choices and design rules:

- SOI, device layer thickness 20 µm
- Gap height 1 µm
- Released area < 800 × 800 µm
- Pull-in voltage 10 V
- Capacitance > 1 pF
- Electrode material Al, Mo or MoSiN
- Double electrodes for four terminal point measurement.

3.2.1 Geometry

The seesaw component is shown in Fig. 26 and its dimensions are listed in Table 3. The seesaw was fabricated with two different spring width w_s values: 26 µm and 34 µm. The electrode length z is measured from the edge of the seesaw.

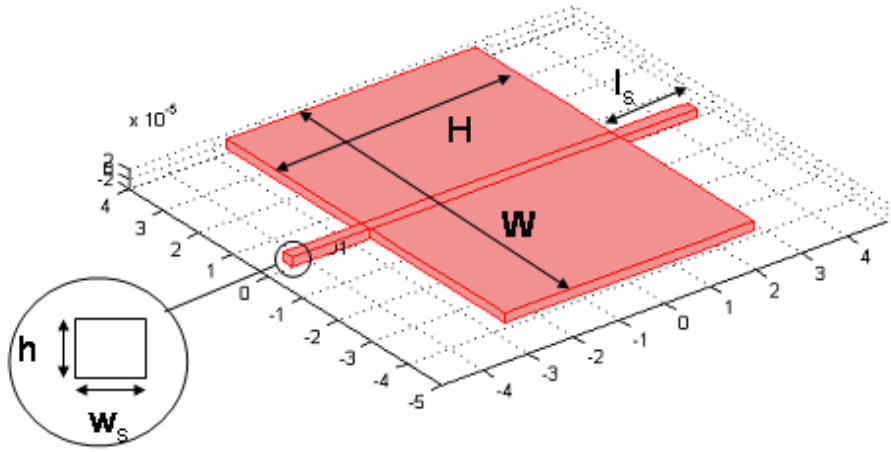

Figure 26. Seesaw design for the DC voltage reference use.

Table 3. Dimensions, materials constants, and calculated parameters for the DC voltage reference.

Dimensions and constants	**Symbol**	**Value**	**Calculated parameters**	**Symbol**	**Value**
Plate thickness	$h = 2a$	20 μm	**Capacitance (x = 0)**	C_0	1.22 pF
Spring length	l_s	180 μm	**Pull-in voltage**	V_{pi}	9.7 (19.4) V
Spring width	$w_s = 2b$	26 (34) μm	**Resonance frequency**	f_{res}	27 (54) kHz
Plate length	W	800 μm	**Mass**	m	0.02 μg
Plate width	H	550 μm	**Spring constant**	k	1.8 (13) kN/m
Electrode length	z	250 μm	**Momentum of inertia**	I	1.12×10^{-15} kgm^2
Gap	d	1 μm	**Center of the electrode**	C	275 μm
Vacuum permittivity	ε_0	8.85×10^{-12} J/K	**Electrode surface area**	$A_{el} = H\times z$	0.14 mm^2
Si density	ρ	2330 kg/m^3	**Plate surface area**	$A = H\times W$	0.44 mm^2

3.2.2 Eigencurve

The calculated eigencurve of the seesaw component is shown in Fig. 27. The pull-in point corresponds to the maximum of the curve, $V_{pi} \approx 9.7$ V for the 26 μm thick spring and $V_{pi} \approx 19.4$ V for the 34 μm thick spring.

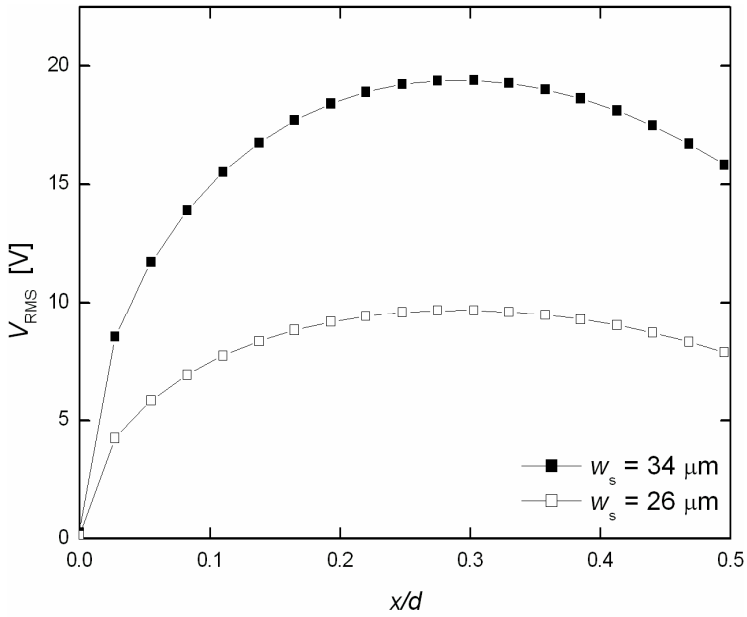

Figure 27. Eigencurve of the seesaw component as a function of deflection x divided by gap d.

3.2.3 FEM simulations

Ansys 7.0 was used to simulate the moving plate deflection due to the electrostatic force by an external voltage source and to calculate the resonance frequencies for the eigenmodes of the moving plate modals. Since Ansys is not a multiphysical program, the voltage (or electrostatic force) could not be applied into the model as such. It was assumed that the voltage causes a uniform pressure P on the electrode according to equation $P = F_e / A$, where F_e is calculated from Eq. (2). The simulation parameters used are listed in Table 4, and the boundary conditions are displayed in Fig. 28. The analytical deflection values and simulated values are compared in Fig. 29. The results agree quite well. The simulated deflection values are larger than analytically calculated because the simulation takes into account the silicon deformation at the spring anchoring areas.

Table 4. Ansys model parameters.

Materials parameters	**Value**	**Calculation parameters**	
Young modulus	130 GPa	Element type	SOLID92
Poisson ratio	0.27	Number of elements	2691
Shear modulus	66 GPa		

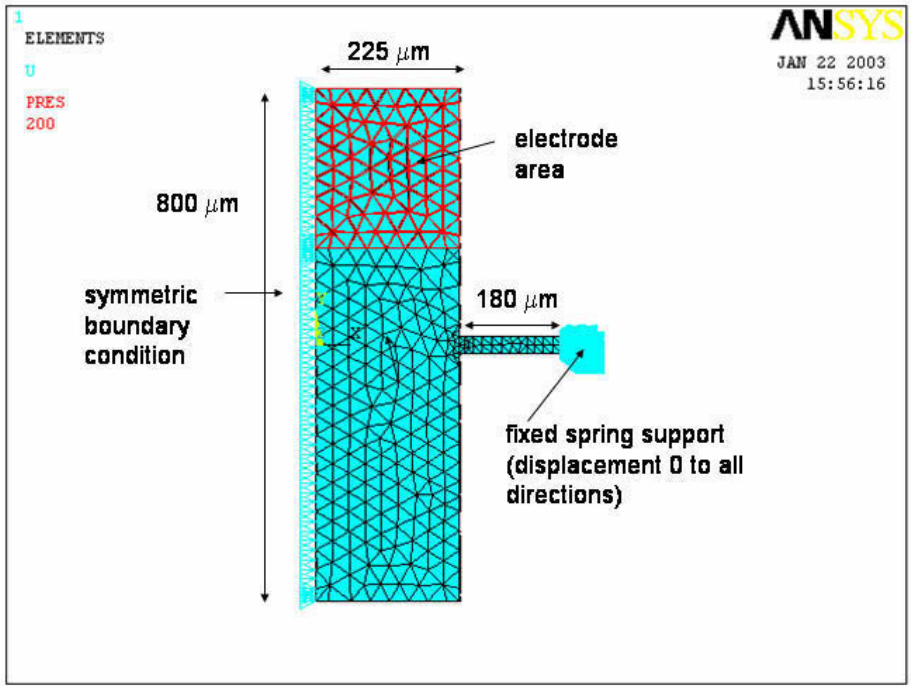

Figure 28. The boundary conditions used in the simulations.

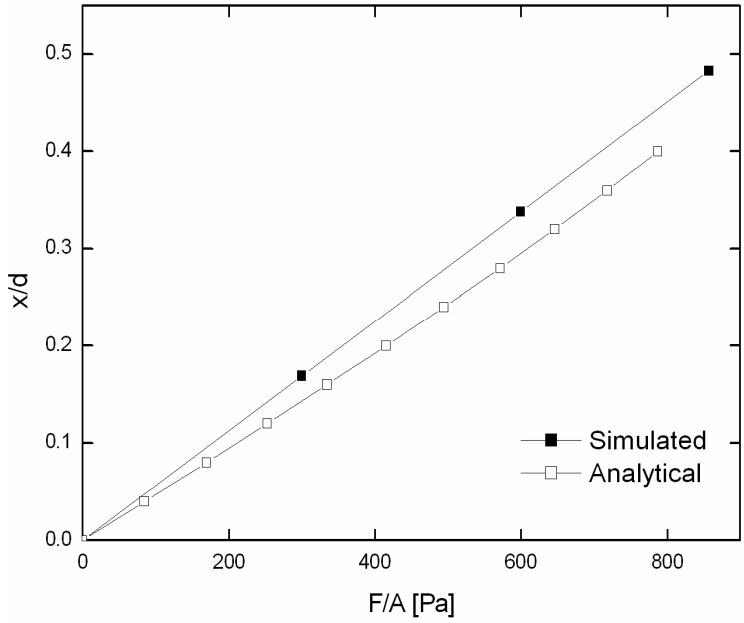

Figure 29. Analytically calculated deflection values for the seesaw as a function of the applied voltage compared against simulation results (spring width 26 μm).

3.2.4 Resonance frequency

The lowest mechanical resonance frequency of the seesaw component can be calculated from [24]

$$f_{\mathrm{m}} = \frac{1}{2\pi}\sqrt{\frac{k}{I}} \tag{52}$$

where the moment of inertia I is

$$I = m\left[\frac{W^2 + h^2}{12}\right]. \tag{53}$$

The theoretical value for the resonance frequency is 27.1 kHz and the simulated value is 23.6 kHz. The first four modals and their characteristic frequencies are shown in Fig. 30.

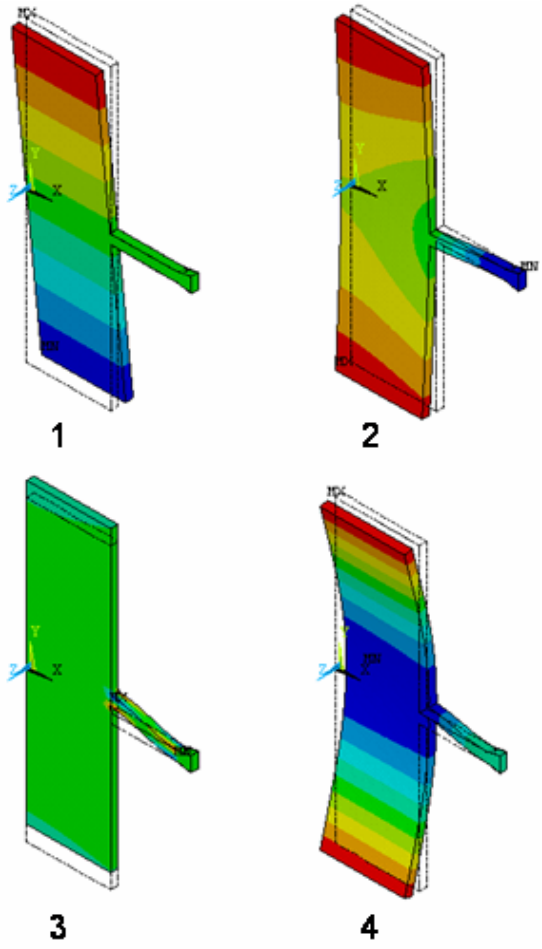

Figure 30. The first four modals of the seesaw component. The corresponding characteristic frequencies are 23.6 kHz, 71.9 kHz, 137.6 kHz, and 276.6 kHz.

3.2.5 Electrodes

The upper electrode of the seesaw component is a simple rectangle whereas the substrate wafer electrodes are divided as shown in Fig. 31. The two sections in the middle are the sense electrodes for displacement control (3 and 4). The top electrodes (1 and 2) are used for actuating the seesaw to the pull-in position while the other electrodes (5 and 6) are grounded. The effective built-in voltage (V_{bie}), *i.e.* the contact potential difference of the silicon-metal junction V_{bi}

together with the voltage V_c due to charges on the native oxide layers, can be compensated by splitting the actuation electrode into two equal sections and applying slightly different voltages with opposite polarity on the electrodes. If a positive voltage V_p is applied to electrode 1 and a negative voltage V_n is applied to electrode 2, so that $V_p = V_0 + V_{bie}$ and $V_n = -V_0 + V_{bie}$, with V_0 being the average of positive and negative pull-in voltage values, the electrostatic force F_e, $F_e \propto V_p^2 + V_n^2 \approx 2V_0^2$, is independent of V_{bie} in the first order.

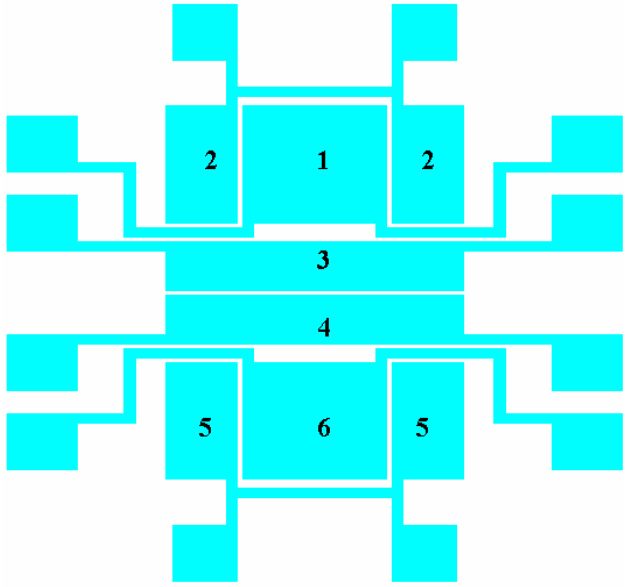

Figure 31. Divided substrate wafer electrodes enable effective built-in voltage compensation.

3.2.6 Component characteristics

The average nominal capacitance (electrodes 1 and 2 together, see Fig. 31) of the components was measured to be about 1.4 pF and the pull-in voltages varied between 6…14 V. The average built-in voltage was about -0.7 V (low potential contacted to the moving electrode). The *C-V* curve of a seesaw component is shown in Fig. 32.

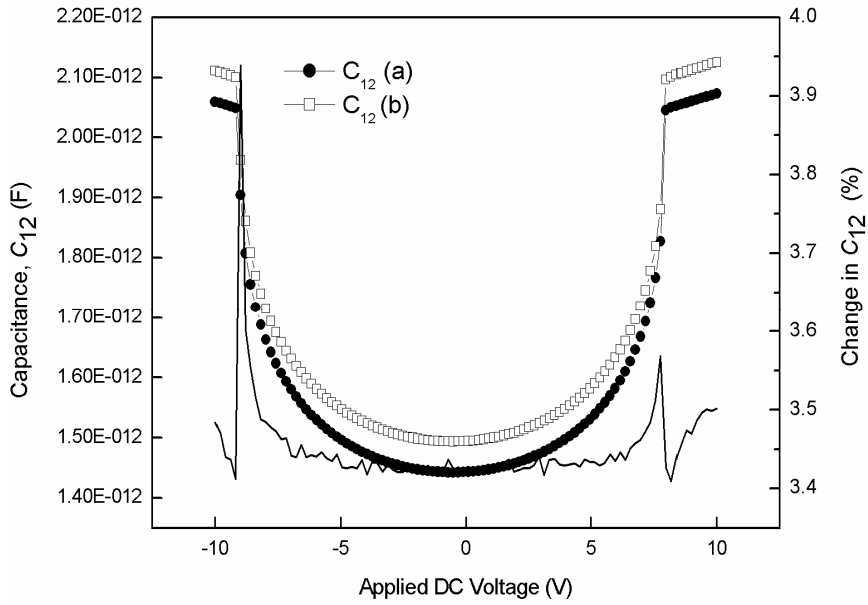

Figure 32. The characteristic C-V curves (a and b) of a component showing the measured pull-in voltage and the effective built-in voltage (the shift of the minima from 0 V).Curve b was measured after curve a and the difference of the curves is also shown (on the right hand side).

3.3 Component for the AC voltage reference

The component for the AC voltage reference was manufactured at the same time (on the same wafer) as the DC reference component. Hence the same design rules applied. The AC voltage component did not need the counter-electrode for the feedback, hence it is advantageous to utilise the whole released area for the work capacitance and hence the translational mode of operation was selected.

3.3.1 Geometry

The round component for the AC voltage reference is shown in Fig. 33 and the corresponding dimensions are displayed in Table 5. There were two variations of the sensor regarding the spring width w_s: 20 μm and 30 μm. All the calculations are done accordingly.

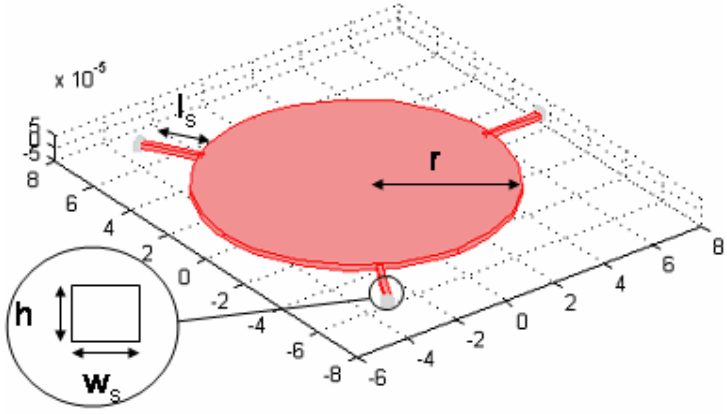

Figure 33. Round component for the AC voltage reference.

Table 5. Component dimensions, materials constants and analytically calculated characteristics.

Values	**Symbol**	**Value**	**Calculated values**	**Symbol**	**Value**
Plate thickness	h	20 µm	**Capacitance**	C_0	4.45 pF
Radius	r	400 µm	**Pull-in voltage**	V_{pi}	15.4 (18.8) V
Spring length	l_s	260 µm	**Spring constant**	k	3.5 (5.3) kN/m
Spring width	w_s	20 (30) µm	**Mass**	m	0.024 µg
Gap	d	1 µm	**Surface area**	A	0.5 mm^2
Si density	ρ	2330 kg/m^3	**Resonance frequency**	f_m	61 (74) kHz
Young's modulus	E	131 GPa	**Deflection due to gravity**	x	0.7 Å

3.3.2 Eigencurve

The calculated eigencurve for the round component is shown in Fig. 34. The voltage V_{RMS} as a function of deflection x is displayed for the two different spring width values w_s = 20 μm and w_s = 30 μm.

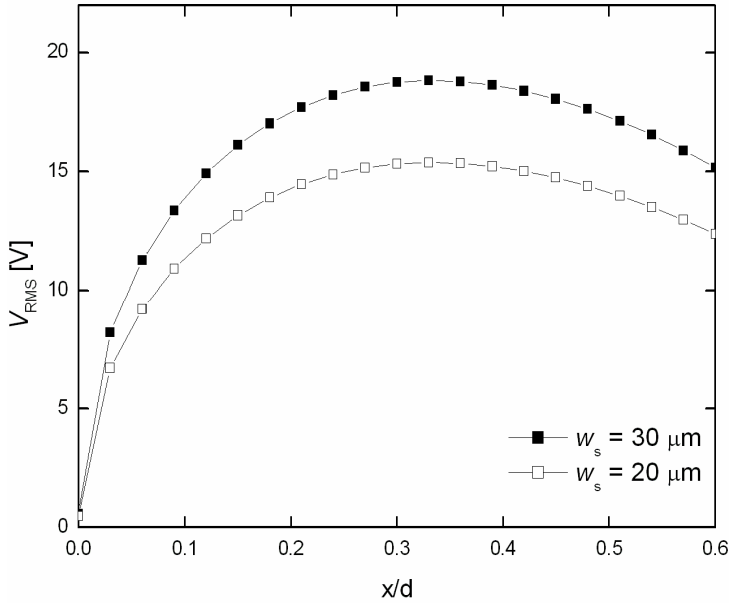

Figure 34. Eigencurve of the round component.

3.3.3 FEM simulations

Ansys 7.0 was used to simulate the component deflection by an external voltage and find out the moving plate modals and their characteristic frequencies. The simulation model used is shown in Fig. 35 and the simulation parameters are listed in Table 6. The simulated deflection values and analytically calculated values are compared in Fig. 36. The simulated deflection values for a component, the spring width of which is 30 μm, approximately equals the values analytically calculated for a component, which has 20 μm wide springs. The simulation gives larger deflection values because it takes into account the silicon deformation at the spring anchoring points. Also the analytical equation used for

the deflection calculations is known to be too stiff, *i.e.* it gives too small deflection values.

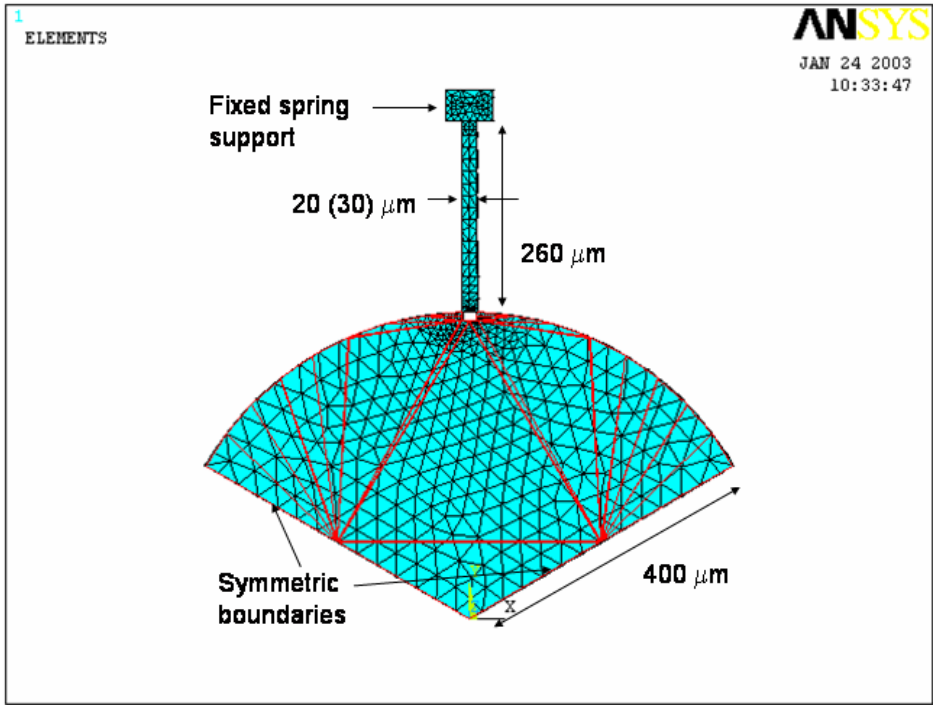

Figure 35. FEM model for the round component.

Table 6. Ansys model parameters.

Material parameters	**Value**	**Calculation parameters**	**Value**
Young modulus	130 GPa	**Element type**	SOLID187
Poisson ratio	0.27	**Number of elements**	2576
Shear modulus	66 GPa	**Number of nodes**	5157

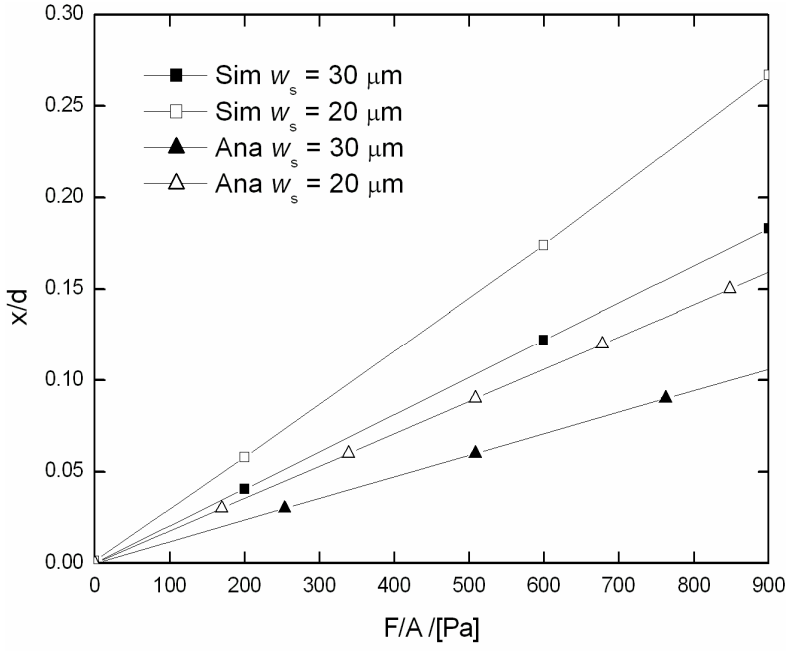

Figure 36. Analytical plate deflection compared to simulated values for two components, the spring widths of which are w_s = 20 μm and w_s = 30 μm.

The first four characteristic modals are displayed in Fig. 37.

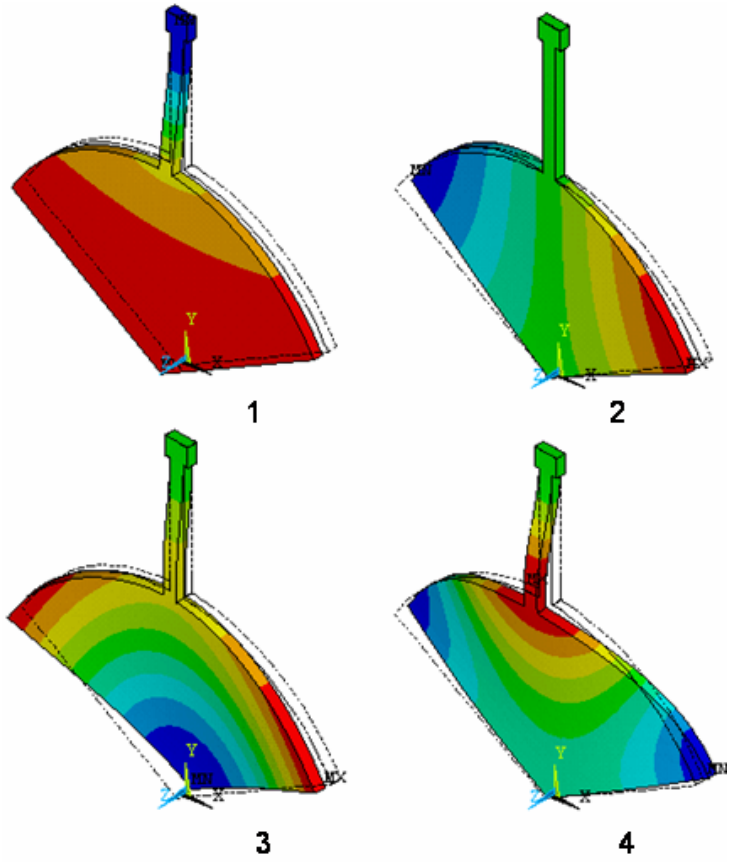

Figure 37. The first four modals of the round component. The corresponding characteristic frequencies are 53.5 kHz, 145 kHz, 442 kHz, and 606 kHz.

Also the deflection due to gravity was simulated with Ansys. It was 1.35 Å for w_s = 20 µm and 0.9 Å for w_s = 30 µm, which are slightly higher than the analytically calculated values 0.67 Å and 0.45 Å.

3.3.4 Electrodes

The substrate wafer electrode for the round component is displayed in Fig. 38. There is one central electrode and a 10 µm thick guard electrode around it. The guard electrode suppresses the stray field between the capacitor plates. Double electrodes are designed for four terminal point measurement connections. The two outermost connectors are connected to the guard and the two innermost to the electrode.

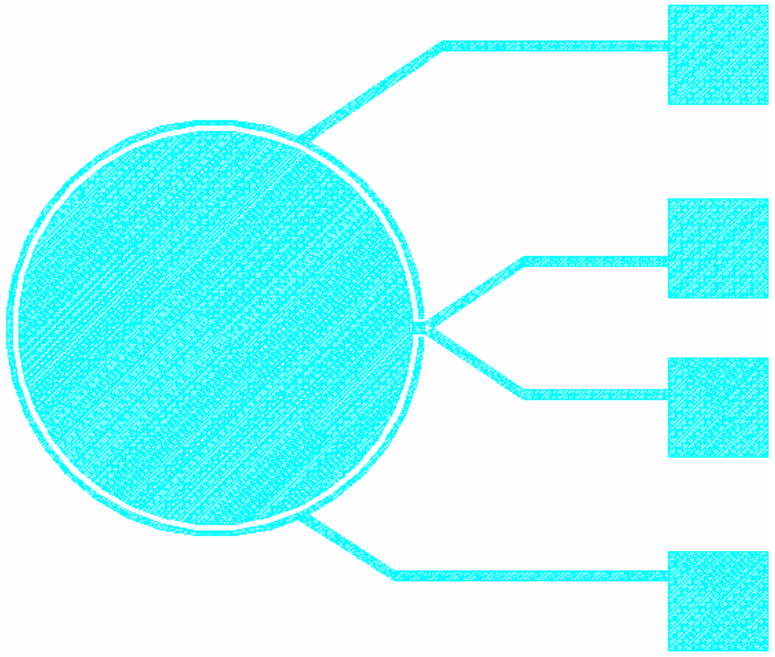

Figure 38. The substrate wafer electrode for the round component.

3.3.5 Component characteristics

The average of the nominal capacitance was measured to be about 5.2 pF and the pull-in voltages varied between 7…16 V for the round components. The built-in voltage was about -0.7 V.

3.4 Stability of the component

The component stability comprises of electrical stability, mechanical stability and stability against changes in environmental conditions. The same considerations apply both to the DC voltage reference component and to the AC voltage reference component and are hence discussed together.

3.4.1 Electrical stability

When a MEMS component is actuated with a DC voltage, the electrostatic charging will cause the reference voltage drift. This can be avoided by using AC current instead of DC voltage as is experimentally demonstrated in [I]. However, even in the absence of an external DC voltage source there is a DC voltage over the component due to the contact potential difference of the silicon-metal junction and charging of the dielectric layer as discussed in Section 2.5. In the case of DC voltage actuation, it is impossible to distinguish the different DC components from each other. The additional DC components due to the built-in voltage and charging will simply reduce the reference voltage value. However, if the component is actuated with a AC current $I(t) = \hat{I} \sin \omega t$ V_{AC}, and there is also a DC component present, V_{DC}, the force balance equation is

$$\frac{\hat{I}^2}{2\varepsilon A \omega^2} \cos^2(\omega t) + \frac{1}{2} V_{DC}^2 \frac{\varepsilon A}{(d-x)^2} = kx \,. \tag{54}$$

V_{DC} is a sum of all DC terms effecting on the component

$$V_{DC} = V_{bi} + V_C + V_{bias}\,, \tag{55}$$

where V_{bi} is the built-in voltage, V_C is the voltage due to charges on the dielectric layers, and V_{bias} is the externally applied DC bias voltage. Also, surface effects can contribute to the DC voltage term. For example, a thin layer of process residual on the top of the electrode surface can change the surface potential of the metal.

Assuming that the angular frequency of the oscillation, ω, is much higher than the component mechanical resonance frequency, the RMS voltage V_{AC} across the plate is (see Eq. (23))

$$V_{AC} = \frac{\hat{I}(d-x)}{\sqrt{2}\omega\varepsilon A} = \sqrt{\frac{2k}{\varepsilon A}(d-x)^2 x - V_{DC}^2}\,. \tag{56}$$

The maximum of V_{AC}, *i.e.* the reference voltage, can be calculated from $dV_{AC}(\hat{I})/d\hat{I} = (dV_{AC}(x)/dx)(\, dx/d\hat{I}\,) = 0$ Since $dx/d\hat{I} \neq 0$, the maximum is reached

when $dV_{AC}(x)/dx = 0$, which occurs at $\hat{I} = (3/\sqrt{2})\omega\varepsilon A V_{pi}/d$ (or $x = d/3$). The maximum of V_{AC} is

$$V_{AC}^{max} = \sqrt{V_{pi}^2 - V_{DC}^2}\ . \tag{57}$$

Since $V_{DC} << V_{AC}$ small time variations ΔV_{DC} of the V_{DC} can described as $V_{DC} = V_{DC,0} + \Delta V_{DC}$, where $V_{DC,0}$ is a constant, and Eq. (57) can now be expressed as

$$V_{AC}^{max} = V_{pi} - \frac{V_{DC,0}^2}{2V_{pi}} - \frac{V_{DC,0}}{V_{pi}}\Delta V_{DC} \tag{58}$$

Equation (58) demonstrates that selecting $V_{DC,0} = 0$, small changes in the DC voltage, ΔV_{DC}, have no effect on the reference voltage in the first order.

3.4.2 Packaging

Two different packages were experimented with: a TO-8 can and a LTCC package as shown in Fig. 39. TO-8 can was selected because it was easily available and the equipment for hermetic enclosing in a nitrogen atmosphere existed. The LTCC package was expected to induce less mechanical stress to the MEMS component due to temperature changes since the linear coefficient of temperature expansion is about 6 ppm/ºC, *i.e.* close to that of silicon (3 ppm/ºC). However, the hermetic enclosing of the LTCC packages failed, hence a comparison between the LTCC and the TO-8 could not be made. Also, that was concluded to be the major reason why the stability of the component did not reach the level of the VTI hermetically packaged component. The stability of the AC voltage reference was measured to be ± 60 ppm in 14 hours [II] using the round component while the stability was measured to be ± 1 ppm in 22 days [V] using the VTI component. The readout electronics and the measurement setup were improved for the latter measurement complicating the direct comparison of these results.

The component was attached in the package using a small drop of soft adhesive in one corner. Also conductive silver epoxy was tested in order to ground the substrate wafer. Al bond wires were used for electric contacts.

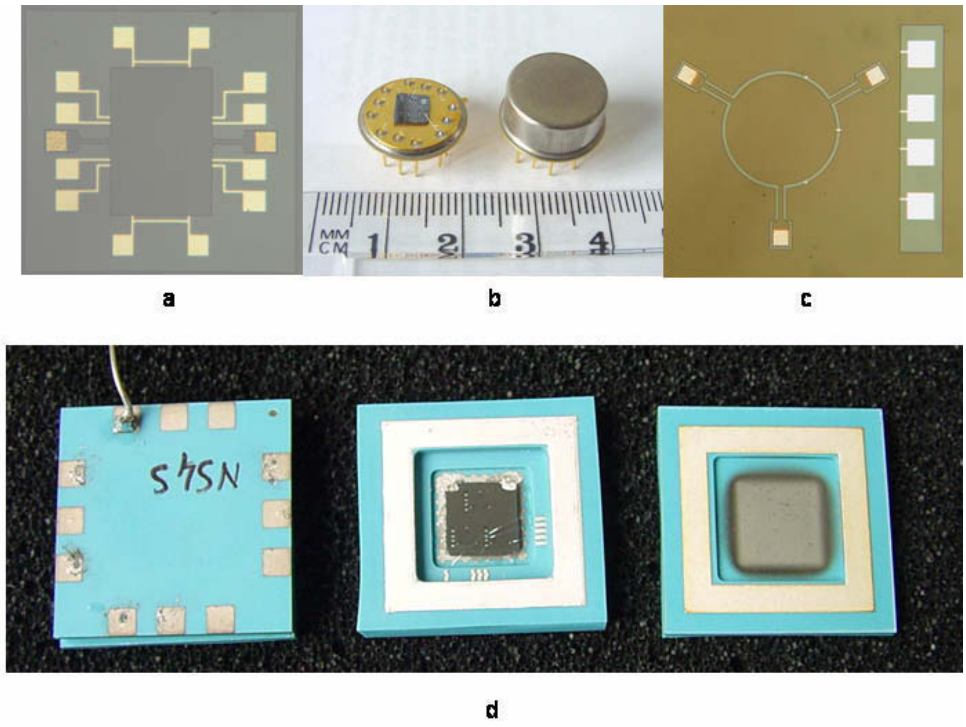

Figure 39. a) Photograph of a seesaw component, b) component mounted in a TO-8 can and hermetically enclosed TO-8 can, c) photograph of a round component, and d) LTCC package for the seesaw component.

3.4.3 Stability against changes in the environmental conditions

Calibration standards, like voltage references, are usually operated in a room environment. Still, the device is subject to modest changes in temperature, pressure, and humidity. Changes in ambient pressure can deform the package or the component structure. The mechanical stability was already discussed in Section 2.5.5. Temperature coefficient, effect of humidity and the ambient gravity for the component manufactured are discussed below.

3.4.3.1 Temperature

The temperature coefficient for a component manufactured using EMMA process, shown in Fig. 25, can be derived from the pull-in voltage equation calculated in Section 2.1.1 (Eq. 7)

$$V_{\mathrm{pi}} = \sqrt{\frac{8}{27}} d_0 \sqrt{\frac{k}{C_0}}, \tag{59}$$

where d_0 is the initial height of the gap, C_0 the initial capacitance and k the spring constant. The gap in the EMMA process is determined by the depth of the cavity in the substrate wafer. The temperature dependences of the parameters above are

$$d_0(T) = d_0(1+\alpha T), \tag{60}$$

$$k(T) = 3E(1+\beta T) w_{\mathrm{s}} (1+\alpha T) \left(\frac{h}{l_{\mathrm{s}}}\right)^3 \approx k\left[1+(\alpha+\beta)T\right] \tag{61}$$

and

$$C_0(T) = \varepsilon \frac{A(1+\alpha T)^2}{d_0(1+\alpha T)} \approx C_0\left(1+2\alpha T\right), \tag{62}$$

where h and A are the thickness and area of the moving plate, w_{s} and l_{s} are the thickness and the length of the spring, and E is Young's modulus. The linear coefficient of thermal expansion for Si and the temperature coefficient of Young's modulus are α (= 2.6×10^{-6}/ºC) and β (= -65×10^{-6}/ºC) respectively. The temperature dependence of the pull-in voltage can now be calculated by differentiating Eq. (59). If he second order terms with respect to the temperature T are neglected the result is

$$\frac{\partial V_{\mathrm{pi}}}{\partial T} = V_{\mathrm{pi}}\left(\frac{1}{d_0}\frac{\partial d_0}{T} + \frac{1}{2k}\frac{\partial k}{T} - \frac{1}{2C_0}\frac{\partial C_0}{T}\right) \approx V_{\mathrm{pi}}\left(\frac{1}{2}(\alpha+\beta) - \frac{1}{2}\alpha\right) \quad (63)$$
$$= V_{\mathrm{pi}}\frac{\beta}{2}$$

Theoretically the temperature coefficient of the pull-in voltage, about -33 ppm/ºC, is determined by the temperature coefficient of the Young's modulus. However, the measured temperature coefficient of the AC reference voltage was about -140 ppm/ºC for the round component and -240 ppm/ºC for the VTI component [III]. In the case of the round component it was assumed that the major part of the temperature coefficient arises from the component mounting. The VTI component was resting on the top of a TO-8 can and connected to the package only via the bond wires. It is assumed that the higher temperature coefficient of the VTI component is dominated by the component bending due to the different temperature coefficients of silicon and glass.

The theoretical temperature coefficient calculated above is not the ultimate limit since it is possible to design a component, where temperature coefficients arising from different sources cancel each other resulting in a negligible temperature coefficient. For example [53] presents a RF MEMS capacitor utilizing a compensation structure to eliminate the effect of intrinsic and thermal stress.

3.4.3.2 Humidity

Open capacitive structures are very sensitive of changes in humidity so that they are even used as humidity sensors [2]. Especially silicon surface is very hydrophilic unless cleaned with hydrofluoric acid [31]. Hence the components for the voltage reference application need to be packaged hermetically. However, even with hermetic package, there are residuals of process chemicals inside the component enclosure. Their adsorption and desorption on the surfaces of the component electrodes can cause noise or drift [30]. The importance of vacuum encapsulation has been demonstrated using silicon microresonators [43]. The long term stability (*df/f*) of the resonator was improved from about 40 ppm below 1 ppm during 42 days by packaging the component in vacuum. The relative humidity was 20…35 RH % during the measurement period.

3.4.3.3 Gravity

Depending on the moving plate suspension and position, ambient gravity can decrease the gap between electrodes. The effect of gravity on the reference voltage has already been calculated in Section 2.1.1.4 and is presented in Eq. (25). The change in the reference voltage V_{ref} is

$$V_{\mathrm{ref}} = V_{\mathrm{pi}}\left(1 - \frac{F_{\mathrm{m}}}{kd}\right)^{\frac{3}{2}}, \tag{64}$$

where V_{pi} is the pull-in voltage, F_{m} the force due to gravity acting on the moving mass m, $F_{\mathrm{m}} = mg$, and g is the constant of gravity. The change of the reference voltage is -216 ppm for a typical component positioned and suspended as shown in Fig. 3. Component parameters given in the Table 5 were used in the calculation.

4. Readout electronics

The readout electronics is important to the overall device performance. A good review is given in [23]. If not carefully designed, it can limit the performance and the range of applicability of the MEMS component. A capacitive readout has a high resolution and low power consumption, which makes it suitable for this purpose. Usually the displacements to be detected are in the order of nanometers. The corresponding capacitance changes are typically in the order of femtofarads which can be resolved with a 4.0 $aF/\sqrt{Hz}$ resolution even with a commercial capacitive readout circuit [54]. However, when ultimate stability and sensitivity is required, custom made electronics is necessary. Two dedicated electronics, one for the DC voltage references and one for the AC voltage references, were designed and manufactured.

4.1 DC voltage reference

A block diagram of the DC voltage reference electronics utilizing feedback is displayed in Fig. 40. It is designed for the seesaw component shown in Fig. 26. A DC voltage is connected to the electrodes on one edge (C_1 and C_2) to actuate the component, while the electrodes on the other edge (C_5 and C_6) are grounded. The DC voltage on electrodes C_1 and C_2 is adjusted by the feedback loop to keep the component at the pull-in point and this voltage is the reference voltage. The plate displacement is detected by a capacitive bridge formed by the electrodes in the middle (C_3 and C_4).

The plate displacement could be detected using one capacitor only, but it is advantageous to use two capacitors since the electrostatic force acting on the plate, due to the position detection voltage V_{ext}, can be minimized. By selecting equal values for the resistors $R_1 = R_2$ results to voltage values

$$V_1 = \frac{1 - x/d}{1 + x/d} V_{ext} \text{ and } V_2 = -V_{ext} \tag{65}$$

on capacitors C_3 and C_4 respectively. Here x is the plate deflection at the position detection point as shown in Fig. 40. The electrostatic forces, F_1 and F_2, caused by the position detection voltage V_{ext} on electrodes C_3 and C_4 are

$$F_1 = \frac{C_m V_1^2}{d(1-x/d)^2} \text{ and } F_2 = \frac{C_m V_2^2}{d(1+x/d)^2}, \tag{66}$$

assuming that C_3 and C_4 are equal in size and their nominal capacitance is C_m. At the pull-in point $x_{pi} = d/3$ the forces balance each other, *i.e.* $F_1 = F_2$.

Also, if the voltage V_{ext} varies with time, the amplitude ratio V_1/V_2 remains unchanged, which improves the displacement detection accuracy. Hence the plate displacement is determined only by the voltages over C_1 and C_2.

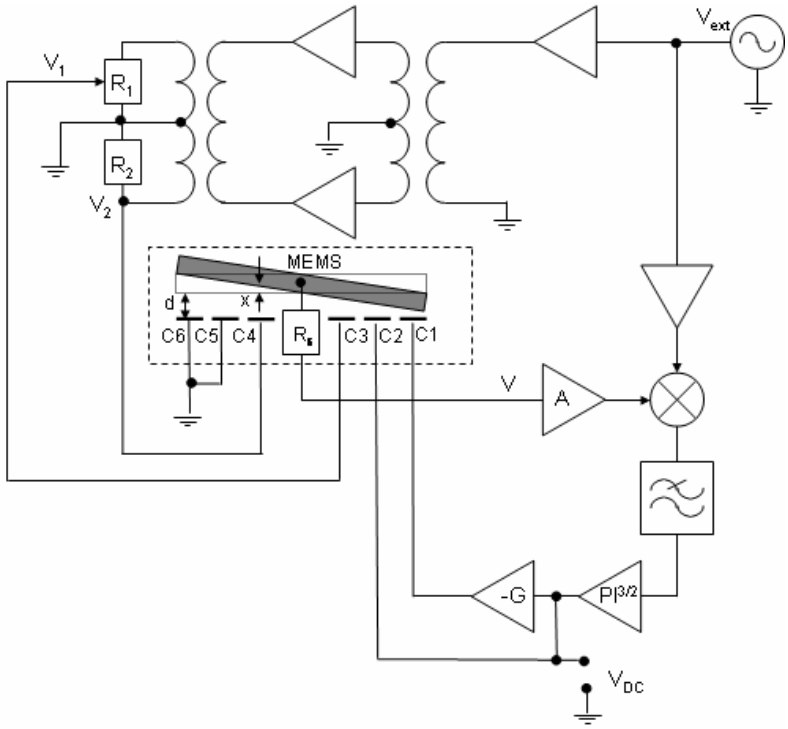

Figure 40. An electronics block diagram of a DC voltage reference based on feedback control.

In order to compensate the built-in voltage and minimize the component drift, the component is actuated to the pull-in point using slightly different voltages of opposite polarity on the electrodes C_1 and C_2, as discussed in Section 3.2.5. The actuation voltage difference is controlled by gain G.

The voltage V at the moving plate is zero at the pull-in point $x = x_{pi}$. If the plate deflects from the pull-in point, there will be a voltage and hence a current through the silicon spring, the resistivity of which is R_s. The current will be amplified by A and the output voltage of A is combined with the reference voltage from the bridge oscillator V_{ext} by a mixer. The output of the mixer is a DC voltage with superimposed harmonic components of the input voltages. The harmonics are filtered out using a low pass filter leaving only a DC signal. This is fed to the $PI^{3/2}$ controller [55], which restores the pull-in displacement by adjusting the voltage V_{DC}, which is the DC reference voltage. A photograph of the electronics is shown in Fig. 41.

Figure 41. Photograph of the DC voltage reference.

The circuit model for the electronics is shown in Fig. 42, which takes also into account the parasitic capacitances C_{p3} and C_{p4}, mainly arising from the spring attachment points (see Section 2.3.3). In that case the voltage ratio V_1/V_2 should be adjusted from ½ in order to remain the voltage V zero at the moving plate. If the AC readout voltages are $V_1 = rV_{ext}e^{j\omega}$ and $V_2 = -V_{ext}e^{j\omega}$, the voltage division ratio r should now be

$$r = \frac{\frac{3}{4}C_m + C_p}{\frac{3}{2}C_m + C_p}, \tag{67}$$

assuming that the parasitic capacitances are equal, $C_{p3} = C_{p4} = C_p$. In that case the force balance $F_1 = F_2$ is not exactly true anymore unless C_p is negligible. For example if $C_p = C_m/2$, $F_1 / F_2 = 1.5$. Hence the detection voltage V_e will cause an error in the pull-in voltage V_{pi}. The error can be minimized by using as small a detection voltage as is feasible and minimizing the component parasitic capacitance.

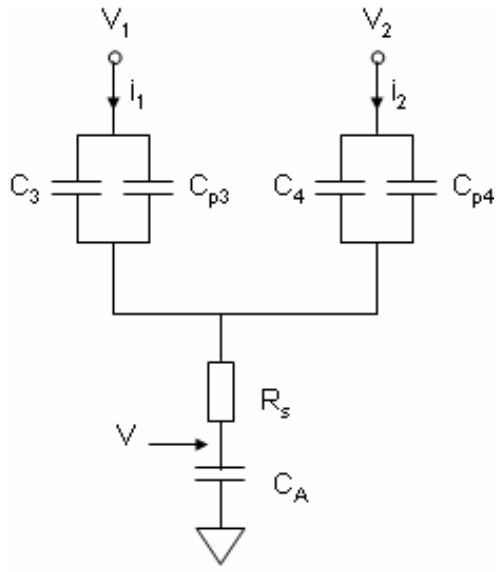

Figure 42. Circuit model for the readout electronics.

The voltage V at the moving plate can easily be derived:

$$V = \frac{(C_3 + C_{p3})V_1 + (C_4 + C_{p4})V_2}{(C_3 + C_{p3} + C_4 + C_{p4})(1 + j\omega R_s C_A) + C_A}, \tag{68}$$

where C_A is the amplifier input capacitance. Near the pull-in point, $x=d/3+\delta x$, the capacitances C_3 and C_4 are

$$C_3 = \frac{3}{2}C_m\left(1 + \frac{3}{2}\frac{\delta x}{d}\right) \quad \text{and} \quad C_4 = \frac{3}{4}C_m\left(1 - \frac{3}{4}\frac{\delta x}{d}\right). \tag{69}$$

Inserting Eq. (69) into Eq. (68) results in

$$\frac{\mathrm{Re}(V)}{\delta x} = \frac{9}{16}\frac{V_{\mathrm{ext}}}{d}\frac{\left(\frac{C_{\mathrm{A}}}{C_{\mathrm{m}}}+2\frac{C_{\mathrm{p}}}{C_{\mathrm{m}}}+\frac{9}{4}\right)\left(\frac{9+10C_{\mathrm{p}}/C_{\mathrm{m}}}{3+2C_{\mathrm{p}}/C_{\mathrm{m}}}\right)}{\left(\frac{C_{\mathrm{A}}}{C_{\mathrm{m}}}+2\frac{C_{\mathrm{p}}}{C_{\mathrm{m}}}+\frac{9}{4}\right)^2+\left(R_{\mathrm{s}}\omega C_{\mathrm{A}}\left(\frac{9}{4}+2\frac{C_{\mathrm{p}}}{C_{\mathrm{m}}}\right)\right)^2}. \tag{70}$$

This is the position detection transfer function *G4* (Eq. (18), if C_{p} is set to zero) discussed in Section 2.1.1.3.

The parasitic capacitance and amplifier input capacitance reduce the sensitivity of the readout which is demonstrated in Fig. 43 for different parasitic capacitance C_{p} values and amplifier input capacitance C_{A} values. Typical values for the spring resistance, angular frequency, and amplifier input capacitance are $R_{\mathrm{s}} = 50\ \Omega$, $\omega = 628$ kHz and $C_{\mathrm{A}} = 3$ pF which have been used in the calculation.

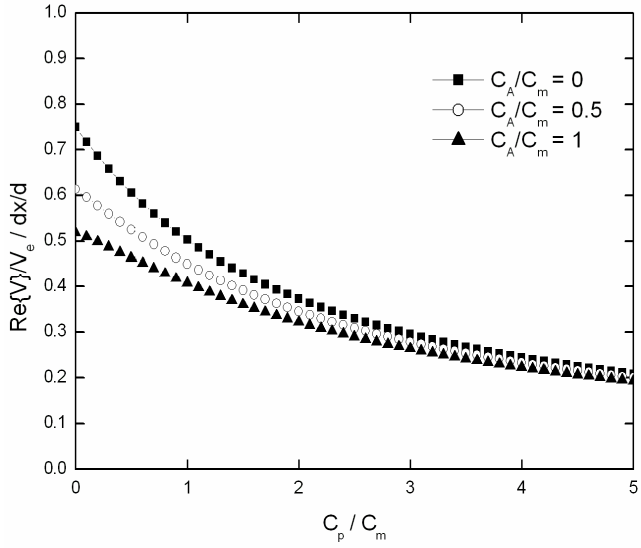

Figure 43. Relative sensitivity of the readout $Re(V)/V_e/(\delta x/d)$ as a function of the parasitic capacitance C_p for different amplifier input capacitance C_A values.

4.2 AC reference electronics

The electronics for a current actuated AC voltage reference can be realised using only a few component as show in Fig. 44. An AC voltage, the frequency of which is well above the mechanical resonance frequency, is fed to the inverting input of the main operational amplifier OA2 which acts as a voltage to current converter. The amplitude of the input current is slowly varied over the maximum point and the maximum output voltage is the AC reference voltage (the AC component of V_{out} in Fig. 44). The instrumentation amplifier IA1 isolates the source V_{AC_in}. The stability of the OA2 gain is recorded at the output of the unity gain buffer amplifier OA3. The DC bias voltage for the built-in voltage compensation is fed to the non-inverting input of OA2. A trimmer resistor is needed to find out the right DC compensation voltage, but once found, the trimmer can be replaced with a fixed resistor. Temperature, pressure and humidity are recorded during the measurement and used for the multi-regression analysis to correct the measurement data.

It has been experimentally demonstrated, that small changes in the parasitic capacitance or in the parasitic resistance over the component have no effect on the pull-in voltage [III]. Hence the stability of the electronics depends only on the stability of the MEMS component and the stability of the OA2 gain.

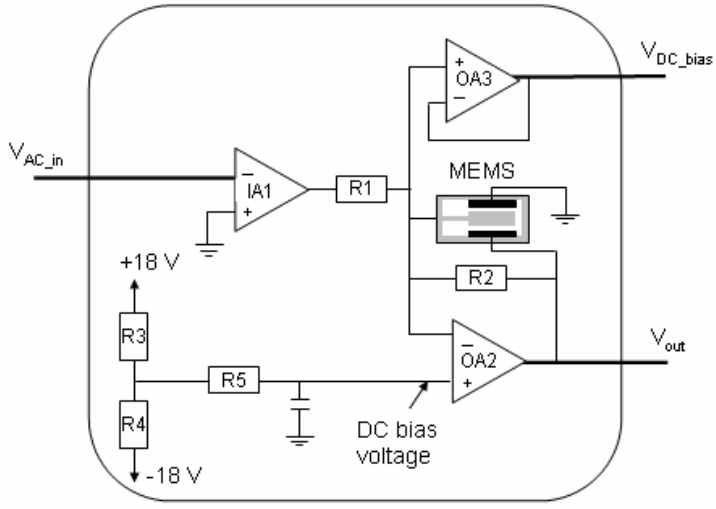

Figure 44. An electronics block diagram for the AC voltage reference.

A photograph of the readout electronics including a VTI component mounted in a TO-8 can is shown in Fig. 45.

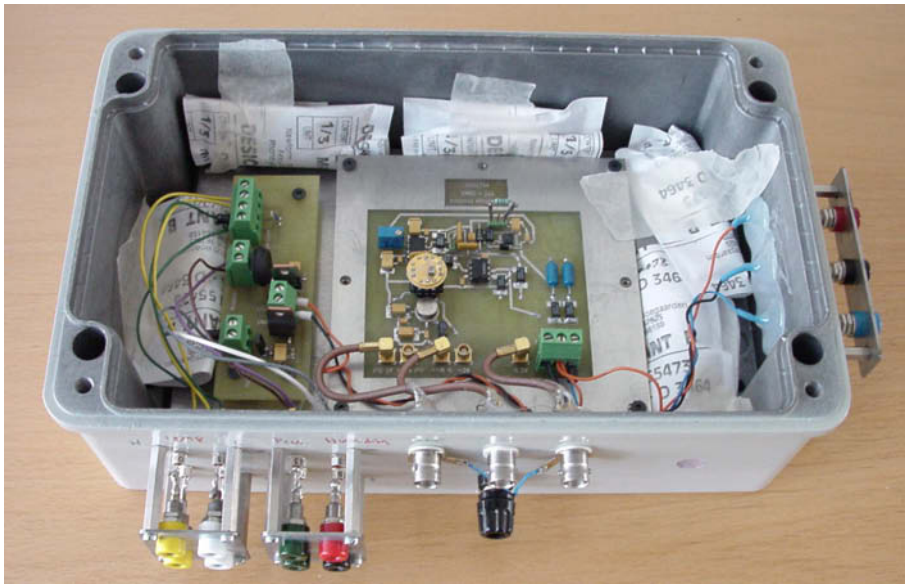

Figure 45. A photograph of the AC voltage reference including the humidity absorbing gel bags on the sides.

5. Measurement results

5.1 Stability of the DC voltage reference

The long-term stability of the DC voltage reference using a seesaw component and feedback electronics described in Section 4.1 was measured in a laboratory environment. Fig. 46 shows the measurement result. After the initial rapid change in the reference voltage the device stabilizes at approximately 60 μV/V over the next 10 hours. The result does not include any ambient temperature corrections to the measured data.

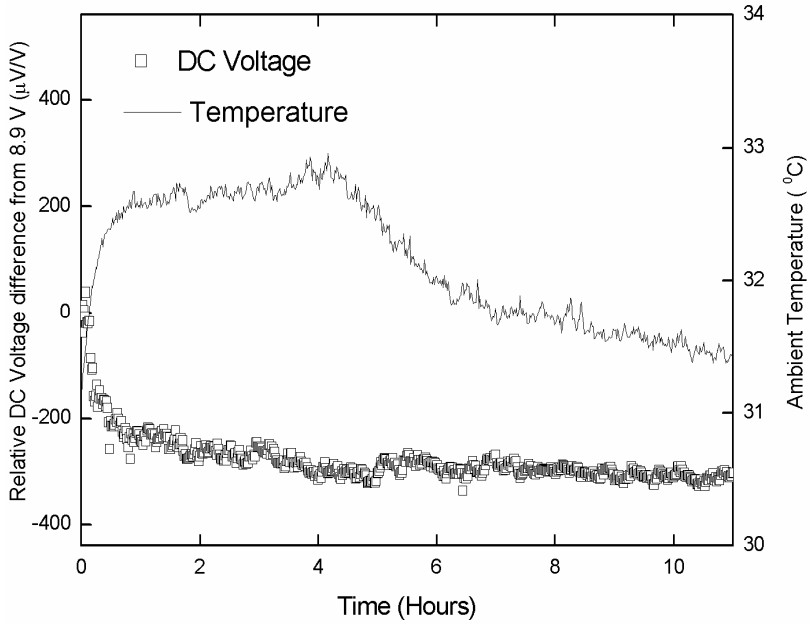

Figure 46. Long-term stability of the DC voltage reference over 11 hours. The solid curve shows the corresponding ambient temperature recorded during the measurements.

The first experimental results of the new device show an order of magnitude improvement with respect to earlier work [18]. However, the long-term stability of the reference is not sufficient for reference application. The device would still require improvements in the feedback electronics and in the component mounting as well as hermetic packaging.

5.2 Drift of the AC reference voltage

The voltage drift of the AC reference was measured when different bias voltages where applied over the MEMS component. The measurement was done in laboratory environment where the temperature varied less than 3 °C around the average value of 34 °C inside the enclosure. The bias voltage was set close to the built-in voltage value by changing the values of resistors R3 and R4 (see Fig. 44), and the AC reference voltage was monitored with an HP 3458A DVM for 4–21 days for each bias voltage setting. Two MEMS components (VTI accelerometers) were experimented: one with a thin native oxide layer (typically in the order of 1–2 nm) and the other with a 50 nm thick SiO_2 layer on top of the non-moving electrode. The non-moving electrodes of the components were coated with AlCu and the moving electrodes had an additional boron doping ($N_A = 4^{19}$ cm^{-3}). The surface areas of the electrodes were almost equal, but the spring constants (30 N/m and 105 N/m) and the gaps (5.7 μm and 2 μm) of the components (native oxide and thick oxide) were different. The measured pull-in voltage values were 9.0 V and 3.9 V respectively. The relative change of the reference voltage V_{AC} is shown in Fig. 47 for the thick oxide component. The slope of the curve is the drift rate, displayed in Fig. 48 for the thick oxide component and in Fig. 49 for the native oxide component.

Within the time span and bias voltage range used in the experiment, the drift is linear for both of the components. For the native oxide component the drift is at its minimum when the bias voltage is set to compensate the built-in voltage as explained in Section 3.4.1 and will be demonstrated in the next Section. For the thick oxide component the minimum drift is achieved at a bias voltage value of 300 mV while the built-in voltage, measured from the component *C*-*V* curve, is 61 mV. This discrepancy might be related to the component mechanical drift or variation of the initial charging state of the component. Although the component was short circuited several days between the measurements, the initial charging state might have varied due to the long (de)charging time constant.

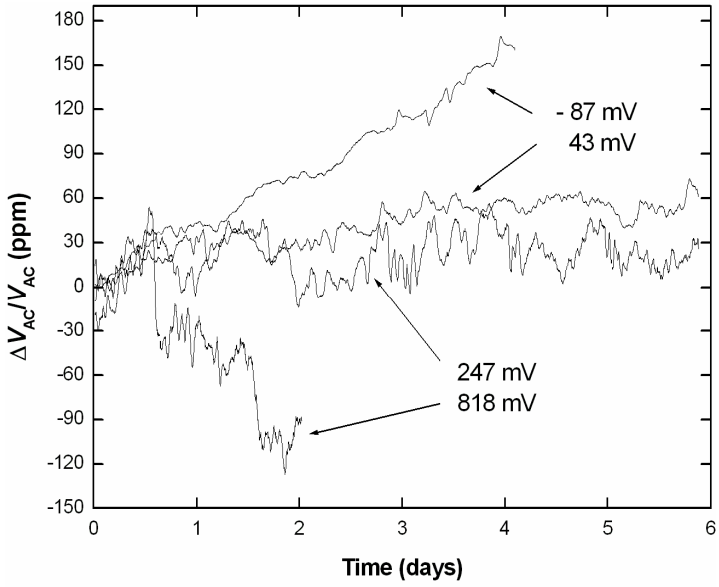

Figure 47. Measured voltage drift of the AC reference. The applied DC bias is shown in the legend.

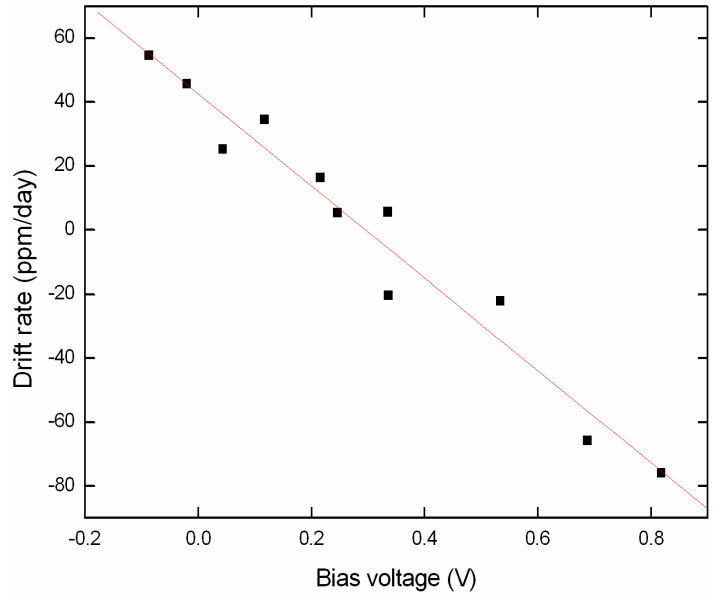

Figure 48. Measured drift rate of the AC voltage reference and a linear fit. The MEMS component was a VTI accelerometer having a 50 nm oxide layer on the non-moving electrode.

The effective built-in voltage of the thick oxide component (61 mV) compares favourably with that of the native oxide component (245 mV). However, the drift rate of the thick oxide component is approximately 20 times larger than that of the native oxide component. The built-in voltage compensation for the thick oxide component turned out to be very difficult due to the large drift rate and long time constant associated with it.

5.3 Built-in voltage compensation

The drift of the AC reference voltage due to component dielectric charging can be avoided by applying an external bias voltage which eliminates the built-in voltage over the MEMS component. The right bias voltage can be determined either from the component *C-V* curve, as the voltage corresponding to the minimum point of the *C-V* curve (with opposite polarity), or scanning the bias voltage of the AC reference. The bias voltage corresponding to the maximum of the reference voltage is the right compensation voltage (see Eq. 57). Figure 49 shows the measured voltage drift for a VTI component as a function of the applied bias voltage. The figure also includes the compensation voltages derived by different ways. The compensation voltage corresponding to the *C-V* curve minimum, $V_{\text{C-V}}$, is -245 mV, the maximum point of the AC reference voltage, $V_{\text{AC\_ref}}$, is -278 mV, and the zero point of the curve fitted to the measured drift rates with different bias voltages, V_{drift}, is -256 mV. The values agree fairly well especially taking into account that the original charging state of the component may have varied between the different measurements. The component was short circuited for several days between the measurement, which is enough to decharge the mobile ionic and the interface trap charges but the deep states in oxide may have time constants much longer than that.

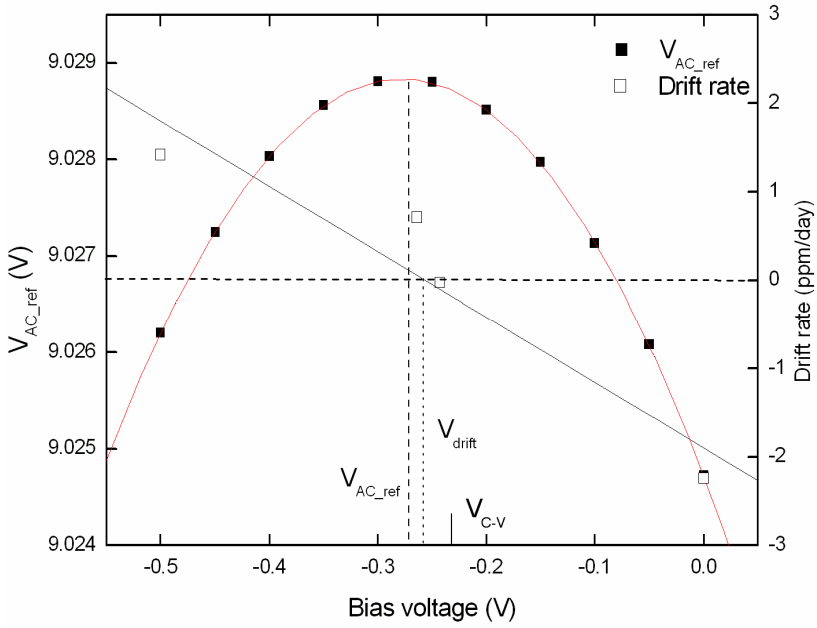

Figure 49. Measured voltage drift of the AC reference as a function of applied DC bias voltage. The C-V curve minimum, $V_{C\text{-}V}$, marked to the figure with the opposite polarity.

5.4 Stability of the AC voltage reference

The experimental setup for the long-term stability measurement of the AC voltage reference is shown in Fig. 50. The measurement was done at the Centre for Metrology and Accreditation MIKES. The AC voltage reference, including a VTI accelerometer as the MEMS component, was mounted on a stone table closed in a temperature stabilized chamber. The temperature varied less than 0.1 °C around the average value of about 23.5 °C during the 3-week measurement. The output voltage was measured using a HP 3458A DVM, the stability of which was periodically (about once in a day) checked against a Datron 4920 AC measurement standard and a Fluke 5700 A calibrator (the upper part of Fig. 50). No drift between these three devices was observed during the three-week measuring period within the scatter of about 2 ppm, which indicates that the repeatability of the DVM during the experiment was of the order of 2 ppm.

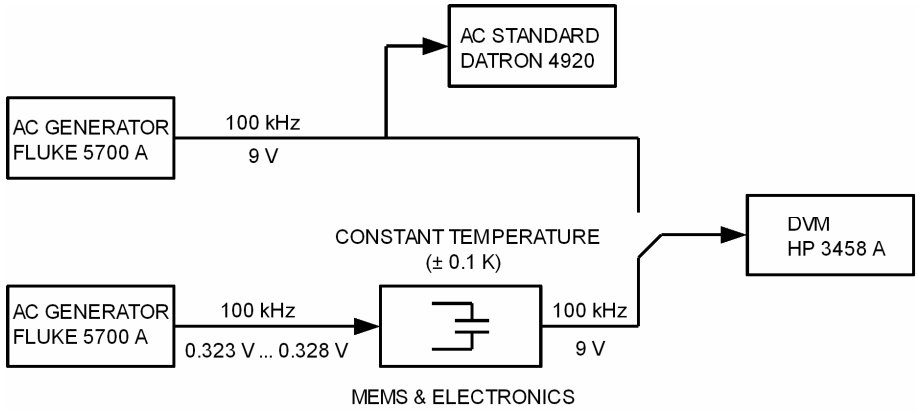

Figure 50. Measurement setup for the long-term stability measurement. The lower part is the actual measurement system, and the upper part was used for calibration of the DVM. (courtesy of MIKES).

The bias voltage was first set to the measured value of the built-in voltage -0.245 V (with opposite polarity) and fine tuned later to -0.243 V (see Fig. 49). The measurement was made by changing the amplitude of the 100 kHz driving current across the maximum point, and by recording the RMS value of the reference output voltage with the DVM for each amplitude value. A second-order polynomial fit was made to the data and the voltage at the maximum was determined. Essentially identical results, with slightly larger scatter, would have been obtained by monitoring the output voltage at a fixed amplitude of the driving current set to the pull-in point. The results are plotted in Fig. 51 after correcting the data for ambient pressure (-6 μV/hPa) and temperature (-180 μV/ºC). No drift could be observed in the 100 kHz output voltage of the device within the measurement accuracy of about 2 ppm. After the stability test was finished, both AC drive and DC bias (built-in voltage compensation) were disconnected but the device was kept in the temperature isolated measurement chamber. After one day the voltages were reconnected and the experiment was started again. After a relaxation period of about 8 hours, the output voltage returned to the original level within the measurement accuracy of about 2 ppm.

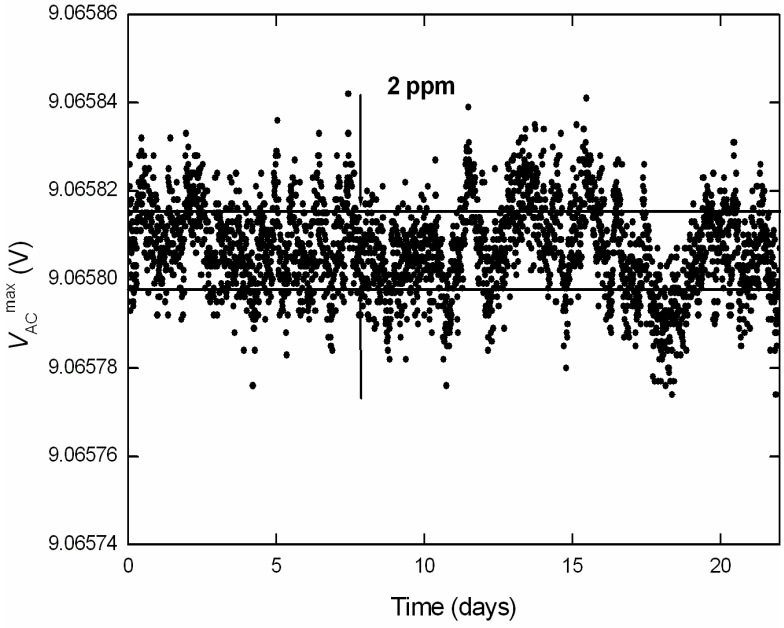

Figure 51. Long-term stability of the AC voltage reference (courtesy of MIKES).

6. Conclusions

This dissertation investigates a DC voltage reference and an AC voltage reference based on the pull-in phenomenon of a micromechanical moving plate capacitor. The main emphasis is on the device stability which is one of the main criteria of the device applicability in metrology. The stability of the AC voltage reference was improved to the ppm-level. This level of performance is sufficient for many applications.

The major achievements of this work are solving the electrostatic stability of the MEMS component by applying AC voltage actuation together with the built-in voltage compensation, and creating a new silicon-on-insulator (SOI) process which enables metallization of the moving electrode. Metal electrodes significantly increase the component stability although with increased complexity of the manufacturing process. The methods for improving the stability of MEMS components can be generally exploited in MEMS applications and the new process has already been applied in manufacturing of a MEMS magnetometer.

This work demonstrates that MEMS based voltage references can be very stable if manufactured from single-crystal silicon and mounted in a hermetic package, which causes no mechanical stress to the component. MEMS references compare favourably to the existing devices by size, price and power consumption. The value of the pull-in voltage depends on the component dimensions and can be set to a wide range of values. MEMS components can be integrated with the readout electronics, as is illustrated in Fig. 52.

MEMS based voltage references can provide a competitive alternative to the conventional voltage reference devices. However, plenty of work still remains to commercialize these devices. The manufacturing process is not suitable for mass production, mechanical design of the component could be improved and a new stress free hermetic packaging developed.

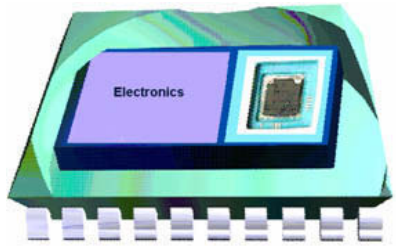

Figure 52. Future vision of the MEMS based voltage reference.

References

[1] Maluf, N. An Introduction to Microelectromechanical Systems Engineering, Artech House, 2000, ISBN 0-89006-581-0.

[2] Gardner, J.W. Microsensors, John Wiley & Sons, 1994, ISBN 0-471-94145-2.

[3] Krueger, S., Müller-Fiedler, R., Finkbeiner, S. and Trah, H.-P. MST News 1/05, pp. 8–10.

[4] Taylor, B.N. (Ed.) The International System of Units (SI). Washington, DC: U.S. General Printing Office, 1991, NBS Special Publ. 330.

[5] Benz, S.P. and Hamilton, C.A. Application of the Josephson Effect to Voltage Metrology, Proceedings of the IEEE, Vol. 92, No. 10, Oct. 2004, pp. 1617–1629.

[6] http://nvl.nist.gov/pub/nistpubs/sp958-lide/html/315-318.html (22.6.2006).

[7] Gray, P. and Meyer, R.G. Analysis and design of analog integrated circuits, John Wiley & Sons, 2nd edition, 1994, ISBN 0-471-59984-0.

[8] Horrowich, P. and Hill, W. The art of electronics, Cambridge University Press, 2nd edition, 1989, ISBN 0-521-37095-7.

[9] http://www.intersil.com/Vref/index.asp (22.6.2006).

[10] Klonz, M., Laiz, H. and Kessler, E. Development of Thin-Film Multijunction Thermal Converters at PTB/IPHT, IEEE Trans. Instrum. Meas., Vol. 50, Dec. 2001, pp. 1490–1498.

[11] Wolffenbuttel, R.F. and van Mullem, C.J. The Relationship Between Microsystem Technology and Metrology, IEEE Trans. Instrum. Meas., Vol. 50, Dec. 2001, pp. 1469–1474.

[12] van Drieënhuizen, B.P. and Wolffenbuttel, R.F. Integrated Micromachined Electrostatic True RMS-to-DC Converter, IEEE Trans. Instrum. Meas., Vol. 44, No. 2, 1995. pp. 370–373.

[13] van Drieënhuizen, B.P. Integrated Electrostatic RMS-to-DC Converter, Ph.D. Thesis, Delft University, 1996.

[14] de Graaf, G., Bartek, M., Xiao, Z., van Mullem, C.J. and Wolffenbuttel, R.F. Bulk Micromachined Electrostatic True RMS-to-DC Converter, IEEE Trans. Instrum. Meas., Vol. 50, No. 6, Dec. 2001. pp. 1508–1512.

[15] Kyynäräinen, J., Oja, A.S. and Seppä, H.A Micromechanical RMS-TO-DC Converter, in Digest, CPEM2000, Sydney, May 2000, pp. 699–700.

[16] Suhonen, M., Seppä, H., Oja, A.S., Heinilä, M. and Näkki, I. AC and DC Voltage Standards Based on Silicon Micromechanics, in Digest, CPEM98, Washington DC, July 1998, pp. 23–24.

[17] Seppä, H., Kyynäräinen, J. and Oja, A. Microelectromechanical Systems in Electrical Metrology, IEEE Trans. Instrum. Meas., Vol. 50, No. 2, Apr. 2001, pp. 440–444.

[18] Kyynäräinen, J., Oja, A.S. and Seppä, H. Stability of Microelectro-mechanical Devices for Electrical Metrology, IEEE Trans. Instrum. Meas., Vol. 50, No. 6, Dec. 2001, pp. 1499–1503.

[19] Cretu, E., Rocha, L.A. and Wolffenbuttel, R.F. Micromechanical Voltage reference Using the Pull-In of a Beam, IEEE Trans. Instrum. Meas., Vol. 50, Dec. 2001, pp. 1504–1507.

[20] Rocha, L.A., Cretu, E. and Wolffenbuttel, R.F. Full characterisation of pull-in in single-sided clamped beams, Sensors and Actuators, A110, 2004, pp. 301–309.

[21] Seeger, J.I. and Boser, B.E. Charge Control of Parallel-Plate, Electrostatic Actuators and the Tip-In Instability, Journal of Microelectromechanical Systems, Vol. 12, No. 5, Oct. 2003, pp. 1–16.

[22] Rocha, L.A. Dynamics and Nonlinearities of the Electro-Mechanical Coupling in Inertial MEMS, Ph.D. Thesis, Delft University, 2005.

[23] Senturia, S.D. Microsystem design, KluwerAcademic Publishers, 2001, ISBN 0-7923-7246-8.

[24] Roark, R.J. and Young, W.C. Formulas for Stress and Strain, McGraw-Hill, 6th edition, 1989, ISBN 0-07-100373-8.

[25] Nadal-Guardia, R., Dehé, A., Aigner, R. and Castañer, L.M. Current Drive Methods to Extend the Range of Travel of Electrostatic Microactuators Beyond the Voltage Pull-In Point, Journal of Microelectromechanical Systems, Vol. 11, No. 3, June 2002, pp. 255–263.

[26] Lewis, P.H. and Yang, C. Basic Control Systems Engineering, Prentice Hall International, Inc., 1997, ISBN 0-13-744434-6.

[27] Castañer, L.M., Pons, J., Nadal-Guardia, R. and Rodríguez, A. Analysis of the extended operation range of electrostatic actuators by current-pulse drive, Sensors and Actuators, A 90, 2001, pp. 181–190.

[28] Veijola, T., Kuisma, H., Lahdenperä, J. and Ryhänen, T. Equivalent-circuit model of the squeezed gas film in a silicon accelerometer, Sensors and Actuators, A 48, 1995, pp. 239–248.

[29] Veijola, T., Kuisma, H. and Lahdenperä, J. The influence of gas-surface interaction on gas-film damping in a silicon accelerometer, Sensors and Actuators, A 66, 1998, pp. 83–92.

[30] Kovacs, G.T.A. Micromachined transducers source book, McGraw-Hill Companies Inc., 1998, ISBN 0-07-290722-3.

[31] Franssila, S. Introduction to Microfabrication, John Wiley & Sons Ltd, 2004, ISBN 0-470-85105-8.

[32] Kiihamäki, J. Fabrication of SOI micromechanical devices, Ph.D. Thesis, Helsinki University of Technology, 2005. VTT Publications 559. Espoo: VTT. 87 p. + app. 28 p. ISBN 951-38-6435-9; 951-38-6436-7. http://virtual.vtt.fi/inf/pdf/publications/2005/P559.pdf.

[33] Cabuz, C. Tradeoffs in MEMS materials, Proc. SPIE, Vol. 2881, 1996, pp. 160–170.

[34] Guckel, H., Burns, D.W., Visser, C.C.G., Tilmans, H.A.C. and Deroo, D. Fine-Grained Polysilicon Films with Built-In Tensile Strain, IEEE Trans. Electron Devices, Vol. 35, No. 6, 1988, pp. 800–801.

[35] Madou, M.J. Fundamentals of Microfabrication, CRC Press LLC, 1997, ISBN 0-8493-9451-1.

[36] Sze, S.M. Semiconductor devices, John Wiley & Sons Ltd, 2nd edition, 2002, ISBN 0-471-33372-7.

[37] Bourgeois, C., Steinsland, E., Blanc, N. and de Rooij, N.F. Design of resonators for the determination of the temperature coefficient of elastic constants of monocrystalline silicon, in Proc. IEEE Int. Frequency Control Symp., Orlando, FL, May 1997, pp. 791–799.

[38] Rusanen, O. Adhesives in micromechanical sensor packaging, Ph.D. Thesis, University of Oulu, 2000. VTT Publications 407. Espoo: VTT. 74 p. + app. 54 p. ISBN 951-38-5558-9.

[39] http://parts.jpl.nasa.gov/docs/JPL%20PUB%2099-1.pdf (22.6.2006).

[40] http://www.vti.fi (22.6.2006).

[41] Pohjanen, J. Sahköstaattiset pintailmiöt kapasitiivisessa kiihtyvyys-anturissa, M.Sc. Thesis, Helsinki University of Technology, 2003.

[42] Rytkönen, V.-P. Built-in voltages of metal semiconductor junctions and structures, M.Sc. Thesis, Helsinki University of Technology, 2005.

[43] Koskenvuori, M., Mattila, T., Häärä, A., Kiihamäki, J., Tittonen, I., Oja, A. and Seppä, H. Long-term stability of single-crystal silicon microresonators, Sensors and Actuators, A 155, 2004, pp. 23–27.

[44] Kaajakari, V., Kiihamäki, J., Oja, A., Seppä, H., Pietikäinen, S., Kokkala, V. and Kuisma, H. Stability of Wafer Level Vacuum Encapsulated Single-Crystal Silicon Resonators, The 13th International Conference on Solid-State Sensors, Actuators and Microsystems, Seoul, Korea, June 5–9, 2005.

[45] Wibbeler, J., Pfeifer, G. and Hietschold, M. Parasitic charging of dielectric surfaces in capacitive microelectromechanical systems (MEMS), Sensors and Actuators, A 71, 1998, pp. 74–80.

[46] Schröder, D.K. and Babcock, J.F. Negative bias temperature instability: Road to cross in deep submicron silicon semiconductor manufacturing, J. Appl. Phys. 94, 2003, pp. 1–18.

[47] Rebeiz, G.M. RF MEMS: theory, design, and technology, John Wiley & Sons, 2003, ISBN 0-471-20169-3.

[48] Rashkeev, S.N., Fleetwood, D.M., Schrimpf, R.D. and Pantelides, S.T. Proton Induced Defect Generation at the Si-SiO2 Interface, IEEE Trans. Nucl. Sci. 48, 2001, pp. 2086–2092.

[49] Liu, C.-H., Lee, M.T., Lin, C.-Y., Chen, J., Loh, Y.T., Liou, F.-T., Schrueffer, K., Katsetos, A.A., Yang, Z., Rovedo, N., Hook, T.B., Wann, C. and Chen, T.-C. Mechanism of Threshold Voltage Shift (ΔVth) Caused by Negative Bias Temperature Instability (NBTI) in Deep Submicron pMOSFETs, Jpn. J. Appl. Phys. Vol. 41, 2002, pp. 2423–2425.

[50] van Spengen, W.M., Puers, R., Mertens, R. and De Wolf, I. A comprehensive model to prodict the charging and reliability of capacitive RF MEMS switches, J. Micronech. Microeng. 14, 2004, pp. 514–521.

[51] Mizsei, J. Ultra-thin insulator covered silicon: potential barriers and tunnel currents, Solid-State Electronics, Vol. 46, 2002, pp. 235–241.

[52] Zafar, S., Lee, B.H., Stathis, J., Callegari, A. and Ning, T. A Model for negative Bias Temperature Instability (NBTI) in Oxide and High κ pFETs, IEEE VLSI Symp., 2004, pp. 208–209.

[53] Nieminen, H., Ermolov, V., Silanto, S., Nybergh, K. and Ryhänen, T. Design of a Temperature-Stable RF MEM Capacitor, Journal of Micro-electromechanical systems, Vol. 13, No. 5, October 2004, pp. 705–714.

[54] http://www.irvine-sensors.com/pdf/MS3110%20Datasheet%20USE.pdf (22.6.2006).

[55] Kiviranta, M. and Seppä, H. DC-SQUID electronics based on the noise cancellation scheme, IEEE Transactions on Applied Superconductivity, Vol. 5, No. 2, June 1995, pp. 2146–2148.

PUBLICATION I

Stability of Electrostatic Actuation of MEMS

In: Physica Scripta 2004. Vol. T114, pp. 193–194.
Reprinted with permission from the publisher.

Physica Scripta. Vol. T114, 193–194, 2004

Stability of Electrostatic Actuation of MEMS

Anu Kärkkäinen[1], Aarne Oja[1], Jukka Kyynäräinen[1], Heikki Kuisma[2] and Heikki Seppä[1]

[1]VTT Microsensing, P.O. Box 1207, FIN-02044 VTT, Finland
[2]VTI Technologies, P.O. Box 27, FIN-01621 Vantaa, Finland

Received August 28, 2003; accepted October 2, 2003

PACS Ref: 85.85+

Abstract

The increased electrostatic stability of MEMS sensors enables new application areas for the sensors, and decreases the manufacturing costs of existing products. Especially in the applications where the MEMS component is operated under bias voltage close to the pull-in point, the undesired instability phenomenon becomes a major source of inaccuracy. We demonstrate that biasing the sensor to the pull-in point using AC voltage is significantly more stable than the conventionally used DC voltage biasing.

1. Introduction

Electrostatically actuated MEMS components find many applications today in areas such as inertial sensors, pressure sensors, relays, switches, etc. A serious limitation on the use of these devices lies in electrostatic stability. For example the instability results in increased tolerance in a varactor capacitor value and uncertainty of a sensor reading. Sensors with increased stability can be utilized with reduced test procedures hence decreasing the manufacturing costs of the final product. Also new application areas are enabled for sensors with increased performance values. For example improved inertial sensors could be used for short range navigation. Stable MEMS devices can also be utilized in precision applications like DC voltage reference and AC RMS converter as presented in [1].

The stability of capacitive transducers has been studied earlier [2, 3, 4]. The instability of capacitive MEMS components originates form electrostatic surface phenomena. Thin oxides are electrically leaky and therefore the electrical field between the surface of the oxide and the underlying bulk silicon tends to vanish due to surface charging. Another source of non-ideality is due to the surface potentials of MEMS electrodes. Surface potentials are not determined solely by the work functions of the electrode materials. Adsorption, e.g., can change surface potentials by several hundreds of millivolts.

2. Theory

The electrostatic force can be modeled as $F_{el} = (1/2)(\mathrm{d}C/\mathrm{d}x)(V - V_{offset})^2$ where V_{offset} is the component CV curve asymmetry, schematically illustrated in Fig. 2. V_{offset} depends on surface potentials and charges [1]. Typically $|V_{offset}| = 5\,\mathrm{mV} \ldots 500\,\mathrm{mV}$. If the MEMS structure is biased with a DC voltage $V = V_{DC}$, much larger than $V = V_{offset}$, the (relative) uncertainty in the electrostatic force is $\Delta F_{el}/F_{el} \approx -2\Delta V_{offset}/V_{DC}$. If the actuation is achieved by using an AC voltage $V = V_{AC}(t) = \sqrt{2}V_{AC}^{rms}\sin(\omega t)$, the uncertainty is lower, $\Delta F_{el}/F_{el} \approx 2\Delta V_{offset}V_{offset}/(V_{AC}^{rms})^2$. Here we have assumed that the frequency of the AC voltage is much higher than the mechanical resonance frequency of the MEMS structure to result only in a static displacement.

3. Measurement set-up

The measurement set-up, shown in Fig. 1, uses a HP Precision LCR Meter as an accurate capacitance bridge. The component used in the experiments was a bulk-micromachined silicon transducer [5]. The effective gap was 2.2 µm and electrode area 1.4 mm^2. The non-moving electrode on top of a glass layer was coated with 150 nm thick sputtered molybdenum and the moving electrode was coated with 200 nm thick evaporated molybdenum. The component was hermetically shielded in inert gas. The variation of the capacitance between the fixed electrode and the electrode attached to the bending beam as a function of the DC bias voltage, i.e. the component CV-curve, is shown in Fig. 2. The

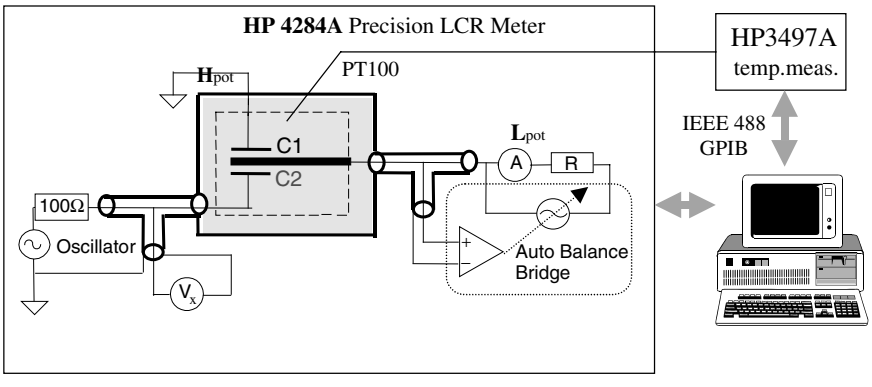

Fig. 1. Four terminal pair capacitance measurement set-up.

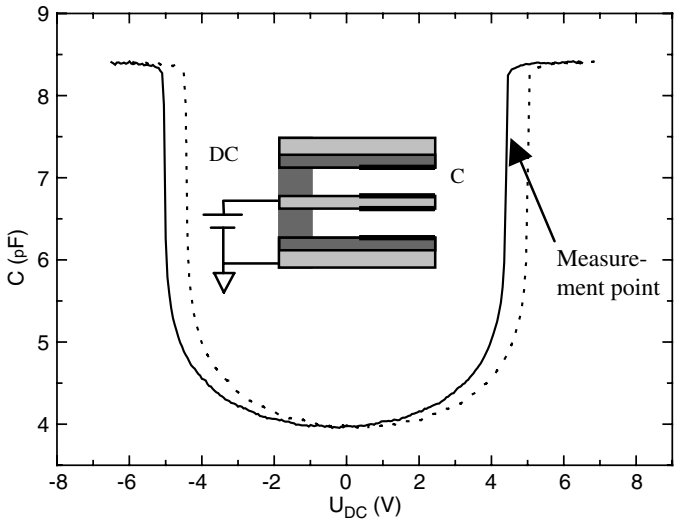

Fig. 2. Component capacitance as a function of the DC bias voltage. The offset voltage $V_{offset} = -0.29\,\mathrm{V}$. The dashed line schematically illustrates a large positive change in V_{offset} which decreased the capacitance under a constant DC bias voltage.

component pull-in occurs at 4.3 V. The stability of the component was studied by measuring the capacitance and the capacitance derivative $\mathrm{d}C/\mathrm{d}V$ of the component as a function of time near the component pull-in point by varying the bias voltage. The pull-in voltage was generated in case (1) by a DC bias voltage, using $V = V_{DC} = 4.1\,\mathrm{V}$ and $V_{AC}^{rms} = 180\,\mathrm{mV}$ for the capacitance measurement, and in case (2) an AC voltage, $V_{AC}^{rms} = 4.1\,\mathrm{V}$ and $V_{DC} = 0\,\mathrm{V}$. The measurement frequency was in both cases $f = 1\,\mathrm{MHz}$, i.e. well above the component mechanical resonance frequency, which was in the order of 10 kHz. The temperature of the component was maintained at $T = 23.2 \pm 2\,^{\circ}\mathrm{C}$.

4. Results

The measurement results are displayed in Fig. 3 and Fig. 4. The considerably larger drift of the capacitance when the bias voltage was generated using DC bias can be attributed to a change in the offset potential by $\Delta V_{offset} = 10\,\mathrm{mV}$. This can be concluded from the data correlating $C(t)$ and $\mathrm{d}C(t)/\mathrm{d}V$, shown in Fig. 4, which suggests that the biasing position moves away from the pull-in point due to the drift in V_{offset}, as schematically illustrated in the Fig. 2. The measured offset voltage V_{offset} change is $-[C(t = 450\,\mathrm{min}) - C(t = 0)]/[\mathrm{d}C(t)/\mathrm{d}V]_{\mathrm{ave}} = 10\,\mathrm{mV}$.

5. Conclusions

Stability of electrostatic actuation is important in several MEMS applications. Actuation using a DC voltage is prone to drifts due to surface charging and changes in surface potentials. We have show theoretically and experimentally that actuation using AC voltage is significantly more stable against electrode surface effects than actuation using DC voltage. These results have been confirmed by measurements of MEMS devices from completely different fabrication processes.

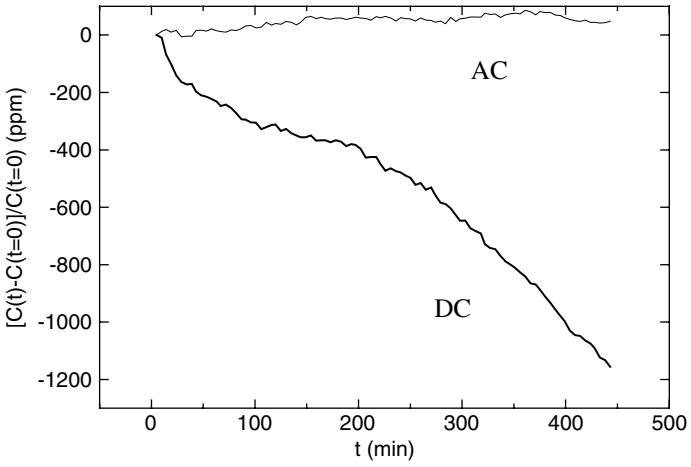

Fig. 3. Stability of the component capacitance near the pull-in voltage for DC bias voltage and AC bias voltage. The capacitance values have been normalized to the respective initials values.

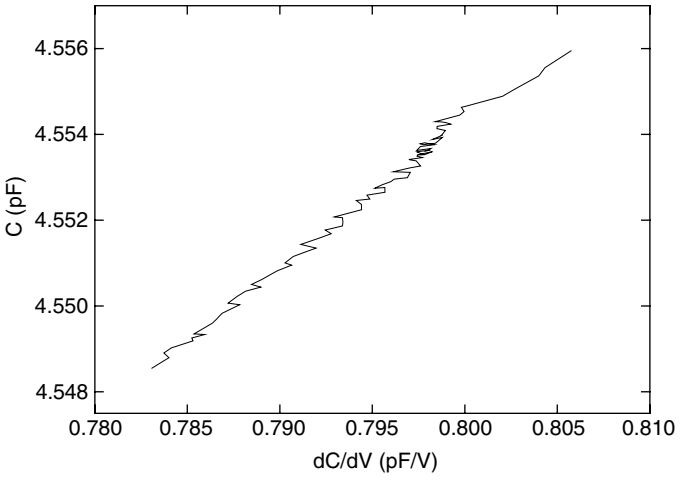

Fig. 4. Capacitance $C(t)$ as a function of $\mathrm{d}C(t)/\mathrm{d}V$, the voltage derivative of the capacitance.

Acknowledgements

This work has been carried out under EMMA project (IST-2000-28261) financed by EC and Finnish National Technology Agency Tekes.

References

1. Suhonen, M., Seppä, H., Oja, A., Heinilä, M. and Näkki, I., CPEM (Conf. Prec. Electron. Meas.) 2000 Conference Digest, p. 23–24 (2000).
2. Oja, A., Kyynäräinen, J. and Seppä, H., SPIE (Int. Soc. Opt. Eng.) Proc. **4408**, 463 (2001).
3. Cabuz, C., SPIE vol. **2881**, 160 (1996).
4. Wibbeler, J., Pfifer, G. and Hietschod, M., Sensors Actuators **A71**, 74 (1998).
5. Kuisma, H., Micro Structure Bulletin No. **3**, 4 (1997).

PUBLICATION II

Stable SOI Micromachined Electrostatic AC Voltage Reference

In: Journal of Microsystem Technologies 2005.
Vol. 12, pp. 169–172.

STABLE SOI MICROMACHINED ELECTROSTATIC AC VOLTAGE REFERENCE

Anu Kärkkäinen, Panu Pekko, James Dekker, Nadine Pesonen, Mika Suhonen, Aarne Oja, Jukka Kyynäräinen, and Heikki Seppä

VTT Information Technology, Microsensing P.O. Box 1207 FIN-02044 VTT, Finland
VTT Information Technology, Microelectronics P.O. Box 1208 FIN-02044 VTT, Finland

ABSTRACT

We have designed and manufactured a micromachined moving plate capacitor to be used as an AC voltage reference in electrical metrology. The reference is based on the characteristic AC current – voltage curve of the component having a maximum, the value of which depends on the geometry of the component and material properties of single crystalline silicon. The electrode surface stability is essential in this application and hence a new fabrication process has been developed to metallize both surfaces of an electrostatically actuated micromachined structure. The stability of the AC reference voltage at a frequency of 100 kHz and an RMS voltage value 6.4 V was measured to be ± 60 ppm over 14 hours.

1. INTRODUCTION

Electrostatically actuated capacitive MEMS components can be used as electrical references. Examples of a MEMS DC voltage reference [1], an AC voltage RMS converter [2], and a true RMS-to-DC converter [3] have been published. The targeted benefits of using MEMS components as references are improved stability compared to conventional devices (Zener diodes, for example), low 1/f noise, large operation voltage range, small size and small power consumption. The major difficulty is to achieve the excellent long term stability required for metrological applications.

Electrostatic surface phenomena cause instability in capacitive MEMS components. A silicon semiconductor surface is unstable, hence metal electrodes are needed. However, metal surfaces can charge if they are covered with a native oxide layer, as is typical. Electrode charging effects are negligible when an AC signal is used for actuation of the moving electrode [4]. Also, the built-in voltage of the device, which originates from the surface potential difference of the metal electrode and silicon spring, is temperature dependent and a potential source of instability. Slowly changing surface potentials due to, e.g., adsorption and desorption of gas molecules, also contribute to electrical instability.

2. PRINCIPLE OF OPERATION

A parallel-plate capacitor with a spring-suspended moving plate exhibits a well-known pull-in phenomenon [1]. The pull-in voltage is given by

$$V_{pi} = \sqrt{\frac{8kd^2}{27C_0}} \qquad (1)$$

where k is the spring constant, d and C_0 are respectively the air gap and the capacitance at zero voltage.

If a sinusoidal current with an RMS amplitude I_{RMS} and angular frequency ω is driven through the capacitor, the amplitude of the AC voltage across the plates is given by [1]

$$V_{ac} = \frac{I_{RMS}}{\omega C_0}\left[1 - \frac{4}{27}\left(\frac{I_{RMS}}{\omega C_0 V_{pi}}\right)^2\right], \qquad (2)$$

where we assume that the device is operated at a frequency much higher than its mechanical resonance frequency, f_0. This avoids movement of the plate due to electromechanical coupling. The amplitude V_{ac} reaches a maximum value $V_{ac,\max} = V_{pi}$ at $I_{RMS,\max} = (3/2)\omega C_0 V_{pi}$. This amplitude can be used as an AC voltage reference since a small change in the current I_{RMS} has a negligible effect on $V_{ac,max}$ near the pull-in point. The eigencurve of the component is shown in Fig.1 as a function of the moving plate deflection x from the centre position ($V_{ac} = 0$).

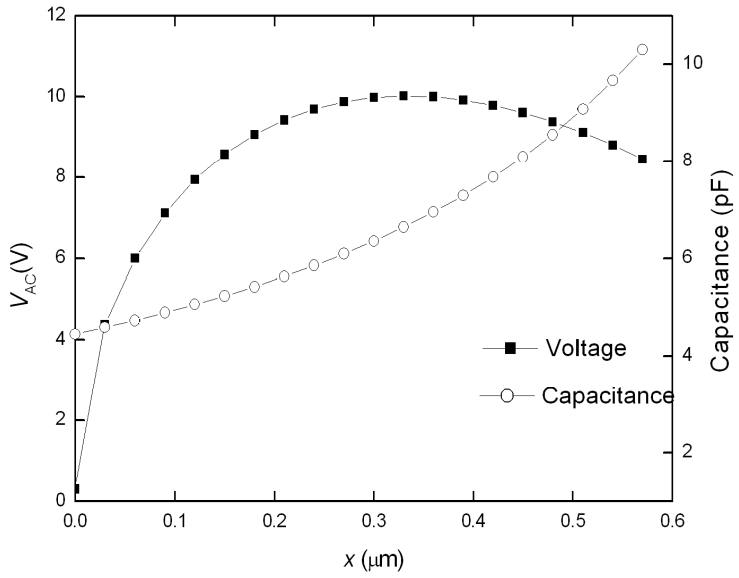

Fig.1. Calculated eigencurve for the component shown in Fig.2. (d=1μm and C0 = 4.45 pF).

3. COMPONENT DESIGN

The component is a large (r = 400 μm) round silicon plate suspended with three 260 μm-long springs, as shown in Fig. 2. The upper moving plate and lower fixed plate form a capacitor, which moves in a piston mode. The bottom of the moving plate is coated with sputtered aluminum, and the top of the fixed lower plate is coated with sputtered molybdenum. The metal thicknesses are 100 nm and 50 nm correspondingly. The component was designed for a 10 V pull-in voltage and as low a resonance frequency (about 60 kHz) as feasible, which can be achieved by fabricating the device as large as the manufacturing process allows. A large component is beneficial also for the readout electronics since the work capacitance value increases. The ambient gravity decreases the pull-in voltage by 2.2 mV (calculated).

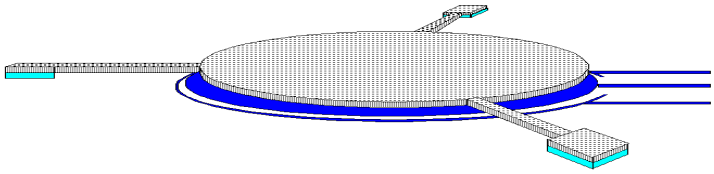

Fig.2. AC reference MEMS component

A SOI wafer was selected as the starting point of the design because of single crystal silicon springs and well defined device layer thickness. The device layer of the SOI forms the moving plate. Although the handle layer is removed during the process, this manufacturing scheme is expected to give the best results. A 20 μm-thick SOI is easily available and thick enough to withstand stress arising from the different thermal expansion coefficients of silicon and deposited metal layer.

Parasitic capacitances are a nuisance in capacitive sensors. They cause loss of sensitivity since the relative change of capacitance vs. displacement decreases. In addition, they limit the actuation range of the moving-plate capacitive actuator under charge control. Hence parasitic capacitances, mainly originating from the spring attachment areas, are minimized in the sensor design. A guard also surrounds the bottom electrode.

4. FABRICATION

A new fabrication process has been developed in order to realize the metallization on both capacitor surfaces. The approach chosen is based on aligned direct bonding of separately metallized and patterned wafers. The device wafer was a SOI with 20 μm thick device layer and 1 μm buried oxide layer and the substrate wafer was a 380 μm thick double side polished Si wafer. Both of the wafers were Boron doped and the resistivity was 0.015 - 0.02 Ωcm. The metal electrodes are placed in wells to avoid problems in wafer bonding. The well depth and oxide thickness of the substrate wafer define the gap height, which is 1 μm.

To enable bonding of the metallized wafers low temperature wafer bonding is utilized. After wafer bonding the handle layer of the SOI wafer and the buried oxide are removed by etching. Then the upper component surface is metallized and patterned and finally the device is formed with ICP etching. The process consists of three parts: 1) processing of the device (moving part) wafer, 2) processing of the substrate wafer, and 3) processing of the bonded pair as shown in Fig.3. The final component is step 4 in Fig. 3. The process requires 10 lithography steps.

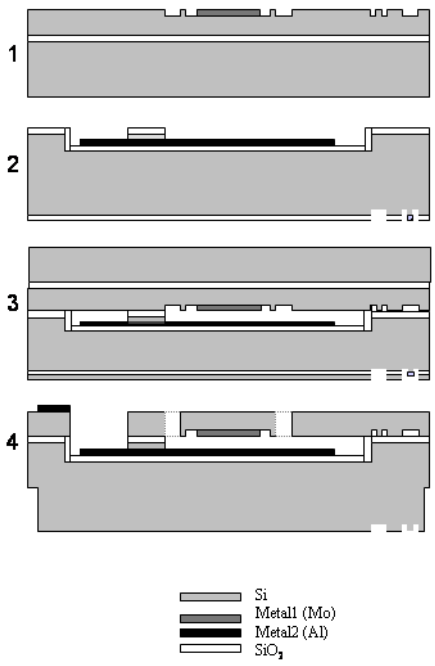

Fig.3. Major process steps.

The most critical step in the process is the wafer bonding. If the bonding surface quality is not sufficient, large non-bonded areas can be observed in optical or acoustical measurements. In the worst case, the wafers will not bond at all. To keep the surfaces in bondable condition, careful process planning and frequent cleaning procedures are demanded throughout the process. Because metallizations are needed on the capacitor surfaces, metal residues have to be removed from bonding surfaces with great care. Also, trapped gas bubbles between the bonded wafers can cause large non-bonded areas, as experienced in our process. The component yield from the successfully bonded areas was very good.

A photograph of the final component is shown in Fig. 4. The three small contact pads at the end of the springs are connected to the capacitor moving plate (only two of them are used) and the two middlemost large contact pads on the right are connected to the bottom plate. This enables a four terminal point capacitance measurement. The two remaining large contact pads on the right are connected to the guard (grounded).

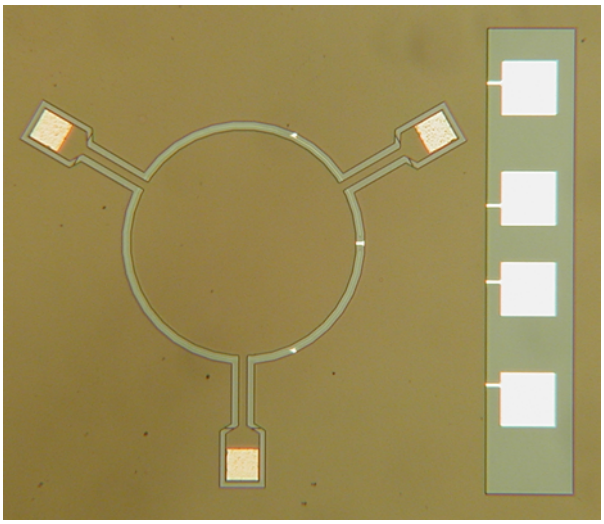

Fig.4. Final component.

5. PACKAGING

Open capacitive structures are very sensitive to changes in temperature, pressure, humidity, etc. Hence the sensor needs to be encapsulated in vacuum or in protective gas. A high gas pressure was chosen as it works as a mechanical damper. The component was encapsulated into a hermetically sealed TO-8 can containing 1 atm nitrogen gas. Fig 5. shows a component glued in a TO-8 can and a hermetically encapsulated component .

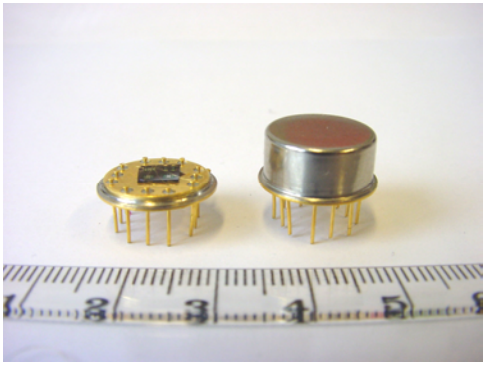

Fig.5. Component glued in TO-8 can and hermetically encapsulated component.

6. CHARACTERIZATION

A schematic drawing of the readout electronics developed for the AC voltage reference is shown in Fig. 6. An AC voltage is fed to the inverting input of the main operational amplifier OA2, which acts as a voltage to current converter to drive the current through the MEMS capacitor. Capacitors C_1 and C_2 as well as the shunt resistor R_4 force the DC voltage offset, which originates from OA2, to be zero across the MEMS capacitor. C_1 and C_2 are both 100 nF, hence much greater than the initial value (V_{ac}=0) of the MEMS capacitor (4.5 pF). The difference amplifier OA1 isolates the AC source from the electronics. The output of the unity gain buffer amplifier, AD549LH, is the AC reference voltage equivalent to the pull-in voltage of the MEMS capacitor. Guarding techniques are employed to minimize the effects of parasitic capacitances. The measurement setup is housed in a temperature, pressure and humidity-controlled environment.

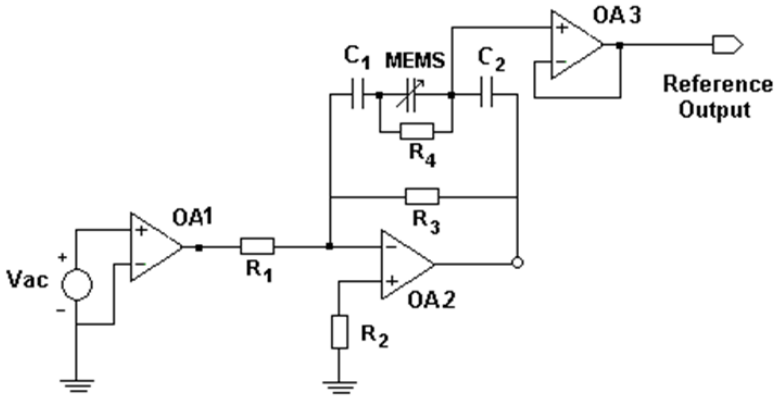

Fig. 6. Readout electronic used in MEMS component characterization.

7. RESULTS

A HP3324A signal generator was used to drive the MEMS capacitor to its pull-in point. The stability of the pull-in voltage 6.4 V was measured at 100 kHz. The stability for a period of 14 hours is shown in Fig. 7 and it is found to be within ± 30 ppm over 14 hours. The data is corrected versus the temperature changes of the input AC voltage source. The temperature inside the environment chamber was 28 ± 0.15 °C.

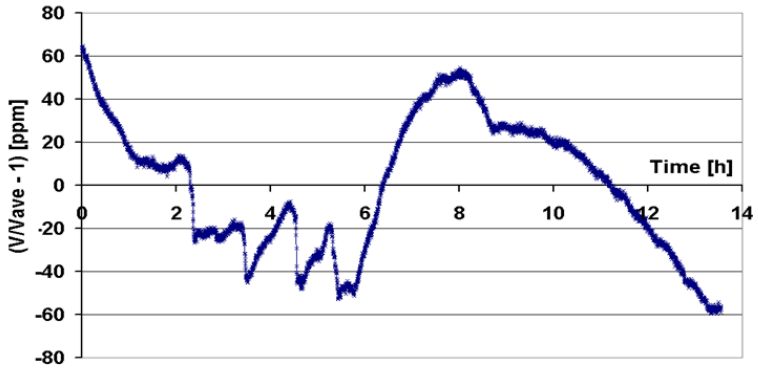

Fig. 7. Measurement results showing the stability of the MEMS component over 14 hours.

The characterization of the component has started only recently. More experiments are needed to find out reasons for the observed voltage behaviour in the measurement data. Potential sources for the slow voltage variation are charging of the MEMS component, instability of the readout electronics and changes in the environmental parameters. Although the component was hermetically packaged, the encapsulation was done at too low temperature (100 °C) to guarantee that there is no residual humidity inside the package that could influence the component stability.

8. CONCLUSIONS

A new MEMS process has been developed, which enables fabrication of moving plate capacitors having both capacitor surfaces metallized. The manufacturing is a straightforward, although lengthy, process. The wafer bonding at low temperature is challenging, especially since the wafers are exposed in many process steps.

The fabricated moving plate capacitors have been used as AC voltage references, which demonstrated rather good short-term stability. Long-term stability measurements have also started. The future work will focus on readout electronics improvement and component packaging. A LTCC package sealed in vacuum will be investigated next.

ACKNOWLEDGEMENTS

This work has been carried out under EMMA project (IST-2000-28261) financed by the European Commission.

REFERENCES

[1] H. Seppä, J. Kyynäräinen and A. Oja, “Microelectromechanical Systems in Electrical Metrology”, IEEE Trans. Instr. & Measurement, Vol. 50, pp. 440-4, 2000.

[2] J. Kyynäräinen, A.S. Oja, and H. Seppä, “A Micromechanical RMS-TO-DC Converter”, in Digest, CPEM2000, Sydney, May 2000, pp. 699-700.

[3] B.P. van Drieënhuizen and R.F. Wolffenbuttel, “Integrated Micromachined Electrostatic True RMS-to-DC Converter”, in IEEE Trans. Instr. & Measurement, Vol. 44, No. 2, pp. 370-3, 1995.

[4] A.Kärkkäinen, A.Oja, J.Kyynäräinen, H. Kuisma, and H.Seppä, “Stability of Electrostatic Actation of MEMS”, Physica Scripta T.Vol.T224, 193-194, 2004.

[5] M. Suhonen, H. Seppä, A.S. Oja, M. Heinilä, and I. Näkki, “AC and DC Voltage Standards Based on Silicon Micromechanics”, in Digest, CPEM98, Washington DC, July 1998, pp. 23 - 24.

PUBLICATION III

MEMS-Based AC Voltage Reference

In: IEEE Transactions on Instrumentation and Measurement 2005. Vol. 54, pp. 595–599.

MEMS-Based AC Voltage Reference

Anu Kärkkäinen, Nadine Pesonen, Mika Suhonen, Aarne S. Oja, Antti Manninen, Nikolai Tisnek, and Heikki Seppä

***Abstract*—An ac root-mean-square (RMS) voltage reference based on a microelectromechanical system (MEMS) component is presented. The device stability is investigated in various experiments. A time stability at a level of a few μV/V in 24 h was measured using an accelerometer MEMS component at an operating frequency of 100 kHz.**

***Index Terms*—AC voltage reference, capacitive sensors, microelectromechanical systems.**

I. Introduction

PROPOSALS for an ac voltage reference based on a capacitive microelectromechanical system (MEMS) were first published in 1998 [1], [2]. The MEMS ac voltage reference is based on the characteristic pull-in point of the MEMS component. This pull-in point depends only on the component geometry and material properties of single crystal silicon. The benefits of MEMS components in reference applications are good stability [3], low $1/f$ noise, large operation voltage range, small size, and low power consumption.

The electronics of a stable ac voltage reference is easier to realize than the electronics of a dc voltage reference. Indeed, while the dc reference requires a feedback circuit [3], only an ac current drive is needed for the ac voltage reference to bias the component to the pull-in position. In addition, electrode charging effects are negligible when using an ac signal for the actuation of the moving electrode [4].

II. Principle of Operation

If a sinusoidal current with an RMS amplitude I_{RMS} and angular frequency ω is driven through a spring suspended moving plate capacitor, the amplitude of the ac voltage across the plates is given by

$$V_{\mathrm{RMS}} = \frac{I_{\mathrm{RMS}}}{\omega C_0}\left[1 - \frac{4}{27}\left(\frac{I_{\mathrm{RMS}}}{\omega C_0 V_{\mathrm{pi}}}\right)^2 - \frac{F_{\mathrm{m}}}{kd} + \varepsilon'(x - x_0)\right] \tag{1}$$

where C_0 is the capacitance at zero voltage, k is the spring constant, and d the gap between the plates. ε' describes the second-order terms due to mechanical movement of the plate and x is the plate deflection from the rest position x_0. The pull-in voltage is

$$V_{\mathrm{pi}} = \sqrt{\frac{8kd^2}{27C_0}}\left[1 - \frac{F_{\mathrm{m}}}{kd} + \frac{4}{9}\left(\frac{\omega_0}{\omega}\right)^2 + \varepsilon''(C_{\mathrm{s}}, Q, R, \ldots)\right] \tag{2}$$

where F_{m} describes all external mechanical forces effecting the component such as vibrations, tensions, and ambient gravity. Again, ε'' describes second-order terms, which depend on parasitic capacitance C_{s}, component mechanical Q value, parallel resistance R, etc. The device is operated at a frequency higher than its resonant frequency, $f = \omega_0/2\pi$, to minimize the influence of the mechanical forces.

The amplitude V_{RMS} has a maximum $V_{\mathrm{RMS,max}}$, which can be used as an ac voltage reference since a small change ΔI_{RMS} in the current near the pull-in point has only a minor effect on V_{RMS}.

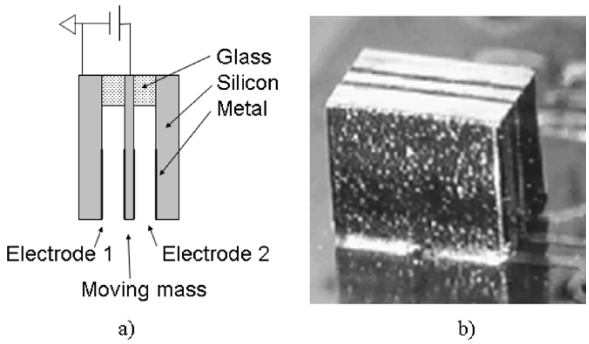

Fig. 1. (a) Photograph of the component and (b) a schematic diagram of the structure of the component.

III. Component Stability

If the external mechanical forces exerting on the MEMS component are small, the stability of the component depends only on the material, the geometry and the manufacturing process selections, which are discussed below.

A. Material and Geometry

Fundamental factors affecting the pull-in voltage stability, according to [2], are the spring constant k, the gap d, the permittivity ε, and the electrode area A of the component. A stable spring constant is achieved by using single crystal silicon springs. Although single crystal silicon is mechanically an extremely stable material, the spring constant has a temperature coefficient arising mainly from the temperature coefficient of the modulus of elasticity, on the order of -6×10^{-5} /°K [5]. However, the temperature coefficient of the device, usually 10–20 times higher, is dominated by the component mounting.

Manuscript received July 2, 2004; revised October 28, 2004. This work was supported in part by the European Commission under EMMA Project IST-2000-28261 financed and in part by Tekes, National Technology Agency of Finland.

A. Kärkkäinen, M. Suhonen, A. S. Oja, and H. Seppä are with VTT Information Technology, Microsensing, FIN-02044 VTT, Finland (e-mail: anu.karkkainen@vtt.fi).

N. Pesonen is with the Centre for Metrology and Accreditation (MIKES), 02150 Espoo, Finland, on leave from the VTT Information Technology, FIN-02044 VTT, Finland.

A. Manninen and N. Tisnek are with the Centre for Metrology and Accreditation (MIKES), 02150 Espoo, Finland.

Digital Object Identifier 10.1109/TIM.2004.843422

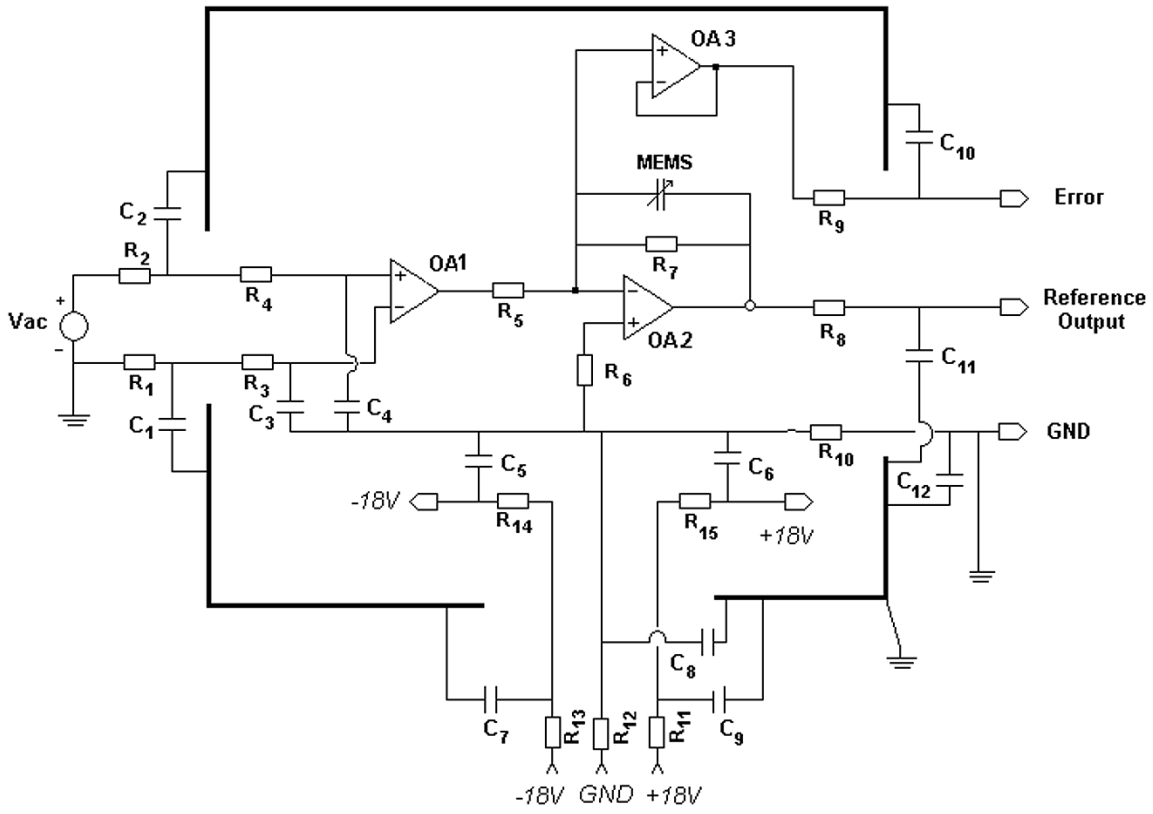

Fig. 2. Readout electronic used in MEMS component characterization.

Consequently, the device needs to be stabilized for temperature or temperature compensated.

Mechanical deformations of the electrode plates can change the distance d between the plates. Residual stress, inherent for epi-poly process [6], strongly influences time and temperature stability of the component. Hence stress-free substrate material, such as silicon-on-insulator (SOI), is essential. Rigid mounting of components can also cause stress and, hence, should be avoided.

B. Mechanics

When the component is operated close to the mechanical resonance frequency, mechanical forces, related to the inertia of the moving plate, will also influence the stability of the pull-in value. In addition, second-order forces due to temperature, humidity, or any dc voltage that may exist across the component, can also effect the device stability.

C. Electrical Charging

Various electrode surface phenomena are potential sources of instability. Charging can be reduced by metallizing the electrode surfaces. But, also, metal electrode surfaces can oxidize. The charged oxide can be observed as an effective gap reduction.

IV. Component Characteristics

All the measurements were performed using bulk micromachined accelerometers. The accelerometer is a cantilever attached at one end as shown in Fig. 1(a). A single component comprises of two identical capacitors, i.e., between the moving mass and the side electrodes. Only one capacitor was monitored at a time while the other one was grounded. The component was either flip-chipped on a printed circuit board or attached to a TO-8 can with bond wires. The component was enclosed in gas atmosphere and was over damped. A photograph of the component is shown in Fig. 1(b). The component was sensitive to inclination changes, which is characteristic for an accelerometer, and it had an influence on the repeatability of the measurements.

V. Electronics

The requirements for the ac voltage reference electronics are high slew rate and high open loop gain. A schematic of the experimental set-up is shown in Fig. 2. An ac voltage is fed to the inverting input of the main operational amplifier OA2, which acts as a voltage to current converter to drive the current through the MEMS capacitor. The output of OA2 is the ac reference voltage. The output of the unity gain buffer amplifier OA3 corresponds to the voltage at the inverting input of OA2. Monitoring this voltage gives information about any variations of the gain of the operational amplifier OA2. The actual error depends also on the phase shift between the output and input signal. The instrumentation amplifier OA1 isolates the ac source from the electronics. Filtering of the power supply and also input and output voltages suppresses EM interference. In addition, shielding techniques are employed to prevent changes

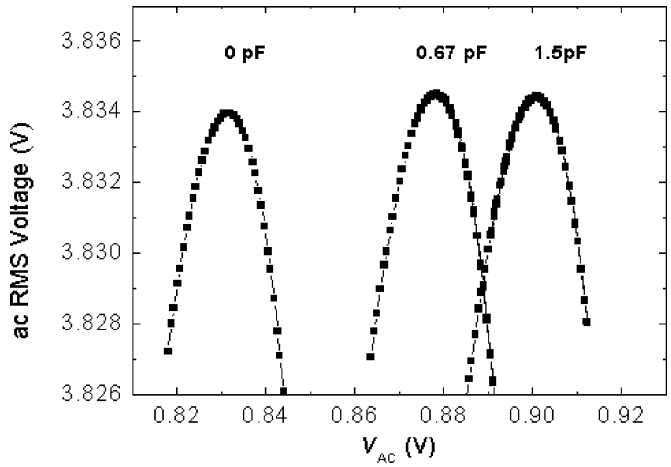

Fig. 3. AC reference voltage curves for stray capacitance values 0, 0.67, and 1.5 pF. AC RMS voltage value change was 143 μV/V and 122 μV/V, accordingly.

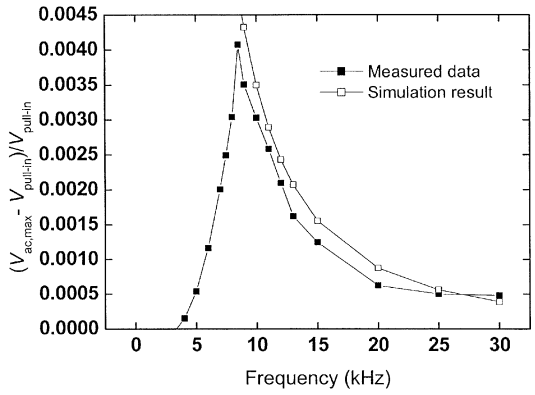

Fig. 4. Dependence of the ac voltage reference with the operating frequency.

in stray capacitances. The MEMS capacitor is measured in a four terminal configuration (not shown in Fig. 2).

VI. Measurement Results

The ac voltage reference was characterized in various experiments. First, we examined the device as an ideal voltage source, which is immune to stray capacitance and to parallel resistance changes. Then, we studied the frequency response, and the sensitivity to environmental parameters such as temperature and humidity. Finally, the stability of the ac voltage amplitude was studied over time. All the measurements were performed at room temperature, which varied from 21 °C to 24 °C, and at a 100 kHz frequency unless otherwise mentioned.

A. The Device as a Voltage Source

1) Stray Capacitance: The effect of stray capacitance was experimentally analyzed by inserting a discrete capacitor in parallel with the MEMS component. For each capacitor being inserted, the signal generator voltage was scanned near the pull-in point and the RMS value of the reference output voltage was measured using a multimeter. The pull-in point, about 4.65 V, was determined from the maximum of the curve. The nominal capacitance of the component was 10 pF. The parallel capacitance values were 0.67 pF and 1.5 pF, about 10% of the nominal value and well above the expected stray capacitance values. The results are shown in Fig. 3. The voltage maximum change for the 0.67 pF capacitor was 143 μV/V and for the 1.5 pF capacitor 122 μV/V. However, these changes are due to component inclination change, which was inevitable when applying a capacitor to the electronics, rather than due to capacitor value changes. This was demonstrated by inserting and removing the same capacitor into the electronics. We could not observe an ac reference voltage change due to stray capacitance within the measurement repeatability.

2) Parallel Resistance: Similarly, a resistor was added in parallel with the MEMS component and the voltage-current curves were recorded in an identical measurement setup as previously. A 90 kΩ additional resistance in parallel with the 1 MΩ resistance changed the ac reference voltage by 7.9 μV/V. The same order of magnitude change was also observed with a parallel resistance of 300 kΩ.

3) Conclusion: The stray capacitance and parallel resistance variations were not observed to effect the value of the ac voltage reference within the measurement accuracy. However, they do effect the input current at which the pull-in point is reached. Therefore, the electronics driving the ac voltage reference should be able to track the maximum of the voltage amplitude even if the stray capacitance and parallel resistance change.

B. Frequency Dependence

The frequency dependence of the ac voltage amplitude was measured by varying the frequency of the input current near the component mechanical resonance frequency (about 10 kHz). The results are plotted in Fig. 4. The results show two phenomena. For frequencies higher than 10 kHz, the voltage exhibits a $(\omega_0/\omega)^2$ frequency behavior. This effect was also verified by simulating a current driven and viscously damped moving plate capacitor, which had a resistor and a capacitor in parallel, using the Runge-Kutta method. The simulation agrees well with the measured data. Below the resonance frequency, the frequency behavior is different because mechanical damping due to residual gas pressure is frequency dependent. The device should be operated at frequencies well above the component mechanical resonance frequency in order to minimize the influence of the mechanical forces.

C. Environmental Changes

1) Temperature Coefficient: The temperature coefficient of the ac voltage reference was measured by cycling the temperature of the component between 32.05 ± 0.05 °C and 34.4 ± 0.05 °C in approximately two hour periods. The mechanical stress arising from the component mounting was minimized by attaching the component only from the bond wires in a TO-8 can. Two 390 kΩ resistors were attached in parallel on top of the TO-8 can lid and the temperature was controlled by changing the voltage across the resistors. The temperature was monitored with a Pt100 thermometer, which was attached on the side of the TO-8 can. The ac RMS voltage values were determined from the maxima of the curves when the signal generator amplitude was scanned near the pull-in point as in previous measurements. Fig. 5 shows the ac reference voltage as a function of time during

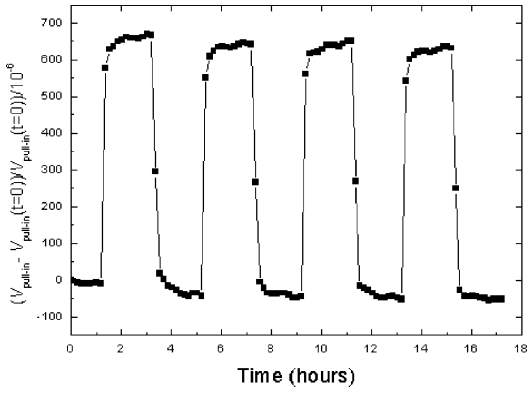

Fig. 5. Variations of the pull-in voltage as a function of temperature.

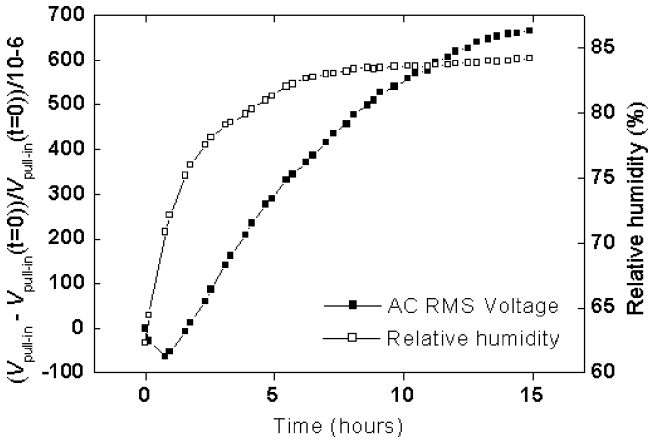

Fig. 6. AC voltage reference response to relative humidity change.

the temperature cycling. The temperature coefficient of the device was measured to be 240 μV/V/°C, which is about four times higher that the temperature coefficient of the modulus of elasticity. Since the mechanical stress arising from the component mounting was minimized, it is assumed that the temperature coefficient is dominated by the component bending due to different temperature expansion coefficients of silicon and glass. In addition, a transient of about 200 min was observed in the beginning of the measurement. A similar transient is also present in the time stability experiment.

2) Humidity: The ac voltage reference sensitivity to humidity was measured by inserting a moist cotton pad in a cup inside the electronics enclosure. Relative humidity inside the enclosure progressively increased from about 60% to about 85%. As previously, the ac RMS voltage was determined from the maxima of the voltage curves, when the input voltage was scanned near the pull-in point. The results are shown in Fig. 6. A 25% change in relative humidity resulted in a 700-μV/V increase in the ac RMS voltage. Since neither stray capacitance nor parallel resistance have an effect on the ac voltage, it is assumed that humidity is absorbed by the glue and/or the ceramic printed circuit board where the component was mounted and, hence, caused the component inclination change.

D. Stability With Time

Preliminary time stability measurement of the ac voltage reference is shown in Fig. 7. The device was closed in a temperature-stabilized chamber, which was mounted on a stone table. The temperature was $23.51 \pm 0.012\,^{\circ}\mathrm{C}$ during the 18 h measurement. The amplitude of the excitation voltage was varied near the pull-in point, and the RMS value of the reference output voltage was measured using a multimeter. A second-order polynomial fit was made to the parabolas similar to those of Fig. 3, and the voltage at the maximum was determined. The values are plotted in Fig. 7. After a transient of about 200 min, the reference output voltage stays constant within the scatter of the data with a standard deviation of about 8 μV (1.7 μV/V). The scatter is mainly caused by the multimeter, which is not an ideal device for voltage measurements at 100 kHz.

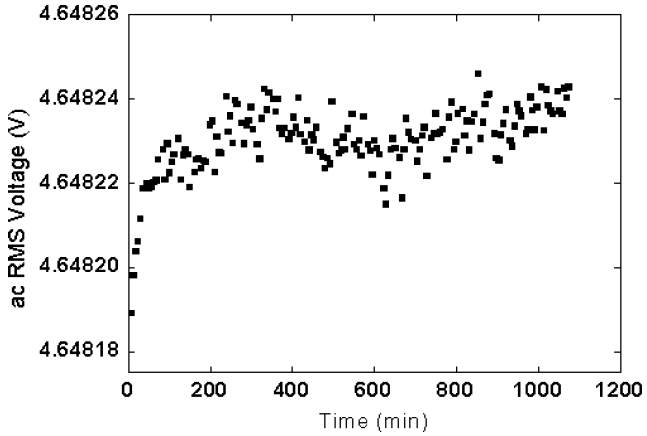

Fig. 7. Time stability of the ac voltage reference.

VII. Conclusion

We have demonstrated that a moving plate MEMS capacitor can be used as an ac RMS voltage reference. The voltage reference should be operated well above the mechanical resonance frequency. Ac voltage amplitude stability of a few μV/V in 24 h has been measured using a MEMS accelerometer as a test component. VTT has designed and manufactured a MEMS component optimized for the ac voltage reference use and it is currently being evaluated. Temperature control or compensation for the ac voltage reference is needed as well as a hermetic package, which should eliminate effects of humidity and pressure on the stability of the ac voltage reference.

Acknowledgment

A. Kärkkäinen and the EMMA team wish to thank H. Kuisma from VTI Technologies for providing test components and useful discussions. J. Penttilä is acknowledged for his excellent technical assistance in the project.

References

[1] M. Suhonen, H. Seppä, A. S. Oja, M. Heinilä, and I. Näkki, "AC and DC voltage standards based on silicon micromechanics," in *CPEM'98 Conf. Dig.*, 1998, pp. 23–24.

[2] H. Seppä, A. S. Oja, and M. Suhonen, "Micromechanical AC and DC Voltage Reference System," W.O. Patent, PCT/FI99/00553, WO 00/02 110, 1999.

[3] H. Seppä, J. Kyynäräinen, and A. S. Oja, "Microelectromechanical systems in electrical metrology," *IEEE Trans. Instrum. Meas.*, vol. 50, no. 2, pp. 440–444, Apr. 2001.

[4] A. Kärkkäinen, A. S. Oja, J. Kyynäräinen, H. Kuisma, and H. Seppä, "Stability of electrostatic actuation of MEMS," *Physica Scripta T*, vol. T, pp. 193–194, 2004.

[5] C. Bourgeois, E. Steinland, N. Blanc, and N. F. de Rooij, "Design of resonators for the determination of the tempeprature coefficients of elastic constants of monocrystalline silicon," in *Proc. IEEE Int. Frequency Control Symp.*, 1997, p. 791.

[6] L. A. Rocha, E. Cretu, and R. F. Wolffenbuttel, "Analysis and analytical modeling of static pull-in with application to MEMS-based voltage reference and process monitoring," *J. Microelectromech. Syst.*, vol. 13, pp. 342–354, 2004.

PUBLICATION IV

Optimized Design and Process for Making a DC Voltage Reference Based on MEMS

In: IEEE Transactions on Instrumentation and Measurement 2005. Vol. 54, pp. 563–566.

Optimized Design and Process for Making a DC Voltage Reference Based on MEMS

Anu Kärkkäinen, Shakil A. Awan, Jukka Kyynäräinen, Panu Pekko, Aarne S. Oja, and Heikki Seppä

***Abstract*—A micromechanical moving plate capacitor has been designed and fabricated for use as a dc voltage reference. The reference is based on the characteristic pull-in property of a capacitive microelectromechanical system (MEMS) component. The design is optimized for stability. A new silicon-on-insulator (SOI) process has been developed to manufacture the component. We also report on improved feedback electronics and the latest measurement results.**

***Index Terms*—Capacitive sensors, feedback electronics, microelectromechanical systems (MEMS), micromachining, silicon-on-insulator (SOI).**

I. Introduction

THE characteristic pull-in voltage of a microelectromechanical system (MEMS) moving plate capacitor depends only, in principle, on its spring constant and geometrical properties. The pull-in voltage of a capacitive MEMS component has been proposed for use as a dc voltage transfer standard in metrology [1]–[6]. The moving plate of a MEMS parallel plate capacitor, suspended by single crystal silicon springs, can be very stable in comparison with, for example, Zener diodes. The latter have an inherent $1/f$ noise and long term stability limitations [7]. The MEMS capacitive devices can be designed to operate at any voltage up to several hundred volts. In theory, the device stability is limited by mechanical noise [5].

The major challenge in the MEMS dc voltage reference development is to achieve high stability, preferably better than 1 μV/V/year. The major improvements introduced in the new design, compared to the earlier published results, are the use of stress-free silicon-on-insulator (SOI) manufacturing process, metallization of both electrode surfaces, and built-in voltage compensation. The major factors effecting the pull-in voltage stability are the spring constant k and the gap d. The spring is made out of single crystal silicon resulting in a very stable spring constant k with time. However, Young's modulus has a temperature coefficient of -60 μV/V/K, which effects the temperature dependence of the spring constant. But even a 10 to 20 times higher temperature coefficient can arise from the component mounting. The sensor needs to be stabilized for temperature or temperature compensated.

Longitudinal and vertical residual stress inherent in an epi poly process, strongly influences the gap and, hence, the time and temperature stability of the device [8]. A new SOI process has been developed for fabrication of a series of components. The seesaw design, a rectangular plate suspended by torsion springs at the symmetry axis, is selected for the component, because it is less sensitive to stress or vibration than a cantilever or beam type capacitor. Stress-free mounting of the component is also essential.

Also, various electrode surface phenomena can have an effect on the pull-in voltage. The charging effect can be reduced by metallizing the electrode surfaces, which is enabled by the new process as well, albeit with significantly increased complexity.

In addition, the built-in voltage of the component is temperature dependent and, hence, a source of instability. The built-in voltage temperature dependence can be eliminated in the first order by applying a compensating dc voltage on the moving plate or using "split" electrodes, explained later in detail.

In our previous work [4], the underlying dc voltage reference stability was found to be 1 μV/V only after subtracting the measured drift of the pull-in voltage from the curve fitted to the data. The actual drift was -6000 μV/V over 60 h.

II. Principle of Operation

When a dc voltage V is applied across a moving plate capacitor, the capacitor plates are pulled towards each other by an electrostatic force $F_{\rm e} = C_0V^2d/2(d-x)^2$, where x is the deflection, d is the gap at $x = 0$, $C_0 = \varepsilon A/d$ is the capacitance at $x = 0$, ε is the dielectric constant, and A the capacitor plate area. The mechanical force $F_{\rm m} = -kx$, where k is the spring constant, acts as a restoring force on the plate position. The maximum dc voltage across the capacitor is known as the pull-in voltage

$$V_{\rm pi} = \sqrt{\frac{8kd^2}{27C_0}} \tag{1}$$

which occurs when $x = d/3$, as can be seen in Fig. 1. The displacement can be stabilized at that point by a force feedback loop. The pull-in voltage can be used as a dc voltage reference. Small deviations in the plate deflection Δx, near $x = d/3$, have only a second order effect in the reference voltage $\Delta V/V_{\rm pi} \sim 27/4\,(\Delta x/d)^2$ which makes the pull-in point excellent for the reference use.

Manuscript received July 2, 2004; revised October 29, 2004. This work was supported in part by the EMMA project (IST-2000-28261) funded by the European Commission Framework V Program and by the National Technology Agency of Finland. S.A. Awan would like to acknowledge support from the Glazebrook Fellowship Award and the NPL Strategic Research 9SRPE140 Project to attend VTT as Guest Researcher between January and March 2004.

A. Kärkkäinen, J. Kyynäräinen, P. Pekko, A. S. Oja, and H. Seppä are with the VTT Information Technology, Microsensing, FIN-02044 VTT, Finland (e-mail: anu.karkkainen@ vtt.fi).

S. A. Awan is with the Division of Enabling Metrology, National Physical Laboratory, Queens Road, Teddington, Middlesex, TW11 0LW, U.K. (e-mail: shakil.awan@npl.co.uk).

Digital Object Identifier 10.1109/TIM.2004.843097

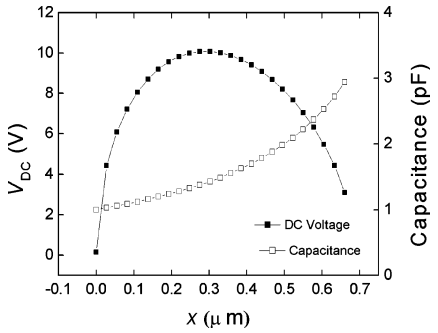

Fig. 1. Calculated eigencurve for a component with 10-V pull-in voltage ($k = 405$ N/m, $d = 1$ μm, $C_0 = 1.2$ pF).

III. Component Manufacturing

A new fabrication process has been developed in order to realize the metallization of both capacitor surfaces. The approach chosen is based on aligned direct bonding of separately metallized and patterned wafers. The device wafer was a SOI wafer with a 20-μm-thick device layer and a 1-μm buried oxide layer and the substrate wafer was a 380 μm-thick double-side polished Si wafer. Both of the wafers were boron-doped and the resistivity was 0.015 to 0.02 Ωcm. The metal electrodes are placed in wells to avoid problems in wafer bonding. The well depth and oxide thickness of the substrate wafer define the gap height, which is 1 μm.

The process consists of four parts: 1) processing the electrodes to the device wafer; 2) processing the electrodes to the substrate wafer; 3) low-temperature fusion bonding of the wafers; and 4) inductively coupled plasma (ICP) etching the bonded pair when the moving part is released. The process diagram is shown in Fig. 2. The process requires 10 lithography steps.

The most critical step in the process is the wafer bonding. If the bonding surface quality (surface roughness and freedom from contaminants) is inadequate, large nonbonded areas can be observed in optical or acoustical measurements. In the worst case, the wafers will not bond at all. To keep the surfaces in bondable condition, careful process planning and frequent cleaning procedures are demanded throughout the fabrication. Also, trapped gas bubbles between the bonded wafers can cause large nonbonded areas, as experienced in our process. The component yield from the successfully bonded areas was very good.

IV. Component Design

The basic design of the dc voltage reference is illustrated in Fig. 3. The top actuator electrode (550 $\times$ 800 μm) is suspended at its center of mass with two 180-μm-long silicon springs. The bottom of the moving plate actuator is coated with sputtered molybdenum, and the top of the lower fixed plate is coated with sputtered aluminum. The upper plate moves in torsion mode and the mechanical resonance frequency is typically 30 kHz. The component was designed to be as large as the manufacturing process allowed in order to achieve high capacitance values.

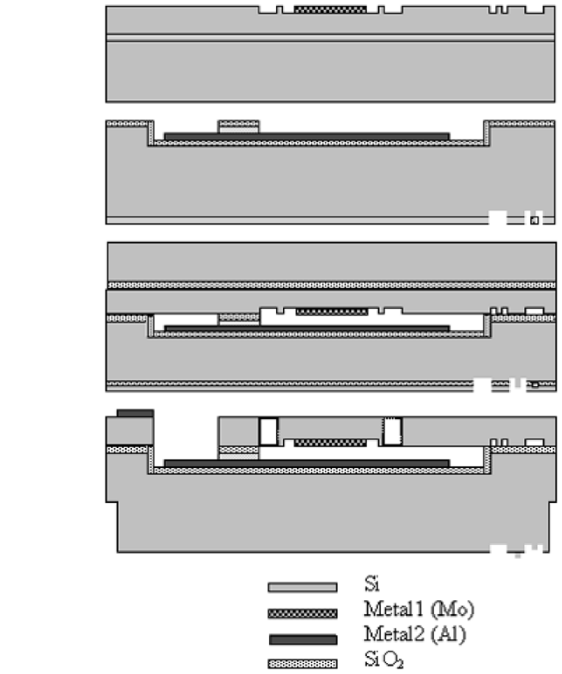

Fig. 2. Major process steps for fabricating the MEMS dc voltage reference.

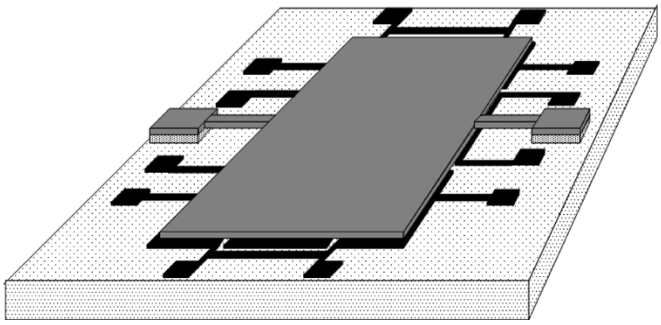

Fig. 3. Silicon-on-insulator (SOI) parallel plate capacitive seesaw component.

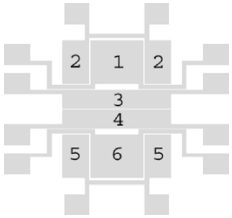

Fig. 4. Bottom electrodes of the component. Double contact pads are needed for the four terminal pair measurements.

The bottom electrode is divided into four sections as shown in Fig. 4. The two sections in the middle are the sense electrodes for displacement control (3 and 4). The top electrodes (1 and 2) are used for actuating the seesaw to the pull-in position while the other electrodes (5 and 6) are grounded. The built-in voltage ($V_{\rm bi}$), which originates from the work function difference of the metal electrode and the silicon spring, can be compensated by splitting the actuation electrode into two equal sections and applying slightly different voltages with opposite polarity on the electrodes. If a positive voltage $V_{\rm p}$ is applied to electrode 1, and a negative voltage $V_{\rm n}$ is applied to electrode 2 so that $V_{\rm p} = V_0 + V_{\rm bi}$ and $V_{\rm n} = -V_0 + V_{\rm bi}$, with V_0 being

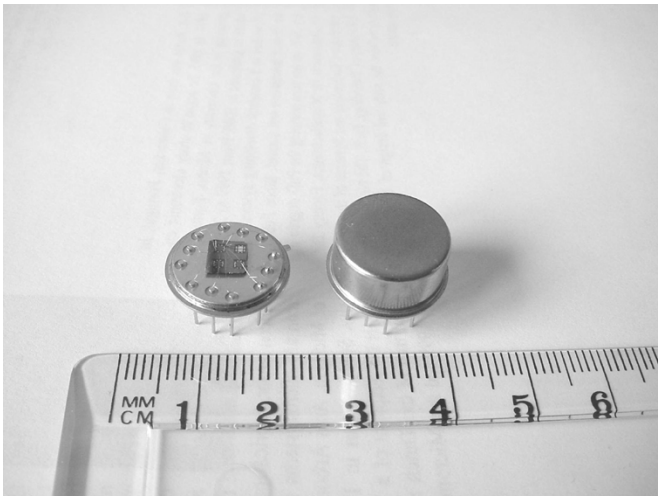

Fig. 5. Component mounted on a TO-8 can and a hermetically encapsulated component.

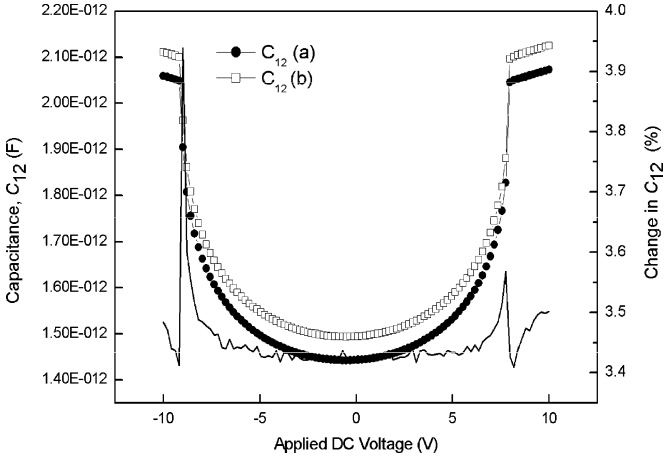

Fig. 6. Characteristic C–V curves (including repeatability a and b) of a component showing the measured pull-in voltage and the built-in voltage (the shift of the minima from 0 V). The solid curve is the change in C_{12} repeatability.

the average of positive and negative pull-in voltage values, the electrostatic force $F_{\rm e}$, $F_{\rm e} \propto V_{\rm p}^2 + V_{\rm n}^2 \approx 2V_0^2$ is independent of $V_{\rm bi}$ in the first order.

Metal surfaces can be very hydrophilic. If there are any residual chemicals from the manufacturing process inside the sensor enclosure, they can out gas with time and effect the device stability. Thus, the component was encapsulated into a hermetically sealed TO-8 can containing 1 atm nitrogen gas. Atmospheric pressure mechanically damps the seesaw electrode, which is also necessary for the stability of the feedback electronics. Fig. 5 shows a component glued in a TO-8 can and a hermetically encapsulated component.

V. Capacitance–Voltage Curve

The characteristic C–V curves of a component are shown in Fig. 6 including repeatability measurements. From Figs. 3 and 4, it is possible to define two capacitances, C_{12} and C_{56}, which exist between the top electrode and the two fixed lower electrodes. The C–V curves of a component were determined by measuring the change in capacitance C_{12} while the dc voltage

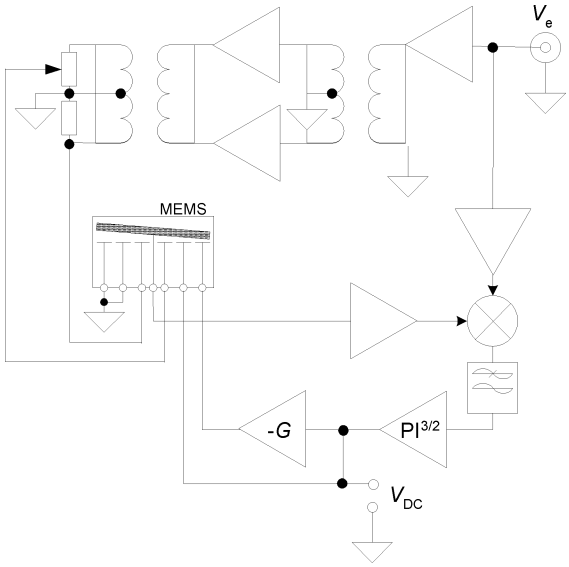

Fig. 7. Feedback electronics used to monitor the stability of the dc voltage reference.

was increased until the pull-in voltage was reached. Capacitance was measured using a HP 4284A four terminal-pair impedance bridge at 1 MHz and 0.5 $V_{\rm rms}$, with the two sections of the lower electrode shorted together. The component capacitance, at $V_{\rm dc} = 0$, was from 1.4 to 1.9 pF, which the HP bridge could resolve to approximately 10 aF. From the C–V curves, both the pull-in voltage and the dc bias voltage needed for the split electrodes, to compensate the built-in voltage, were determined. The repeatability measurements demonstrate that the pull-in and the built-in voltages of these types of components do not change with cycling of the applied dc voltage, and only the shunt capacitance changes due to ambient temperature variations.

VI. Experimental Setup and Feedback Electronics

The schematic of the experimental setup and the force feedback electronics used to monitor the stability of the device is shown in Fig. 7. The elastically supported seesaw electrode is symmetrically positioned above six rigid electrodes to form six capacitances. The position of the seesaw electrode is monitored by the ac capacitive bridge formed of the innermost electrodes (3, 4). The ratio of the ac voltage levels of the two arms is adjusted so that the total current at the seesaw vanishes at $x = d/3$. The deflection of the seesaw is stabilized at $x = d/3$ by controlling the dc voltage on the two rightmost electrodes (1, 2). These electrodes have equal areas and are located equidistant from the springs. Since the electrostatic force is independent of the voltage polarity, the built-in voltage can be compensated by applying slightly different voltages with opposite polarities to the electrodes as discussed in Section IV. The voltage difference is controlled with gain G. The feedback voltage is the result of an output voltage from the bridge, which is proportional to the seesaw fluctuations away from the set value of $x = d/3$. This voltage is combined with a reference voltage from the bridge oscillator in a mixer. The resultant output of the mixer is a dc voltage with superimposed harmonic components of the input voltages. The harmonics of the fundamental are filtered using a

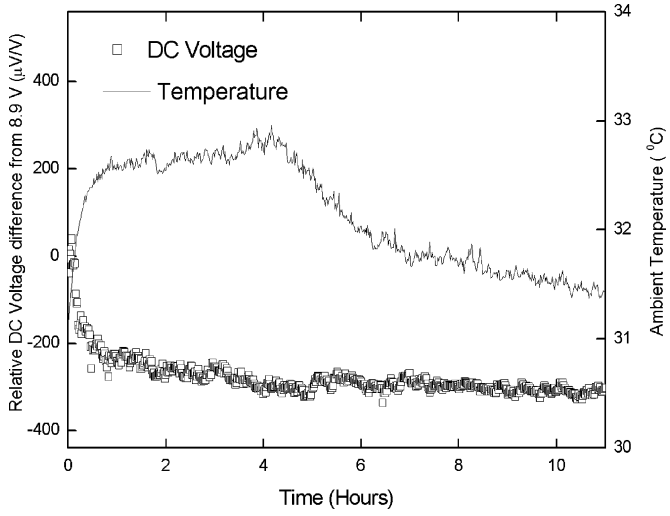

Fig. 8. Stability of the dc voltage reference (component S7/SAW6) over 11 h, showing best stability of 60 μV/V. The solid curve shows the corresponding ambient temperature recorded during the measurements.

lowpass filter, leaving only a dc signal. This is fed to a $\mathrm{PI}^{3/2}$ controller in the feedback loop which restores the position of the seesaw electrode to the set value of $x = d/3$. This controller output voltage can be used as the dc reference voltage.

VII. DC Voltage Experiment

Fig. 8 shows a dc voltage reference measurement result. After the initial rapid change in the reference voltage, the device stabilizes at approximately 60 μV/V stability over the next 10 h. Fig. 8 does not include any ambient temperature corrections to the measured dc voltage reference. Therefore, the inherent stability of the device is likely to be better. Further improvements are still needed for component packaging and feedback electronics.

VIII. Conclusion

We have designed a new MEMS component optimized for a dc voltage reference use and developed a manufacturing process for it. The main target was to eliminate surface charging and mechanical stress effecting the component stability. The first experimental results of the new device show an order of magnitude improvement with respect to earlier work. Further work will include improvements in the feedback electronics as well as stress-free mounting of the component.

References

[1] M. Suhonen, H. Seppä, A. S. Oja, M. Heinilä, and I. Näkki, "AC and DC voltage standards based on silicon micromechanics," in *Proc. CPEM Conf. Dig.*, 1998, pp. 23–24.

[2] H. Seppä, A. S. Oja, and M. Suhonen, "Micromechanical AC and DC Voltage Reference System," W.O. Patent, PCT/FI99/00553, WO 00/02110, 1999.

[3] A. S. Oja, J. Kyynäräinen, and H. Seppä, "A micromechanical DC voltage reference," in *Proc. CPEM Conf. Dig.*, 2000, pp. 701–702.

[4] J. Kyynäräinen, A. S. Oja, and H. Seppä, "Stability of microelectromechanical devices for electrical metrology," *IEEE Trans. Instrum. Meas.*, vol. 50, no. 6, pp. 1499–1503, Dec. 2001.

[5] H. Seppä, J. Kyynäräinen, and A. S. Oja, "Microelectromechanical systems in electrical metrology," *IEEE Trans. Instrum. Meas.*, vol. 50, no. 2, pp. 440–444, Apr. 2001.

[6] L. A. Rocha, E. Cretu, and R. F. Wolffenbuttel, "Stability of a micromechanical pull-in voltage reference," *IEEE Trans. Instrum. Meas.*, vol. 52, no. 2, pp. 457–460, Apr. 2003.

[7] P. Helistö and H. Seppä, "Measurement uncertainty in the presence of low-frequency noise," *IEEE Trans. Instrum. Meas.*, vol. 50, no. 2, pp. 453–456, Apr. 2001.

[8] L. A. Rocha, E. Cretu, and R. F. Wolffenbuttel, "Analysis and analytical modeling of static pull-in with application to MEMS-based voltage reference and process monitoring," *J. Microelectromech. Syst.*, vol. 13, pp. 342–354, 2004.

PUBLICATION V

Electrical Stability of a MEMS-based AC Voltage Reference

Submitted to Sensors and Actuators A.
Reprinted with permission from Elsevier.

Electrical stability of a MEMS-based AC voltage reference

A. Kärkkäinen, N. Tisnek*, A. Manninen*, N. Pesonen,
A. Oja, and H. Seppä

VTT, P.O. Box 1000, 02044 VTT, Finland
(corresponding author phone: +358-20-722 4377; fax: +358-20-722 7029;
e-mail: anu.karkkainen@vtt.fi).

*Centre for Metrology and Accreditation (MIKES),
P.O. Box 9, 02151 Espoo, Finland

Abstract

This paper studies the electric stability of a MEMS based AC voltage reference. The operation of the device is based on the characteristic pull-in phenomenon of a moving plate capacitor. The stability of a MEMS-based AC voltage reference was improved from 3 ppm/day to below 2 ppm/22 days by compensating the built-in voltage with an external DC voltage source. This level of performance is sufficient for several applications and is outstanding compared to results published earlier.

Key Words Microelectromechanical systems, capacitive sensors, micromachining, built-in voltage, voltage reference, oxide charging

I. INTRODUCTION

Voltage references are fundamental building blocks in many instruments like data logging systems, digital multimeters, and calibrators. We have presented the first MEMS based AC voltage reference in [1]. The operation of the AC voltage reference is based on a characteristic property of an electrostatic MEMS component: the pull-in voltage. The component is actuated to the maximum point of the characteristic current-voltage curve using AC current. The maximum voltage depends only on the component geometry and material properties and it is therefore an excellent reference [2]. The benefits of MEMS components in reference applications are good stability [3], low 1/f noise, large operation voltage range, small size, and low power consumption. However, because of a relatively high temperature coefficient, in the order of 100 ppm/°C [2], the reference voltage needs to be compensated for changes in temperature or the component needs to be placed in a temperature-stabilized oven.

In our previous work we have demonstrated that charging of a MEMS component, operated near the pull-in point, can be significantly reduced by using AC voltage for the actuation instead of DC voltage [4]. However, even in the absence of an external DC voltage source, the component will experience an effective DC voltage, which originates from the work function difference of a metal-semiconductor junction, and an offset voltage due to charges in the dielectric layers. In this paper we will demonstrate their effect on the stability of the AC voltage reference. If the effective DC voltage over the MEMS component is constant, it will only reduce the value of the AC reference voltage, but does not jeopardize the device stability. However, if the effective DC voltage changes with time and is not compensated, the change has a first order effect on the stability of the AC reference voltage.

A dielectric layer on top of an electrode of a MEMS component can have a two-fold effect on the component stability. On one hand, the dielectric layer passivates the electrode surface and hence increases the device stability. For example, if there are any process chemicals inside the component enclosure, their adsorption on the electrodes varies with temperature causing a change in the surface potential of the electrode. This effect can be reduced with a dielectric layer. On the other hand,

charge build-up in a dielectric layer is observed in an electric field [5]. Charging of the dielectric layer forms a potential source of instability for the AC voltage reference. Even without a processed dielectric layer, there is always a thin native oxide layer on the electrode surface [3].

II. PRINCIPLE OF OPERATION

The moving plate capacitor, shown in Fig.1, is actuated to the maximum point of its characteristic current-voltage curve using AC current $I(t) = \hat{I}\sin\omega t$. There is also an effective DC voltage, V_{DC}, over the component due to the built-in voltage and charges in the oxide layer. The electrostatic force F_E attracts the electrodes together while the spring force F_M due to the elastically suspended electrode, tries to restore the plate position. The force balance equation is

$$F_E = F_{E,I} + F_{E,V} = -\frac{d}{dx}\left(E_I + E_V\right) = kx = F_M, \tag{1}$$

where $F_{E,I}$ and $F_{E,V}$ are the electrostatic forces due to the AC current I and due to the DC voltage V_{DC}, E_I and E_V are the electrostatic energies, respectively, x is the deflection of the moving electrode, and k is the spring constant. Assuming that the electrodes are in parallel and the movement is translational, $F_{E,I}$ can be calculated from

$$F_{E,I} = -\frac{d}{dx}\left(\frac{q^2(t)}{2C}\right) = \frac{\hat{I}^2}{2\varepsilon A\omega^2}\cos^2(\omega t), \tag{2}$$

where $C = \varepsilon A/(d-x)$ is the component capacitance, ε is the permittivity of the medium, A is the electrode area, d is the gap between the electrodes, and $q(t) = \int \hat{I}\sin(\omega t)dt$ is the capacitor charge. The force due to the DC voltage is

$$F_{E,V} = -\frac{d}{dx}\left(\frac{CV_{DC}^2}{2}\right) = \frac{1}{2}V_{DC}^2\frac{\varepsilon A}{(d-x)^2}. \tag{3}$$

When either the frequency of the actuation current, $\omega/2\pi$, is much higher than the component mechanical resonance frequency or the motion of the moving electrode is sufficiently damped, the position of the moving electrode is stationary over the period of driving frequency and the $\cos^2(\omega t)$ term equals ½.

The rms voltage V_{AC} across the plate as a function of the displacement x can now be calculated from Eq. (1)–(3):

$$V_{AC} = \frac{\hat{I}(d-x)}{\sqrt{2}\omega\varepsilon A} = \sqrt{\frac{2k}{\varepsilon A}(d-x)^2 x - V_{DC}^2}\ . \tag{4}$$

The maximum of $V_{AC}(\hat{I})$, which is the reference voltage, can be calculated from $dV_{AC}(\hat{I})/d\hat{I} = (dV_{AC}(x)/dx)(\, dx/d\,\hat{I}\,) = 0$. Since $dx/d\,\hat{I} \neq 0$, the maximum is reached when $dV_{AC}(x)/dx = 0$, which occurs at $\hat{I} = \left(3/\sqrt{2}\right)\omega\varepsilon A V_{pi}/d$, corresponding to $x = d/3$. The maximum of V_{AC} is

$$V_{AC}^{max} = \sqrt{V_{pi}^2 - V_{DC}^2}\ , \tag{5}$$

where

$$V_{pi} = \sqrt{\frac{8kd^3}{27\varepsilon A}} \tag{6}$$

is the component pull-in voltage.

Small time variations ΔV_{DC} of the V_{DC} can be described as $V_{DC} = V_{DC,0} + \Delta V_{DC}$, where $V_{DC,0}$ is a constant. Since $V_{DC} << V_{AC}$, Eq. (5) can be expressed as

$$V_{AC}^{max} = V_{pi} - \frac{V_{DC,0}^2}{2V_{pi}} - \frac{V_{DC,0}}{V_{pi}}\Delta V_{DC}\,. \tag{7}$$

Equation (7) demonstrates that selecting $V_{DC,0} = 0$, small changes in the DC voltage, ΔV_{DC}, have no effect on the reference voltage in the first order.

III. STABILITY

V_{DC} in Eq. (3) is a sum of all DC voltages effecting on the component:

$$V_{DC} = V_{bi} + V_c(V_{bi}, V_{bias}, t) + V_{bias}, \tag{8}$$

where V_{bi} is the built-in voltage originating from the contact potential difference of silicon and metal, V_c is the voltage due to the charges in the oxide layer, t is time, and V_{bias} the externally applied bias voltage.

Ideally, the built-in voltage is the difference of the materials work functions [5]. For example in the case of silicon aluminum interface, $V_{bi} \approx 4.28$ V – 4.85 V = -0.57 V. However, in practice the situation is more complicated. The disruption of the crystal lattice produces a large number of surface energy states located in the forbidden bandgap. Also, the work function for a thin layer of metal can differ significantly from the bulk value. In addition, the built-in voltage depends on temperature [5].

Charges in the oxide, at the SiO_2 – Si interface, and on the surface of the oxide layer create the voltage V_c. Wibbeler *et al.* [6] have calculated the voltage V_c for a moving capacitor plate structure due to a sheet charge at the dielectric-air interface and van Spengen *et al.* [7] have expanded the model by taking also the trapped charge in the bulk oxide into account. However, these models do not discuss the generation nor the time evolution of charging. These issues have recently been studied for pFET devices under negative bias voltage. It is generally accepted that interface traps and fixed charges are generated from the dissociation of silicon-hydrogen bonds. Diffusion models describing the break of a Si-H bond, where hydrogen diffuses away and reacts with the oxide, have been developed [8]. These models yield a 1-exp(-t/τ) time behavior, where the charging saturates with a time constant τ. The final amount of charge depends, e.g., on the electric field over the oxide layer, oxide thickness, and temperature. Manufacturing process of the oxide, impurity concentration, mechanical stress, and several other parameters are known to have an effect as well.

IV. COMPONENT

A schematic view of the MEMS moving plate capacitor used in this study and its electric equivalent circuit are displayed in Fig. 1. The component is a dice from a bulk micromachined stack of three silicon wafers. A silicon wafer, where the moving structure is etched, is anodically bonded between two glass-covered silicon wafers. The silicon is boron doped, $N_A = 2\times10^{18}$ cm^{-3}, and the surface of the moving mass has additional boron doping $N_A = 4\times10^{19}$ cm^{-3}. The fixed electrode on glass is made of AlCu. The surface areas of the electrodes are 1.45×10^{-6} m^2, the spring constant is 30 N/m and the gap is 5.7 µm. The measured pull-in voltage values are +9.32 V and -8.82 V.

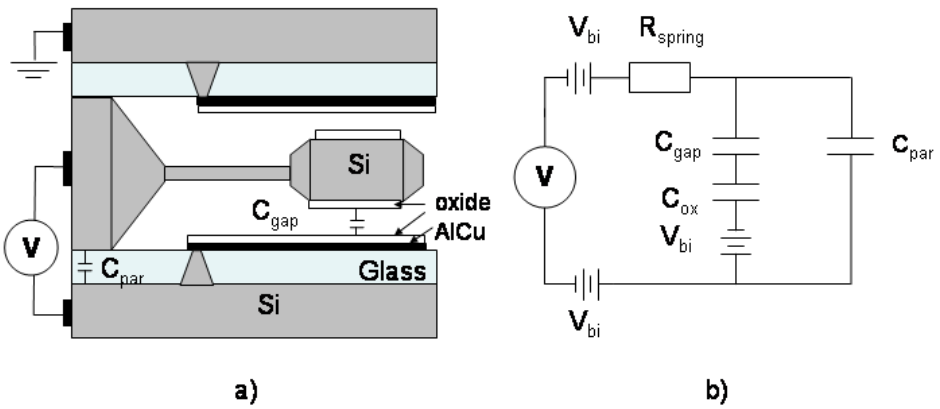

Figure 1. a) Schematic structure of the silicon cantilever used as a moving plate capacitor and b) the equivalent circuit. V is the external voltage source, V_{bi} is the built-in voltage of the metal-silicon junction. C_{gap} is the component capacitance (work capacitance), which has a parasitic capacitance C_{par} in parallel. C_{ox} is the capacitor formed by the dielectric layer (usually SiO_2). R_{spring} is the resistance of the silicon spring.

V. ELECTRONICS

The AC voltage reference electronics block diagram is show in Fig. 2. A 100 kHz AC voltage, V_{AC_in} is fed to the inverting input of the main operational amplifier OA2, which acts as a voltage to current converter. The amplitude of the input current is slowly varied over the maximum point and the maximum output voltage was recorded as the AC reference voltage (the AC component of V_{out} in Fig. 2). The instrumentation amplifier IA1 isolates the AC source. The stability of the OA2 gain is recorded at the output of the unity gain buffer amplifier OA3. The DC bias voltage for the built-in voltage compensation is fed to the non-inverting input of OA2. The DC voltage over the MEMS component is $V_{DC\_out} - V_{DC\_bias}$, where V_{DC_out} is the DC component of V_{out} in Fig. 2. A trimmer resistor is needed to find the right DC compensation voltage, but once found, the trimmer can be replaced with a fixed resistor. Temperature, pressure and humidity are recorded during the measurement and used for the multi-regression analysis to correct the measurement data.

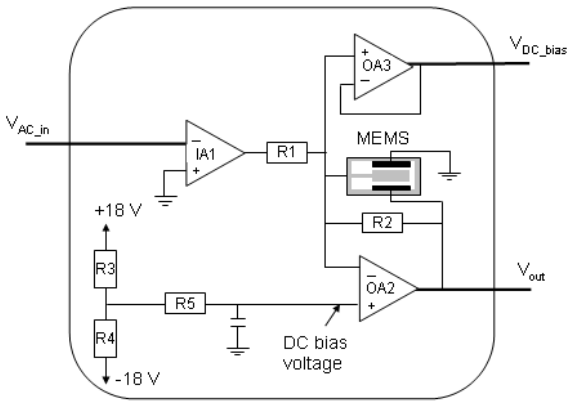

Figure 2. Electronics block diagram of the AC voltage reference. The reference voltage V_{out} contains an AC component V_{AC_out} and a DC component $V_{DC\_out.}$

We have experimentally demonstrated that small changes in the parasitic capacitance or in the parasitic resistance over the component have no effect on the pull-in voltage [2]. Hence the stability of the electronics depends only on the stability of the MEMS component and the stability of the OA2 gain.

VI. DEPENDENCE OF V_{AC} ON THE BIAS VOLTAGE

The dependence of the reference voltage $V_{\mathrm{AC}}^{\max}$ on the applied bias voltage V_{bias} was measured and compared with the calculated values (see Eq. 5). The results are displayed in Fig. 3. The pull-in voltage V_{pi} (Eq. 6) for the calculated curve was derived from the measured *C-V* curve, shown in Fig.4, as the average value of $V_{pull-in}^{+}$ and $-V_{pull-in}^{-}$, where $V_{pull-in}^{+}$ is the run-off point with the positive bias voltage and $V_{pull-in}^{-}$ is the run-off point with the negative bias voltage. If the component is uncharged, *i.e.* $V_{\mathrm{c}} = 0$, V_{bi} is the minimum point of the *C-V* curve, which is 0.245 V. The maximum of the measured $V_{\mathrm{max}}^{\mathrm{AC}}$ curve is obtained when $V_{\mathrm{bias}} = -V_{\mathrm{bi}}$, and it is -0.278 V (in Fig. 3). The measured and calculated values are in fairly good agreement especially considering that the initial charging state of the component may vary, despite of short circuiting the component between the measurements, due to long time constants related to the charging phenomena.

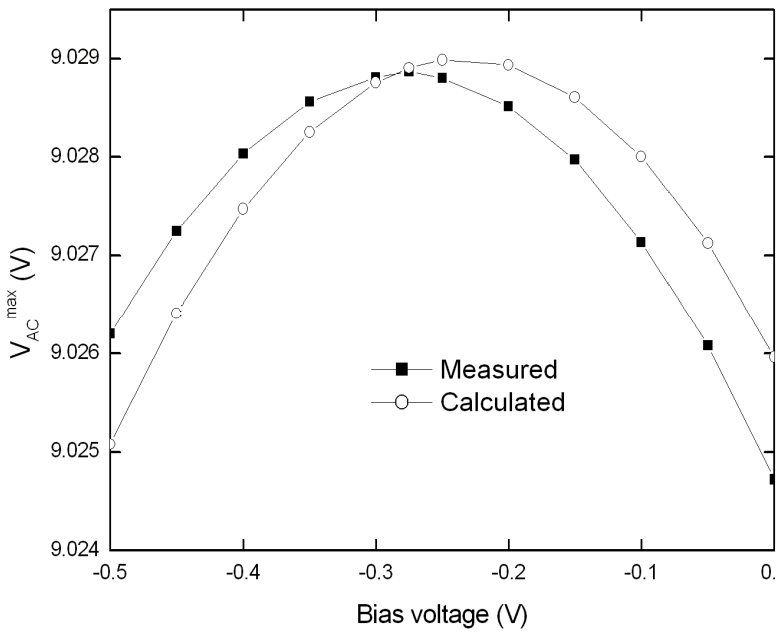

Figure 3. Calculated and measured $V_{\mathrm{AC}}^{\max}$ curves as a function of externally applied DC bias voltage.

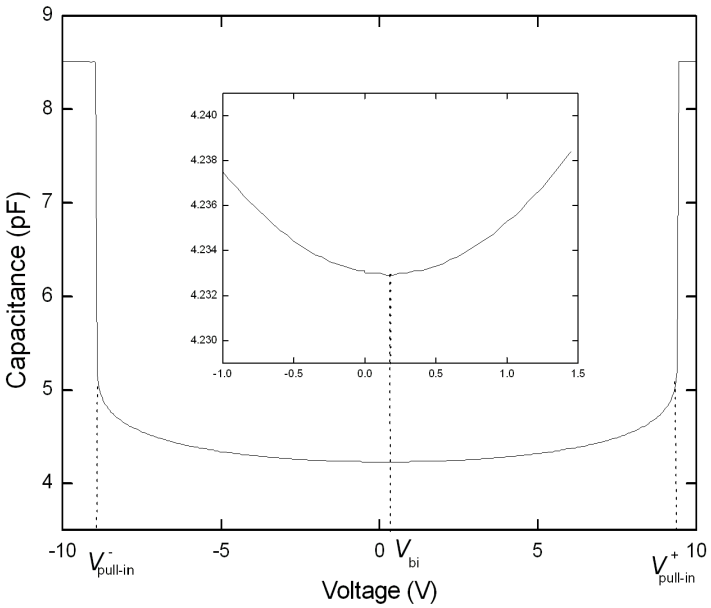

Figure 4. Measured C-V curve of the component and a second order fit to the data points near the zero voltage (insert). The built-in voltage is the minimum point of the C-V curve.

VII. DRIFT OF THE AC REFERENCE VOLTAGE

The stability of the AC voltage reference was monitored when different bias voltages where applied over the MEMS component. The reference was closed in a temperature stabilized chamber mounted on a stone table. The temperature of the chamber varied less than 0.1 °C around the average value of about 23.5 °C. The bias voltage was set close to the built-in voltage value by changing the values of resistors R3 and R4 (see Fig. 2), and the AC reference voltage was monitored with HP 3458A DVM for 4…22 days for each bias voltage setting. The measurement was made by changing the amplitude of the driving 100 kHz current across the pull-in point, and by recording the rms value of the reference output voltage with the DVM for each amplitude value resulting in a curve similar to the one presented in Fig. 3. A second-order polynomial fit was made to the data and the voltage at the maximum, V_{max}, was determined.

The measured AC voltage was corrected for changes in temperature, pressure and humidity using multiple regression analysis. The AC voltage was observed to vary linearly with time. The slope of the curve is the drift rate which is shown in Fig. 5 for different bias voltage values.

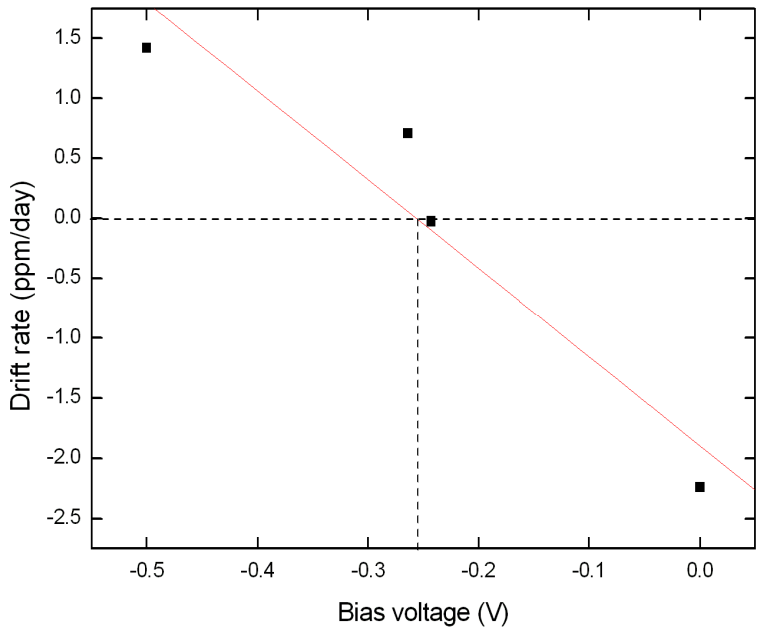

Figure 5. Drift rate of the AC reference voltage as a function of bias voltage.

The results indicate a linear behaviour of the drift rate as a function of the applied DC bias voltage for small bias voltage values. If the bias voltage is larger than $-V_{bi}$, the drift is negative and vice versa. The optimal point of operation for the AC voltage reference is the maximum of the V_{AC}^{max} *vs.* V_{bias} curve, which corresponds to $V_{DC} = 0$. The vanishing DC voltage prevents the charging of the MEMS component and also eliminates possible small changes in the DC voltage in the first order (see Eq. 7).

VIII. STABILITY OF THE AC REFERENCE

Finally, the long-term stability of the AC voltage reference was measured using the bias voltage value of -0.243 V. The measurement setup of the 3-week long experiment was similar to the one described above except that the stability of the HP 3458A DVM was periodically (about once in a day) compared against a Datron 4920 AC measurement standard and a Fluke 5700 A calibrator as shown in Fig. 6 (in the upper part). The uncertainty of the DVM during the experiment was of the order of 2 ppm. V_{max} was determined from a parabolic fit as explained in Chapter VII. Essentially identical results, with slightly larger scatter, would have been obtained by monitoring the output voltage at a fixed amplitude of the driving current set to the pull-in point. The results are plotted in Fig. 7 after correcting the data for changes in ambient pressure (-6 µV/hPa) and temperature (-180 µV/ºC). No drift could be observed in the 100 kHz output voltage of the device within the measurement accuracy of about 2 ppm during a 3-week period. The drift rate without the built-in voltage compensation was measured to be more than 3 ppm per day for the same component. The noise correlated approximately as 1/*f* according to the Fourier analysis made to the data.

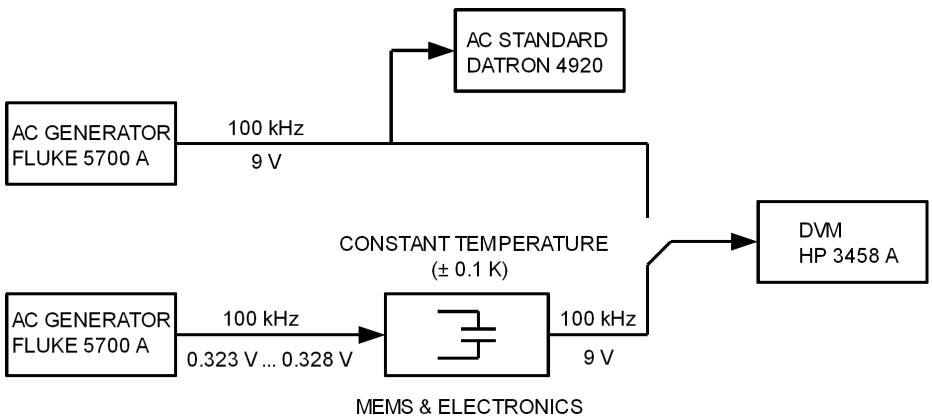

Figure 6. Measurement setup for the time stability measurement.

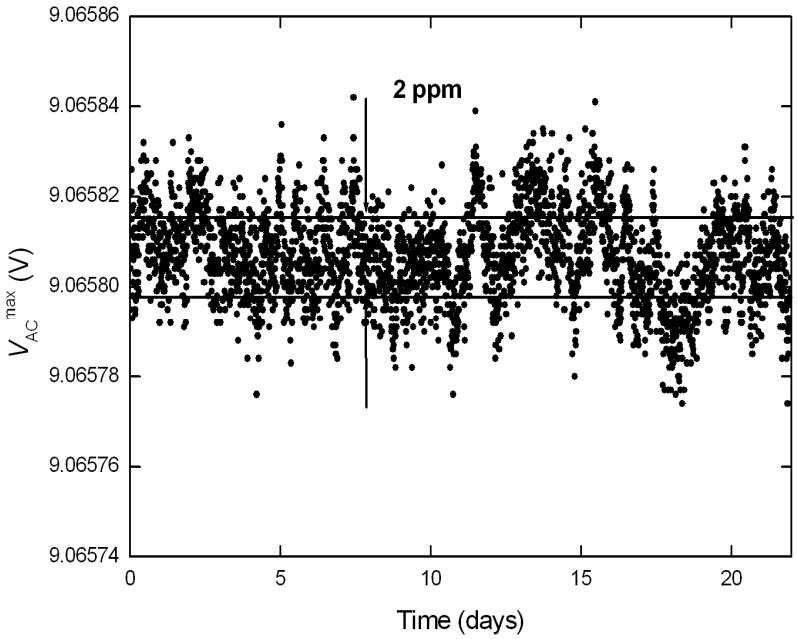

Figure 7. Long-term stability of the built-in voltage compensated AC voltage reference.

After the stability test was finished, both the AC drive and the DC bias (built-in voltage compensation) were disconnected but the device was kept at the temperature isolated measurement chamber. After one day the voltages were reconnected and the measurement continued. After a relaxation period of about 8 hours, the output voltage returned to the original level within the measurement accuracy of about 2 ppm, as shown in Fig. 8.

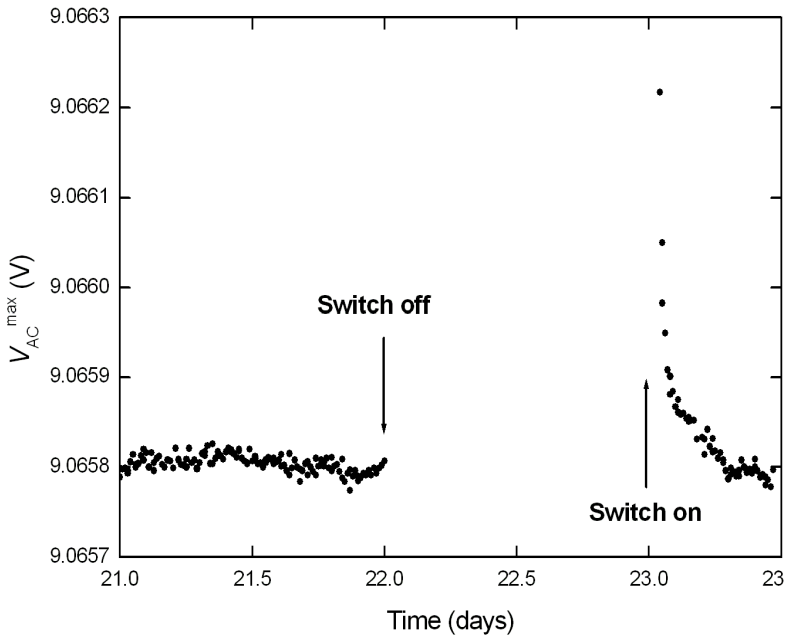

Figure 8. Recovery of the AC voltage after the power has been switched off for one day.

IX. CONCLUSIONS

The long-term stability of a MEMS based AC voltage reference has been studied. Charging of the MEMS component causes significant drift of the AC reference voltage. Charge build-up is observed even when the electrodes are covered only with a thin native oxide layer and the built-in voltage is not compensated. With the compensation the drift was reduced below 2 ppm during a 3-week measurement period. This level of performance is sufficient for several metrological applications and it is so far the best published result for a MEMS based voltage reference. Also, the AC reference can be utilized as a very sensitive device to study the stability of moving plate capacitor structures.

X. ACKNOWLEDGEMENTS

Heikki Kuisma from VTI Technologies Ltd. is acknowledged for providing test components and for useful discussions, and Jari J. Penttilä is acknowledged for his technical assistance in the project. This work has been carried out under EMMA project (IST-2000-28261) funded by the European Commission Framework V Program. Financial support of the National Technology Agency of Finland (TEKES) is also acknowledged.

References

[1] M. Suhonen, H. Seppä, A.S. Oja, M. Heinilä, and I. Näkki, AC and DC Voltage Standards Based on Silicon Micromechanics, CPEM'98 Conf. Dig., 1998, pp. 23–24.

[2] A. Kärkkäinen, N. Pesonen, M. Suhonen, A. Oja, A. Manninen, N. Tisnek, and H. Seppä, MEMS based AC Voltage Reference, IEEE Trans. Instrum. Meas. 54, Apr. 2005, pp. 595–599.

[3] J. Kyynäräinen, A. S. Oja, and H. Seppä, Stability of Microelectromechanical Devices for Electrical Metrology, IEEE Trans. Instrum. Meas. 50, 2001, pp. 1499–1503.

[4] A. Kärkkäinen, A. Oja, J. Kyynäräinen, H. Kuisma, and H. Seppä, Stability of Electrostatic Actuation of MEMS, Physica Scripta, T114, 2004, pp. 193–194.

[5] S.M. Sze, Semiconductor devices, John Wiley & Sons Ltd, 2nd edition, 2002, ISBN 0-471-33372-7.

[6] J. Wibbeler, G. Pfeifer, and M. Hietschold, Parasitic charging of dielectric surfaces in capacitive microelectromechanical systems (MEMS), Sensors and Actuators, A 71, 1998, pp. 74–80.

[7] W.M. van Spengen, R. Puers, R. Mertens, and I. De Wolf, A comprehensive model to predict the charging and reliability of capacitive RF MEMS switches, J. Micromech. Microeng. 14, 2004, pp. 514–521.

[8] D.K. Schröder and J.A. Babcock, Negative Bias temperature instability: Road to cross in deep submicron silicon semiconductor manufacturing, J. Appl. Phys. 94, July 2003, pp. 1–18.

Biographs

Anu Kärkkäinen received the M.Sc degree in 1985 and Licentiate degree in 1987 from Helsinki University. She worked as senior scientist at Vaisala Oyj developing different capacitive sensors and measurement systems (1986–1995). During that time she also visited Arizona State University Optical Detection laboratory. She worked as Product Manager at Vaisala optical sensors (1995–1998) and then she coordinated the Finnish node in the EU funded HPCN-TTN network at CSC, Finnish Supercomputing Centre (1998–2001). Since 2001 Mrs. Kärkkäinen has been working with the MEMS Sensors Group, VTT Technical Research Centre of Finland as project coordinator and researcher in the EU funded project EMMA, which develops capacitive MEMS components for precision applications.

Nadine Pesonen received the M.S. degree in electrical engineering from Ecole Nationale Supérieure d'Electronique, Electrotechnique, Hydraulique, Informatique, Toulouse, France, in 1998 and the D.Sc. degree in electrical engineering from the George Washington University, Washington, DC, in 2002. From 1998 to 2002, she was a Guest Researcher with the IC Technology Group, National Institute of Standards and Technology (NIST), Gaithersburg, MD. At NIST, she developed a non-contact capacitive sensor for chrome photomasks implemented using a Low Temperature Co-Fired Ceramic technology. Since October 2002, she has been with the MEMS Sensors Group, VTT Technical Research Centre of Finland.

Aarne Oja (born 1960) received his Dr. Tech. Degree in 1988 from the Low Temperature Laboratory of the Helsinki University of Technology. He moved to VTT in 1995 and is now the leader of the MEMS sensors group and Research Professor in the field of Sensor Technology. His current research interests include micromachined RF resonators, pressure and ultrasound sensors, RFID technology, and microsystems for ambient intelligence.

Antti Manninen (born 1963) received his M.Sc. (Tech.) and D.Sc. (Tech.) degrees in technical physics from the Helsinki University of Technology, Finland, in 1990 and 1993, respectively. He made D.Sc. thesis work on experimental properties of superfluid He-3 in the Helsinki University of Technology, Finland, and continued research on that field for two years in the University of Manchester, U.K. After that he has studied single electron phenomena in nanostructures in the University of Jyväskylä, Finland, and data transmission using WCDMA techniques in Nokia Research Center, Finland. He joined the Centre for Metrology and Accreditation (MIKES), Espoo, Finland, in the end of 2001. Currently he leads the Electricity Group of MIKES and works in the field of electrical metrology. Research interests include metrological applications of quantum phenomena (Josephson effect, quantum Hall effect, single electron tunnelling) and microelectromechanical devices.

Nikolai Tisnek was born in Russia in 1943. He received the M.Sc.degree in Engineering from Saint-Petersburg State Polytechnical University in 1966. He then began to work at the Ioffe Physico-Technical Institute, Saint-Petersburg, Russia, where he received the Ph.D. degree in Physics and Mathematics in 1971. From 1985 to 1996 he worked as a Research Scientist at the “Electron” National Research Institute in Saint-Petersburg, Russia. Until March 2000 he worked as a Research Scientist at Helsinki University of Technology, Helsinki, Finland. From May 2001 he has been working as a Research Scientist at the Centre for Metrology and Accreditation in Helsinki, Finland, where his research interests include measurements of MEMS devices. He is the author or coauthor of over a hundred journals, conference and technical publications and 7 patents.

Heikki Seppä (born 1953) received the M. Sc., the Licentiate Tech. degree and the Dr. Tech degree in technology, from Helsinki University of Technology, Espoo, Finland in 1977, 1979, and 1989, respectively. From 1976 to 1979, he was an Assistant at the Helsinki University of Technology, working in the area of electrical metrology. He joined the VTT Technical Research Centre of Finland, Espoo in 1979 and since1989 he acted there as a Research Professor. In 1994 he was appointed the Research Manager of the Measurement Technology Field. In 1996 he acted a short period as the Research Director of VTT Automation. He has done research work on electrical metrology, in general, and on superconducting devices for measurement applications, in particular. Currently, he is doing research on DC SQUIDs, quantized Hall effect, SET-devices and microelectromechanical devices.

Published by

Series title, number and report code of publication

VTT Publications 613
VTT–PUBS–613

Author(s)
Kärkkäinen, Anna-Maija

Title

MEMS based voltage references

Abstract

Microsystem technology has enabled a new field in metrology. Voltage references based on MEMS, microelectromechanical systems, are unique in two different ways. First, they are small in size and cost-efficient since they are manufactured using equipment and facilities developed for integrated circuit mass production, where a large number of components are processed on a single silicon wafer. Second, the principle of operation of a MEMS voltage reference is outstanding from the physics point of view. They are electrical references, but their stability is based on material properties of single crystal silicon which is one of the most stable materials. The level of performance of electrical instruments, which utilize voltage references as their key components, like digital multimeters, data logging systems, and calibrators, is proportional to the stability of the voltage reference.

This dissertation provides a comprehensive description of how to make a MEMS based voltage reference. Two references, one for DC voltage and the other for AC voltage, were manufactured as well as the MEMS components for them. The components design and manufacturing, readout electronics and characterisation of the final devices are described. The focus is on the stability of the devices, which has so far been the major limiting factor exploiting commercial MEMS components in high end applications.

The major achievement of this work was the improvement of the electrostatic stability of the AC voltage references to a level applicable in metrology. The innovations related to the stability improvement, as well as the new process developed for the components manufacturing, have general applicability in micromechanics. This work demonstrates that MEMS based voltage references can provide a competitive alternative to the conventional voltage references.

Keywords

MEMS, micro electromechanical systems, DC voltage reference, AC voltage reference, electrostatic charging, pull-in voltage, long-term stability, micromachining

ISBN

951–38–6859–1 (soft back ed.)
951–38–6860–5 (URL: http://www.vtt.fi/publications/index.jsp)

Series title and ISSN	Project number
VTT Publications 1235–0621 (soft back ed.) 1455–0849 (URL: http://www.vtt.fi/publications/index.jsp)	

Date	Language	Pages	Price
October 2006	English	109 p. + app. 42 p.	D

Name of project	Commissioned by

Contact

VTT Technical Research Centre of Finland
Tietotie 3, P.O. Box 1000, FI-02044 VTT, Finland
Phone internat. +358 20 722 111
Fax +358 20 722 7012

Sold by

VTT Technical Research Centre of Finland
P.O.Box 1000, FI-02044 VTT, Finland
Phone internat. +358 20 722 4404
Fax +358 20 722 4374

Julkaisija

Julkaisun sarja, numero ja raporttikoodi

VTT Publications 613
VTT–PUBS–613

Tekijä(t)

Nimeke

MEMSiin perustuvat jännitereferenssit

Tiivistelmä

Mikroelektromekaanisiin systeemeihin, eli MEMSiin, perustuvat jännitereferenssit ovat ainutlaatuisia sekä ominaisuuksiltaan että toimintaperiaatteeltaan. Ne ovat pieniä ja tarkkoja, ja niillä on hyvä hinta-laatusuhde. Referenssin toiminta perustuu mikromekaanisesti valmistettuun levykondensaattoriin, jonka toinen levy on ripustettu piijousien varaan. Levyjen väliin kytketty jännite pyrkii lähentämään levyjä toisiinsa, kun taas piijousi vastustaa tätä liikettä. Voimatasapainoa levyjen välillä voidaan kuvata massa-jousi-vaimennin-mallilla ja sillä on kaksi keskeistä ominaisuutta. Sähköstaattinen voima levyjen välillä on verrannollinen jännitteen neliöön, eli sitä voidaan käyttää todellisena tehollisarvomuuntimena. Lisäksi kondensaattorin ulostulojännitteellä on maksimi, jota voidaan käyttää stabiilina jännitereferenssinä, sillä sen arvo riippuu vain yksikiteisen piin materiaalivakiosta ja jousen geometriasta. Koska referenssijännite on samalla myös käännepiste, ohjausjännitteen pienet vaihtelut eivät vaikuta referenssijännitteen arvoon ensimmäisessä kertaluvussa. Näiden ominaisuuksien ansiosta MEMS-jännitereferenssit tulevat haastamaan olemassa olevat jännitereferenssit, esimerkiksi Zenerdiodit.

Väitöskirjassa tutkitaan sekä teoreettisesti että kokeellisesti kahta jännitereferenssiä, joista toinen on suunniteltu tasajännitteelle ja toinen vaihtojännitteelle. Molemmille suunniteltiin omat MEMS-komponentit. Niiden suunnittelu, valmistus ja ominaisuudet on kuvattu yksityiskohtaisesti samoin kuin referenssien lukuelektroniikat ja valmiiden laitteiden ominaisuudet. Erityisesti huomiota on kiinnitetty referenssien sähköiseen stabilisuuteen, joka on myös nykyisin kaupallisessa tuotannossa olevien MEMS-komponenttien ongelma. Väitöstyön merkittävin saavutus on MEMS-komponenttien sähköisen stabiilisuuden parantaminen tasolle, joka mahdollistaa niiden hyödyntämisen vaativissa metrologisissa sovelluksissa. Näitä innovaatioita, samoin kuin työssä kehitettyä uutta valmistusmenetelmää, voidaan geneerisesti hyödyntää myös muihin MEMS-sovelluksiin.

Avainsanat

MEMS, micro electromechanical systems, DC voltage reference, AC voltage reference, electrostatic charging, pull-in voltage, long-term stability, micromachining

ISBN

951–38–6859–1 (nid.)
951–38–6860–5 (URL: http://www.vtt.fi/publications/index.jsp)

Avainnimeke ja ISSN			Projektinumero
VTT Publications 1235–0621 (nid.) 1455–0849 (URL: http://www.vtt.fi/publications/index.jsp)			
Julkaisuaika Lokakuu 2006	Kieli Englanti, suom. tiiv.	Sivuja 109 s. + liitt. 42 s.	Hinta D
Projektin nimi		Toimeksiantaja(t)	

Yhteystiedot

VTT
Tietotie 3, PL 1000, 02044 VTT
Puh. vaihde 020 722 111
Faksi 020 722 7012

Myynti

VTT
PL 1000, 02044 VTT
Puh. 020 722 4404
Faksi 020 722 4374

Voltage references based on MEMS, microelectromechanical systems, are unique in two different ways. First, they are small in size, stable, and cost-efficient. Second, the principle of operation of a MEMS voltage reference is outstanding from the physics point of view. They are electrical references, but their stability is based on material properties of single crystal silicon. Voltage references are fundamental building blocks in many electrical instruments like digital multimeters, data logging systems, and calibrators. MEMS components are manufactured using equipment and facilities developed for integrated circuit mass production, where a large number of components are processed on a single silicon wafer. Microsystem technology has enabled a new field in metrology.

This dissertation provides a comprehensive description of how to make a MEMS based voltage reference. Two references, one for DC voltage and the other for AC voltage, were manufactured as well as the MEMS components for them. The components design and manufacturing, readout electronics and characterisation of the final devices are described. The focus is on the stability of the devices, which has so far been the major limiting factor exploiting commercial MEMS components in high end applications.

The major achievement of this work was the improvement of the electrostatic stability of the AC voltage references to a level applicable in metrology. The innovations related to the stability improvement, as well as the new process developed for the components manufacturing, have general applicability in micromechanics. This work demonstrates that MEMS based voltage references can provide a competitive alternative to the conventional voltage references.

Tätä julkaisua myy

VTT
PL 1000
02044 VTT
Puh. 020 722 4404
Faksi 020 722 4374

Denna publikation säljs av

VTT
PB 1000
02044 VTT
Tel. 020 722 4404
Fax 020 722 4374

This publication is available from

VTT
P.O. Box 1000
FI-02044 VTT, Finland
Phone internat. +358 20 722 4404
Fax +358 20 722 4374

ISBN 951–38–6859–1 (soft back ed.)
ISSN 1235–0621 (soft back ed.)

ISBN 951–38–6860–5 (URL: http://www.vtt.fi/inf/pdf/)
ISSN 1455–0849 (URL: http://www.vtt.fi/inf/pdf/)

Anna-Maija Kärkkäinen